TITLE

Photoluminescence studies of Silicon doped with Copper & Zinc.

A THESIS FOR THE DEGREE OF MASTER OF SCIENCE

PRESENTED TO THE NATIONAL COUNCIL FOR EDUCATIONAL AWARDS

BY

NIALL O' DONNELL

SCHOOL OF PHYSICAL SCIENCES

NATIONAL INSTITUTE FOR HIGHER EDUCATION DUBLIN.

RESEARCH SUPERVISOR. DATE

DR. M.O. HENRY (INTERNAL) 13/6/88

ABSTRACT

This report investigates the properties of silicon doped with the transition metal impurities copper and zinc. Low temperature photoluminescence measurements reveal an intense luminescence band with zero phonon structure around 919.56mev.Also contained in the spectra is the characteristic copper-copper pair band which has been identified as originating from isoelectronic Cu-Cu pair centres in a <111> configuration.

The 919.56 mev is found to have a slow decay time at low temperatures. This was exploited by the adoption of phase-shift techniques in a phase sensitive lock-in amplifier, which allowed the 919.56 mev band to be studied in isolation from the overlapping copper-copper pair band.

The 919.56mev luminescence spectrum exhibits a strong phonon sideband structure. The most prominent zero phonon line is observed at 919.56mev with phonon replicas separated by 6.3 mev indicating strong coupling to a local mode phonon of energy 6.3 mev. Special features observed at higher temperatures around the principle zero phonon line are identified as anti- Stokes replicas as well as lines originating in electron states at E_1 = 3.3mev and E_2 = 4.6mev above the lower excited state at E_o.

The temperature dependence of the luminescence decay time was studied using deconvolution techniques to correct for the detector response function. A rapid fall off is

observed for the decay time over the temperature range 50 - 100K, corresponding to thermalization over an energy barrier of 65 mev. The data is interpreted in terms of an isoelectronic bound exciton. The energy level structure and luminescence decay time are found to agree well with a model in which the binding centre is axial, with a positive (tensile) stress field and a large electron - hole exchange energy of 14 mev. The model proposed for the centre is a $Cu^{+} - Zn^{2-} - Cu^{+}$ defect, where a substitutional zinc double acceptor complexes with two interstitial copper atoms to produce the isoelectronic binding centre for the excitons.

Acknowledgements.

I would sincerely like to thank my supervisor Dr. Martin Henry for his continued help and advice throughout my studies at the NIHE Dublin. I am also indebted to those in the Physics department whose help and encouragement is deeply appreciated.

I would like to acknowledge the support of Cavan Vocational Educational Committee and the Research and Postgraduate Studies Committee of NIHE Dublin.

Contents. Page

List of Figures. Page

Chapter 1.

Chapter 2.

Chapter 3.

Chapter 4.

list of Tables. Page

List of Equations.

4.5 $\text{Tan}(\phi) = wt$ 89

4.6 $S(t) = k\exp(-t/\tau) \int_0^t D(x) \exp(x/\tau)\, dx$ 95

4.7 $S(t_i) = [S(t_{i-1}) + k\,\Delta t D(t_{i-1})/2]\exp(-\Delta t/\tau) + k\,\Delta t D(t_i)/2$ 95

4.8 $i(t) = k_1\exp(-t/\tau_1) + k_2\exp(-t/\tau_2)$ 98

4.9 $$(T) = \frac{g_o + g_1\exp\left(\frac{-E_1}{KT}\right) + g_2\exp\left(\frac{-E_2}{KT}\right) + g_3\exp\left(\frac{-E_3}{KT}\right)}{X_o + X_1\exp\left(\frac{-E_1}{KT}\right) + X_2\exp\left(\frac{-E_2}{KT}\right) + X_3\exp\left(\frac{-E_3}{KT}\right)}$$ 100

CHAPTER 1. PAGE.

Introduction to Semiconductors.

Chapter 1. Introduction to Semiconductors.

1.1 Introduction.

Semiconductors today are among the most interesting and useful substances of all classes of solids. This is so because of the wide variety of devices employing semiconductors as well as the wide spectrum of phenomena which they exhibit. Since the development of the transistor by Shockley, Bardeen, and Brattain in the late 1940's, semiconductors have become the most actively studied substances in solid state physics. Because of this enormous activity, much has been learned about their basic properties and how to utilize them in designing even more efficient devices.

This chapter begins with a description of crystal structure followed by how the assemblage of similiar atoms into an array leads to the formation of bands of allowed states seperated by an energy gap. This energy gap may contain allowed states, some localized due to impurities and others permeating the crystal (excitons), and so have a major impact on the optical properties of crystals. There then follows a discussion on how an electron once excited to a higher state, decays to its equilibrium position, emitting radiation in the process. This chapter concludes with a brief review of isoelectronic bound excitons occurring in semiconductors such as GaP and Si.

1.2 Crystal structure.

A crystalline solid is one in which the basic units i.e. the atoms are arranged in a lattice, - a repetitive three dimensional framework. For example, the lattice structure of a hypothetical two dimensional crystal is illustrated in figure 1.1.

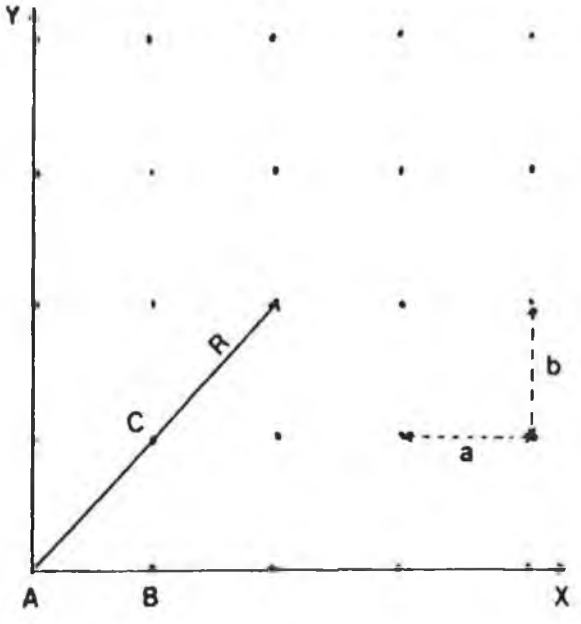

Figure 1.1, A crystalline solid, all atoms are arranged periodically.

The distance between any two neighbours in the x-direction is 'a' and in the y-direction is 'b'.A perfect crystal maintains this periodicity for infinite x and y. Because of this periodicity, then to an observer located at any of the sites A, B or C, the crystal appeares exactly the same. In reality however one cannot prepare a perfect crystal since at the surface the periodicity is interrupted. The atoms near the

surface 'see' a different environment to those deep in the bulk of the crystal and so behave differently. Considering figure 1.1 the position vector of any lattice point relative to point A is given by

$$R = n_1 a + n_2 b \qquad \text{--------1.1}$$

where a and b are as in figure 1.1 and n_1 and n_2 are integers. A unit cell of a two dimensional lattice is defined as an area which, when translated using equation 1.1, will cover the whole lattice once. There are two classes of lattice, the Bravais and the non-Bravais. In a Bravais lattice, all atoms are of the same kind and so all lattice points are equivalent, whereas in the non-Bravais type, some of the lattice points are nonequivalent. There are 14 Bravais lattices which are grouped into seven crystal systems [1,2]. Because of translational invariance, a characteristic feature of crystal structures just described, there are a large number of translations which a perfect crystal may undergo and remain unchanged.

One may view a single atom in free space to have full rotational symmetry but an atom in a crystal has symmetry characteristics which are determined by the lattice. Because of this, its energy levels are less degenerate than those of a free atom. A knowledge of the symmetry of the crystal tells a great deal about the possible behavior which may be found in the crystal. Such properties as the number of possible energy levels and their degeneracy may be determined from

symmetry. All wavefunctions of the Hamiltonian corresponding to the same energy level form a vector space which is invariant under the transformation of the symmetry group From symmetry considerations the group of the Hamiltonian and thus the number and dimensionality of its irreducible representations are known. The symmetry properties of impurity states in semiconductors show that for a single electron or hole in silicon, the appropriate group is the double group T_d. This group has eight different irreducible representations; Γ_1 and Γ_2, are one dimensional Γ_3, Γ_6 and Γ_7, are two dimensional, Γ_4 and Γ_5, are three dimensional and Γ_8 is four dimensional. The possible classifications for electron states are Γ_1, Γ_2, Γ_3, Γ_4, Γ_5, while the hole states are Γ_8, Γ_6, Γ_7.

1.3 Band structure.

When many similiar atoms are brought together to form a crystal structure as described in section 1.2 the wavefunctions describing the electrons on different atoms begin to overlap. To satisfy The Pauli Exclusion principle, the states of all spin-paired electrons accquire energies which are slightly different from their values in the isolated atom. The lowest energy state outside core shells is called the valence band (VB) and is completely filled with electrons. The upper band of states however contains no electrons and is called the conduction band (CB).

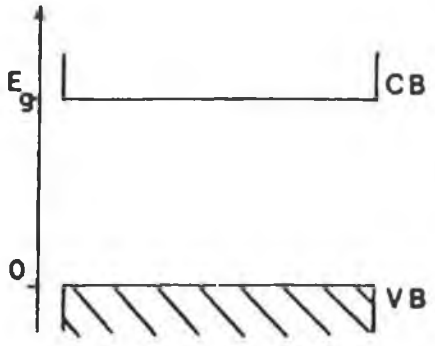

Figure 1.2, Energy band diagram for a semiconductor.

The behaviour of an electron in a crystalline solid is determined by studying the appropriate Schrodinger equation.

$$[-h^2/2m\ \nabla^2 + V(r)]\Psi(r) = E\Psi(r) \qquad \text{--------1.2}$$

where V(r) is the potential 'seen' by the electron and U(r) and E are the state function and energy of this electron respectively. The one feature of the quantum states of crystals which is most important is that the electronic wavefunctions have a special form imposed by the translation periodicity of the crystal. Each electronic wave function is assigned a crystal momentum 'p' and a band index 'n', (p=hk, where h is plank's constant and k is a wave vector). The wave function U_{nk} which satisfies the Schrodinger equation is given by

$$\Psi_{nk}(r) = [\exp(ik.r)]\ U_{nk} \qquad \text{--------1.3}$$

where $U_{nk}(r)$ is a periodic function of r, with the

periodicity of the crystal lattice. Substituting for U(r) in 1.2 yields an expression for E_k.

$$E_k = \hbar^2/2m \left[K_x^2 + K_y^2 + K_z^2 \right] \qquad \text{--------1.4}$$

The band structure of a crystal can be described by the nearly free electron model for which the band electrons are treated as perturbed only weakly by the periodic potential of the ion cores. In this model there occur no solutions of the Schrodinger equation in substantial regions of energy and it is these energy gaps which are of decisive significance in determining whether a solid is an insulator or a conductor.

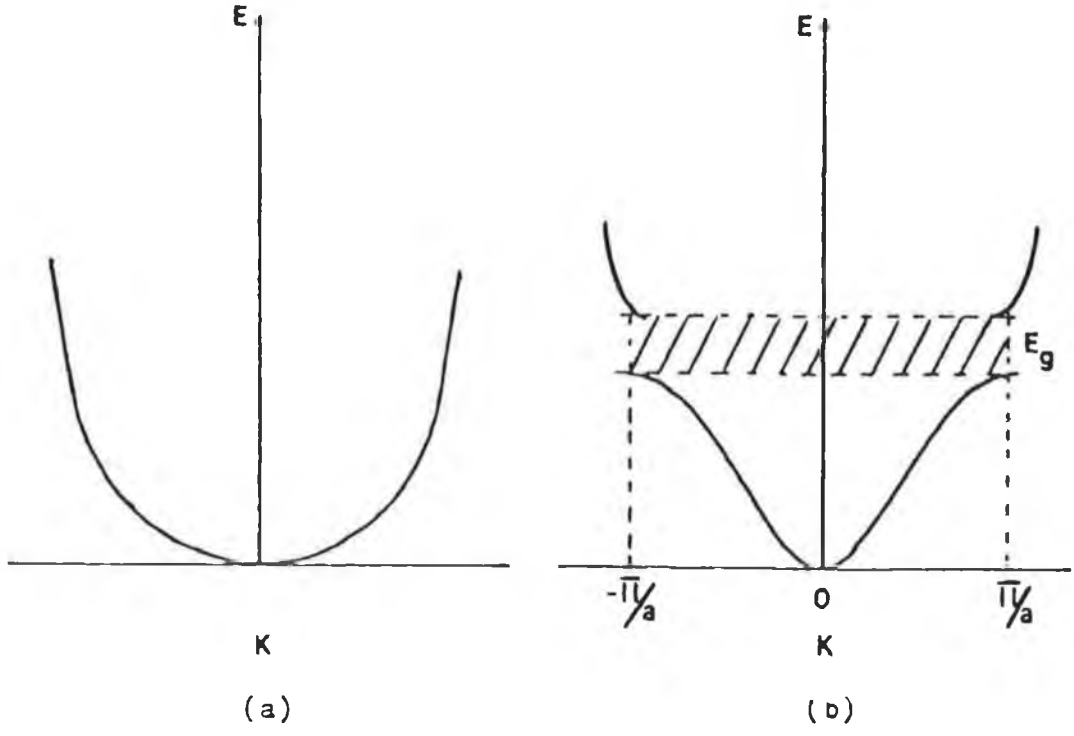

Figure 1.3(a) Plot of E versus K for a free electron (b) Plot of E versus K for an electron in a monatomic linear lattice, of lattice constant 'a'.

The energy gap of a material is defined as the energy separation between the bottom of the CB and the top of the VB. It is the extent of this gap and the availability of electrons that determines whether a material is a metal, an insulator or a semicoductor. In a semiconductor the energy gap extends over less than 3ev and the density of electron states in the upper band or the density of hole states (absence of electrons) in the lower band is generally less than 10^{20} cm^{-3}. However in a metal the density of electron states in the CB is usually greater than 10^{23} cm^{-3} and the energy gap is much smaller or nonexistent. In the case of an insulator the gap is much greater than 3ev but there is a negligible concentration of electrons in the CB.

For almost all semiconductors the perfect crystal will be an insulator at absolute zero temperature. The characteristic properties of such a semiconductor are brought about by thermal excitation, impurities, lattice defects or departure from chemical composition. As the temperature is increased electrons are thermally excited from the VB to the CB and the holes created in the VB contribute to the electrical conductivity of the semiconductor. Certain impurities when introduced into a semiconductor can affect the electrical properties of such a material, eg. the addition of one boron atom to 10^5 silicon atoms increases the conductivity of the sample by a factor of 10^3. To understand this one must look at the actual structure of both boron and silicon. Silicon crystalises into the diamond structure having four valence electrons, each atom forming four

covalent bonds with its nearest neighbours. If an impurity atom is introduced with a valence of three, such as boron, it may reside on one of the silicon sites. As boron is trivalent one of the electron bonds remains vacant. This vacancy may be filled by an electron moving in from another bond. In this way the hole can migrate throughout the crystal. The trivalent atom is known as an acceptor as it accepts electrons to complete its tetrahedral bonds. If on the other hand a pentavalent impurity atom such as phosphorus is introduced into the silicon structure, then only four bonds are needed to complete the bonding, the fifth detaches from the impurity and is free to migrate throughout the crystal. As the impurity atom has lost an electron it becomes positively charged and so the free electron is attracted to the positive ion. Since the pentavalent atom gives an electron to the CB it is known as a donor and creates a level close to the CB, whereas the trivalent atom creates a level close to the VB and is known as an acceptor. The diamond structure of silicon comprises of two interpenetrating face-centered cubic arrays which are based on the points (0,0,0) and (1/4,1/4,1/4). This is clearly shown in figures 1.4 a, b, c.

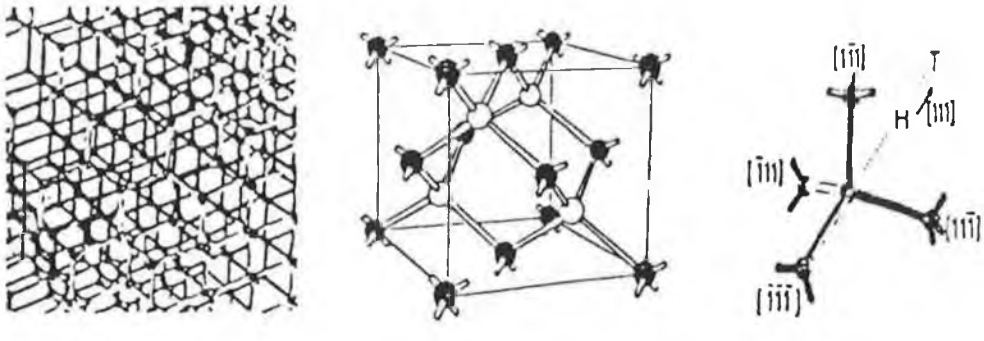

Figure 1.4 (a) Model, (b) Cubic Cell, (c) Tetrahedral Bonding, of the Silicon Lattice.

From figure 1.4 (c) it is evident that the silicon crystal has highly directional valence bonds in the <1,1,1> directions since every atom has four nearest neighbours along the <1,1,1> directions, twelve next nearest neighbours along the <1,1,0> axis and so on. The interstitial sites with tetrahedral symmetry have the same number and spacing of nearest neighbour atoms as the substitutional sites. The volume of these interstitial sites is similiar to that of the substitutional sites thereby emphasising the ease at which impurities can be incorporated into the silicon lattice. Although the substitutional and interstitial sites are by no means the only sites available to impurities within the lattice, they are the sites of higest symmetry and consequently the most commonly occupied.

From the discussion of band structures it is clear that allowed states have definite energy assignments and as such these states are distributed in momentum space. Silicon is an indirect gap semiconductor, i.e. the minimum of the CB and the maximum of the VB do not correspond at the same value of the wavevector k. Silicon has six equivalent conduction band minima located about 80% of the way to the zone boundary along the [1,0,0] directions. The valence band maximum occurs at k=0 where two degenerate bands with different curvatures meet, giving rise to holes with different effective masses. The $P_{3/2}$ band maximum is four fold degenerate while the $P_{1/2}$ maximum is doubly degenerate.

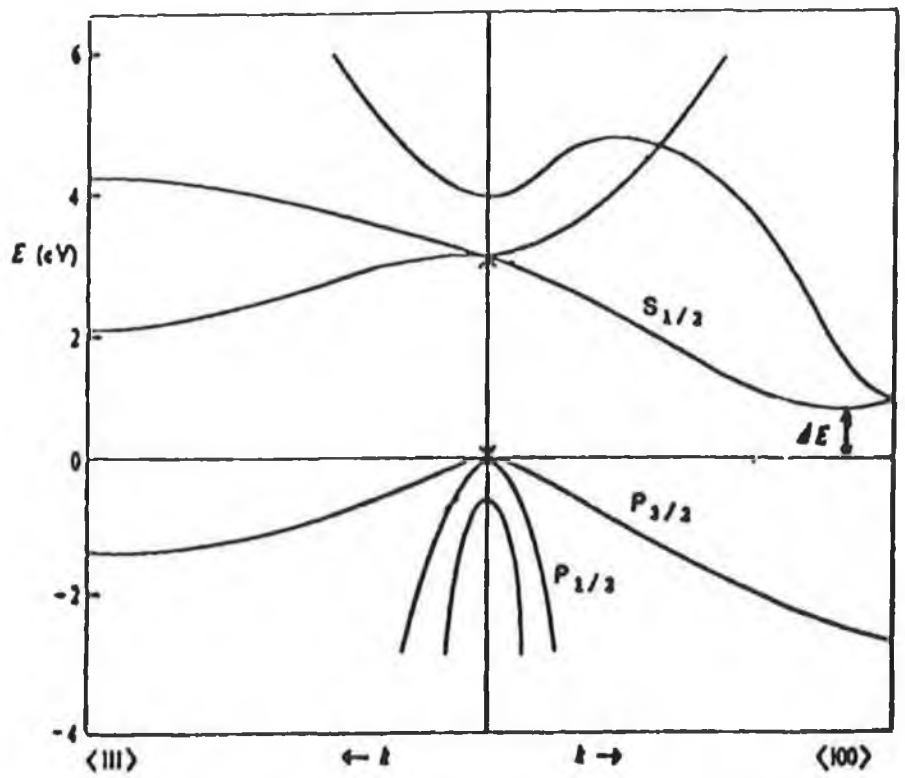

Figure 1.5 Band structure of silicon plotted along the [100] and [111] directions.

1.4 Recombination mechanisms in semiconductors.

The most direct and the simplest method of probing the band structure of a semiconductor is to measure the absorption spectrum. In the absorption process a photon of known energy excites an electron from a lower energy state to a higher one. Therefore by simply placing a semiconductor at the output of a monochromator and studying the changes in the transmitted radiation, one may discover all the possible transitions an electron can make and learn much about the distribution of states. There are many transitions an electron can make when excited by such incident radiation, band -to- band, impurity -to- band, free carrier absorption, etc. Consider the case of the band -to- band transition, i.e. the excitation of an electron from the VB to the CB as shown in figure 1.6 below.

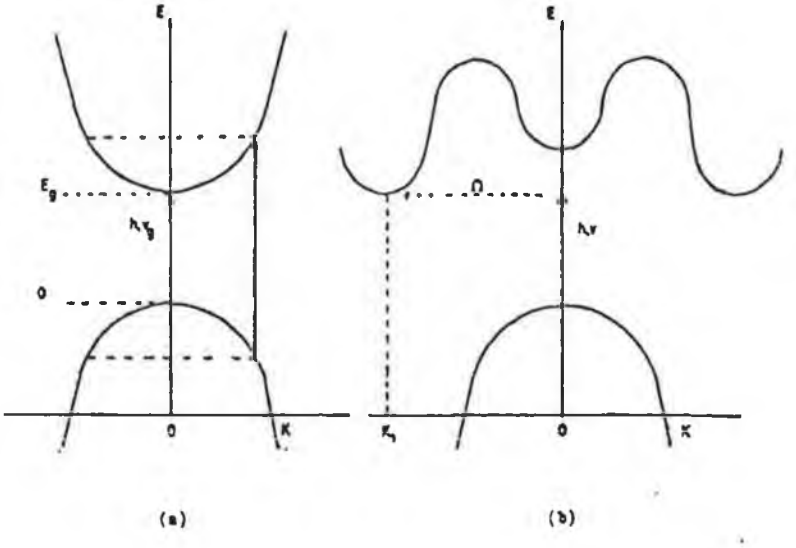

Figure 1.6, Absorption process in (a) a direct, and (b) an indirect gap material.

In (a) above the lowest point on the CB corresponds to the highest point on the VB for the same value of the wavevector k. In this case because the absorbed photon has a small wavevector there is no appreciable change in k in going from the VB to the CB. The threshold frequency F_t for absorption by the direct transition determines the bandgap E_g.

$$E_g = hF_t \qquad \text{--------1.5}$$

However (b) represents an indirect transition as the lowest point of the CB is separated in k space from the VB edge. Because of this the indirect transition involves both a photon and a phonon. The absorption threshold for this case is at

$$E_g = hF + h\Omega \qquad \text{--------1.6}$$

where Ω is the frequency of the phonon. Phonons can either be emitted or absorbed and it is by this process that momentum is conserved in the lattice. A phonon is a quantum of lattice vibration and although a broad spectrum of phonons is available only those with the required momentum change are usable.

Emission of radiation is the inverse of the absorption process. An electron occupying a higher energy state than it would under normal equilibrium conditions makes a transition to an empty lower energy state and all or most

of the energy is emitted as electromagnetic radiation. Most of the examples given above for absorption can also be given for emission and produce a characteristic emission spectrum. There is however an important difference between the information one can obtain by absorption and by emission in a semiconductor. The absorption process can involve all the states of the semiconductor resulting in a broad spectrum whereas the emission process couples a narrow band of states and so produces a narrow spectrum. Photoluminescence is the emission of electromagnetic radiation in excess of thermal radiation from the semiconductor when the excitation source used is light. Luminescence emission involves radiative transitions between electronic energy levels of the material. Luminescence emission may take place during the time of excitation, in which case the phenomenon is known as fluorescence, whereas if the emission continues after the excitation has been removed then it is known as phosphorescence.

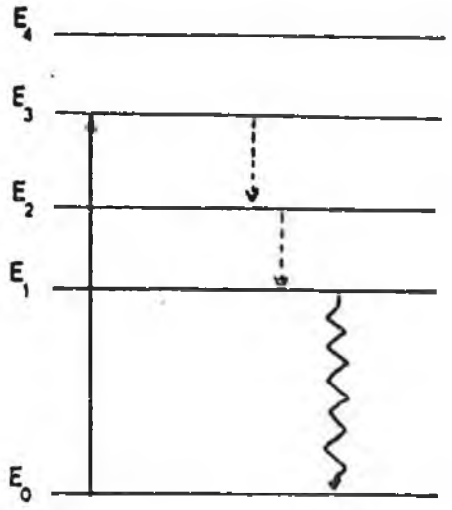

Figure 1.7, Diagramatical representation of both excitation and decay processes.

Figure 1.7, above shows the excitation and the decay process with a ground state energy E_o and excited state energies E_1, E_2, E_3 and E_4. By irradiating the sample with light of suitable wavelength then the material can be raised from Eo to E_3. Because the energy difference between E_3 and E_2 is small, that excited state tends to decay non-radiatively by phonon emission,releasing the energy as heat to the material. Radiative emission occurs when the energy difference is large as in the transition E_1 to E_o. The material decays radiatively between levels 1 and 0 emitting a photon in the process of energy hf, where

$$hf = E_1 - E_o \qquad \text{--------1.7}$$

Non-radiative decay occurs by a multiphonon process and is a consequence of the interaction with the crystal field. The stronger the coupling, the more probable that non-radiative decay will occur. When the optically active atom is in an excited state, radiative and non-radiative decay are possible. In the non-radiative process between two levels, the energy is emitted as a number of phonons, as many as are required to bridge the gap seperating the levels. The larger the number of phonons involved the lower the non-radiative transition probability. Therefore it is acceptable to presume that the non-radiative probability decreases as the energy seperation between levels is large. On the other hand the radiative probabilty increases with

increasing energy separation.

Just as static changes can change the energy levels and as a result change the frequency of the optical transitions, so dynamic strains caused by lattice vibrations, can modulate the frequency of the optical transitions. This can lead to frequency modulation sidebands (phonon sidebands) accompanying the sharp optical lines (no phonon lines). If the initial and final electronic states have a similar (but not identical), sensitivity to strain then the 'modulation index' is small and the sideband is weak. If the difference in sensitivity is large however, the sideband is strong, (section 4.1).

1.5 Bound Excitons.

Structure for photon energies is often shown up by reflectance and absorption experiments just below the energy gap, where the absorption of a photon creats an exciton either in the direct or the indirect process. Because of their attractive nature, an electron and a hole are bound together by coulombic interaction and it is this bound electron - hole that is called an exciton. It has been shown that both a free electron and a free hole are formed whenever the crystal absorbs a photon of energy h f greater than the bandgap E_g. This is true for a direct process; in an indirect phonon assisted process, the threshold is lowered by the phonon energy $h\Omega$, as described above. There are two such kinds of 'Free Excitons' (FE), the Frenkel exciton in which

the exciton is small and tightly bound and the Mott-Wannier exciton in which the exciton is weakly bound, with an electron - hole separation large in comparsion with the lattice constant.

A Bound Exciton (BE) in a semiconductor is the name given to a many - particle electronic excitation containing an electron - hole pair bound to a defect. A BE is an electronic excitation of a defect. The ground state in the case of donors and acceptors already contains one bound particle, an electron in the case of a donor and a hole in the case of an acceptor. However in the case of neutral centres (isoelectronic) the ground state of the excitation is the bare defect. The localization of an additional electron - hole pair to the defect creates the BE excitation, which thus may be regarded as containing two electronic particles for a neutral defect and three particles for a donor or an acceptor (if single donors or acceptors are considered). The defect potential and the local strain field at the defect both interact with the particles present in the BE. The local strain field in the vicinity of the defect is usually a minor perturbation for shallow substitutional defects and a major one for deep defects. Interaction between the electronic particles of the BE are always present to a certain degree and the actual magnitude of these defects will grow with the localization of the wave functions of the particles bound to the defect.

1.5.1 Isoelectronic Bound Excitons.

One can easily distinguish between neutral defects and donor or acceptor type defects, as each has a different number of particles in the BE excitation. Donor and acceptor type defects have been discussed in section 1.2 and a description of neutral defects will be given here. A neutral defect or as it is widely known an isoelectronic defect is a defect which supplies the same number of valence electrons as the atom of the host material which it replaces. Therefore this type of defect is electrically neutral although its electronic structure will differ from that of the replaced atom. It is this difference that may give rise to localized impurity states within the band gap or may give rise to bound states. Hopfield et al [3] proposed a model for isoelectronic traps which explains many of the observed optical properties. An isoelectronic trap can be attractive either to an elecron or a hole. As the trap is neutral, any binding is due to short range forces. It can therefore introduce a bound state for a single particle if it possesses a strong enough short range potential. After binding this electron or hole, the trap becomes positively or negatively charged depending on the particular case. Because of this, the trap can attract either a hole or an electron by strong long range coulombic forces.

This suggests two types of trap depending on which carrier is bound first. Assuming that the first carrier attracted to the trap is a hole and is bound strongly, the

wave function of the second carrier, an electron, will be bound by coulombic interaction and will be donor like. If on the other hand the first carrier bound to the trap is an electron then the second carrier a hole, bound by coulombic forces will be acceptor like. While the energy level ground state for both acceptor and donor isoelectronic traps may be the same, their phonon coupling may be radically different. It is the particle which is strongly attracted to the local potential which is chiefly responsible for the phonon coupling, so that phonon coupling provides a way of determining whether a trap is an isoelecronic donor or an isoelectronic acceptor.

A lot of theoretical work on isoelectronic traps has been concerned with the formulation of an understanding of the mechanisms by which a free carrier becomes bound to a neutral impurity [4,5]. Some information can be derived from a phenomenological approach based on the electronegativity of both the host and the impurity atoms. Experimental data suggests that an isoelectronic impurity may bind a hole (or an electron) only if its electronegativity is smaller (or larger) than that of the host atom it replaces [5,6]. Such a rule is supported by the fact that the electronegativity of the elements decreases with increasing atomic weight. Therefore heavier atoms substituting for host atoms are hole attractive and lighter atoms are electron attractive. Although for many isoelectronic impurities in semiconductors electronegativity differences would indicate the possibility of producing a bound exciton, remarkably few are observed.

This indicates that the influence of strain seems to be very important.

1.5.2 Isoelectronic traps in GaP.

GaP is the most widely studied material concerning isoelectronic traps and much of our present understanding has been obtained from optical studies of recombination mechanisms from excitons bound to these centres. The recombination of the bound electron and hole gives rise to sharp no-phonon luminescence lines, that are very amenable to detailed analysis using high resolution spectroscopy at low temperatures. A typical example of an isoelectronic trap in GaP is the nitrogen (N) related trap in which the substitution of nitrogen for phosphorous creates single excitons bound to isolated nitrogen atoms [6]. This particular example is known as a point substitutional isoelectronic acceptor, while bismuth (Bi) substitution gives rise to an isoelectronic donor. The strength of this centre's luminescence compared with that associated with nitrogen reflects the increased coupling of the exciton to the lattice surrounding the defect. An example of a molecular isoelectronic trap is the Lithium complex (Li-Li-O) in GaP, [7] where three atoms replace a molecule of the GaP lattice. At low temperatures this centre introduces four zero phonon lines.

1.5.3 Isoelectronic traps in Si.

Within the last few years considerable work has emerged on exciton luminescence due to isoelectronic traps in silicon. It is interesting to note that there are no point isoelectronic traps associated with Si in comparsion to GaP. An example of an isoelectronic trap in Si is the Beryllium complex (Be-Be). This centre introduces a molecular type trap suggested from an examination of the phonon sidebands [8].

It is interesting, in view of the fact that it was in Si that donor and acceptor bound excitons were first observed [9], that it is only recently that excitons bound to isoelectronic centres have been detected in this material. Sharp lines in the luminescence spectrum first reported by Vouk and Lightowlers [10] have recently been attributed to bound exciton recombination at an isoelectronic centre [11,12,13] possibly involving iron (14,15) and a similar complex system has been detected in Si:Tl, [13]. Weber et. al. [16] have reported exciton recombination at an isoelectronic defect at low concentrations, while other complex isoelectronic defects have been reported in laser annealed irradiated Si [17] and in irradiated lithium doped material [18].

Recent studies have shown transition metal impurities such as copper (Cu), chromium (Cr), and iron (Fe) to be responsible for the formation of isoelectronic traps. This increase in activity points towards a study of silicon doped with transition metal impurities.

1.6 Conclusion.

A brief review has been given of the crystal and band structures for silicon. Recombination mechanisms and optical properties of semiconductors in general have been reviewed leading to an understanding of isoelectronic type defects that occur in semiconductors.

We have seen that one area of study of isoelectronic traps is still in its infancy, i.e. isoelectronic traps associated with transition metal doping in silicon. The following chapters discuss one such centre which we have examined - associated with a copper - zinc complex. Chapter 2 gives a general overview of transition metal impurities in silicon while at the same time discussing the effect of copper and zinc seperatly incorporated in silicon.

CHAPTER 2. PAGE.

Transition Metal Impurities in Silicon.

Chapter 2: Transition Metal Impurities in Silicon.

2.1 Introduction.

The Transition Metal (TM) elements occupy regions of the periodic table where an inner shell of electrons is being filled as the atomic number increases. Because of its nature, a TM atom can sustain as many as five different charged states in the narrow (1.1ev) bandgap of silicon whereas the various ionizied states of a free TM impurity are spread over a range of many ev's [19,20,21]. This result was first observed experimentally in silicon and was later accounted for by theory. Haldane and Anderson [22] solved the Anderson Hamiltonian model and concluded that many charge states were a result of strong rehybridization between the transition atom d-orbitals and the crystalline s-p orbitals which occur every time an electron is added to, or subtracted from the gap states. Most impurities have more than one electron (or hole) outside of the closed shell. They donate or accept one or in some cases several electrons as the position of the Fermi level is varied within the forbidden gap.

Despite nearly three decades since the first pioneering work of Ludwig and Woodbury [19], the electronic and structural properties of the Si:TM system still remains unclear. The many new experimental techniques which have been

discovered since this early work, and the application of numerous theoretical models to the problem has generated a wealth of new data [23].

2.2 Transition Metal Impurities.

One of the major obstacles in establishing a clear picture of TM impurities in silicon arises from the high diffusivity of these elements. The diffusion coefficients at 1000°C range from $10^{-4}cm^2/sec$ for Ni (as large as typical liquid diffusivities) and decrease to $10^{-8}cm^2/sec$ for lighter impurities such as Ti and V [25a]. Another obstacle arises because the solubilities of these impurities are low (10^{14} or 10^{17} $/cm^3$) and the atoms tend to precipate rather than being retained in supersaturated solution.

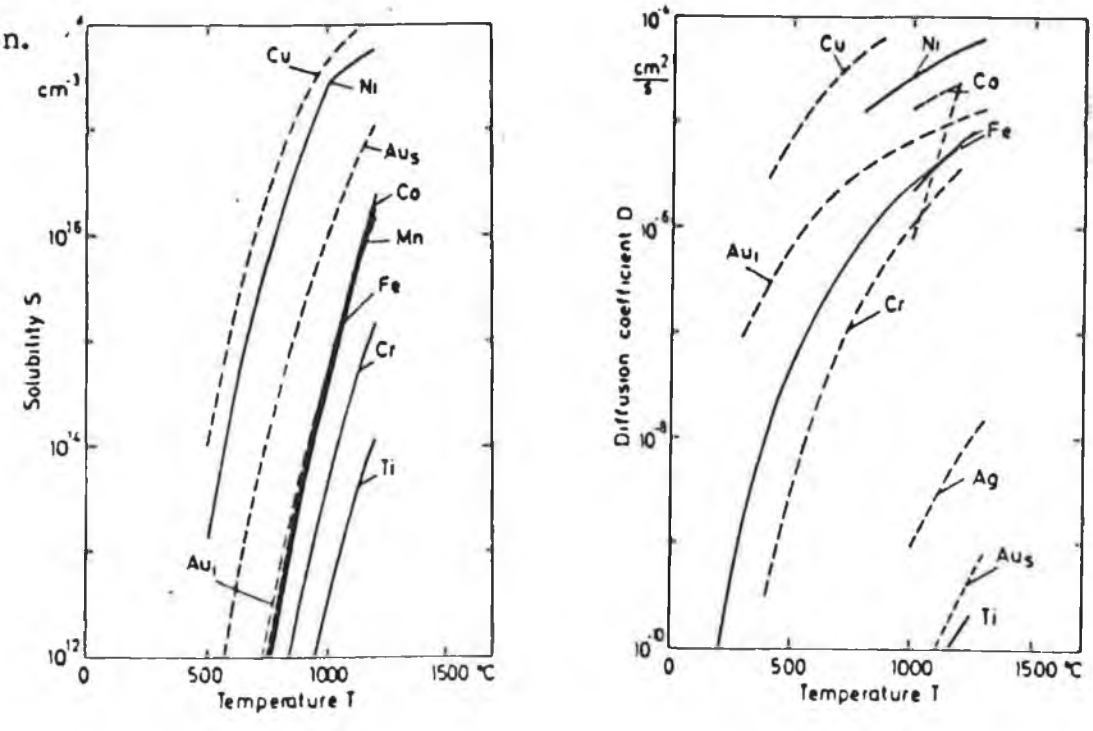

Figure 2.1 Solubilities and Diffusivities of 3d transition metals in silicon [25].

Because of this fact, mobile atoms experience a strong thermodynamic force to find more stable configurations. The fastest diffusing elements Ni, Cu and Co precipate even when using fast quenching techniques so that it has not been possible to assign any energy level to a well defined configuration of these elements. Iron and manganese in silicon can be found as isolated interstitials after sufficiently rapid cooling down but are unstable at room temperature. For a mobile interstitial metal atom the first most stable configuration is the formation of a complex with another impurity atom [26,27]. Heat treatment to temperatures in the range 200°C --- 900°C results in dissociation and subsequent further complexing of the very mobile transition metal atoms [28].

The evidence of the TM lattice site preference (substitutional versus interstitial) and aggregation state (isolated impurities versus impurity clusters) is very inconclusive. It has been known for a long time that the site preference depends on a fine control of the material preparation parameters as much as on the nature of the impurity atom itself [19,20]. For example impurity acceptor pairs are often produced by the diffusion of TM's into P-type silicon near its melting point followed by a slow quenching procedure [19,20]. However if a more rapid quenching procedure is achieved then interstitials may be produced. Diffusion into N-type material followed by a slow quenching may produce impurity clusters (e.g. Mn^4 clusters or Fe^i

clusters) [29]. If the sample contains impurities such as Cu, Ag or Zn, a diffusion of an additional transition element can produce an impurity in a substitutional site [3]. For many of the TM's pairing reactions of interstitials with substitutional acceptors are found to occur [25].

2.3 The Ludwig & Woodbury Model.

The first systematic study of TM's in silicon was performed over twenty years ago by Ludwig and Woodbury [25]. Their work primarly on Electron Paramagnetic Resonance (EPR) of TM doped silicon constitutes a source of valuable information today [19,25]. The electronic properties of semiconductors, in particular silicon, are altered by the presence of both substitutional and interstitial 3d TM impurities. For a wide variety of these elements energy levels are produced within the bandgap. These levels are termed 'deep' levels since they are not close to either of the allowed bands, as opposed to 'shallow' levels introduced when impurities such as boron and phosphorus are incorporated into silicon. Shallow impurities introduce minor perturbations in the crystal (as manifested by the fact that they give rise to bound states in the fundamental band gap very close to the band edge) and generally contribute extra charge carriers, electrons or holes. However TM impurities constitute a more severe local perturbation, giving rise to bound states that are considerably more localized and often have energies deep in the band gap. Unlike shallow

impurities, deep centres act primarily as carrier traps or recombination centres. Evidence of this fact is seen from experiments undertaken by Ludwig et al [25]. These experiments also suggest that the interstitial site is favoured over the substitutional site for the iron group TM elements which consists of the elements scandium through to copper.

When incorporated into silicon at a site of tetrahedral symmetry, the 3d level, whose electrons have two units of angular momentum and has available to it five orbital states, splits into two levels which belong to the doublet 'e' and the triplet 't_2' states. According to the Ludwig and Woodbury model, an atom entering the host lattice interstitially obeys Hund's rule, i.e. the splitting between the 'e' and 't_2' levels is small so that the orbitals are filled in such a way to maximise the total spin while satisfying the Pauli Exclusion principle. Most EPR spectra of TM doped silicon have been described by the Ludwig & Woodbury model. They developed a model for electron states of interstitial and substitutional 3d metals in silicon which successfully explains the observed EPR sepctra. The basic assumption of this model is the promotion of the 4s electrons into the 3d shell for a 3d metal in silicon.

The essential features of the Ludwig & Woodbury model are indicated in figure 2.2. According to the model when a substitutional site is filled by an impurity then four of the impurity's electrons are involved in the bonding. The remaining electrons outside the n=2 shell occupy the 3d level

which has been stated above to be split into e and t_2 states by the tetrahedral crystal field. In effect the model assumes formation of covalent bonds with the silicon neighbours by the hybridization of four of the 3d electrons. The substitutional atom is in an effective cubic crystal field of negative charges from the surrounding valence electrons. The interstitial position is also characterized by tetrahedral symmetry and the 3d level splits as before. However the sign of the crystal field is reversed with 't_2' level now below the 'e' level. The strongly localized covalent bonding of the surrounding silicon atoms concentrates the valence electron density between the host atoms. The interstitial thus experiences a cubic crystal field as before but in this case arising from not completely shielded nuclear positive charges. In this case electrons are not required for bonding and according to the model all electrons outside the n=2 shell are contained in the 3d shell.

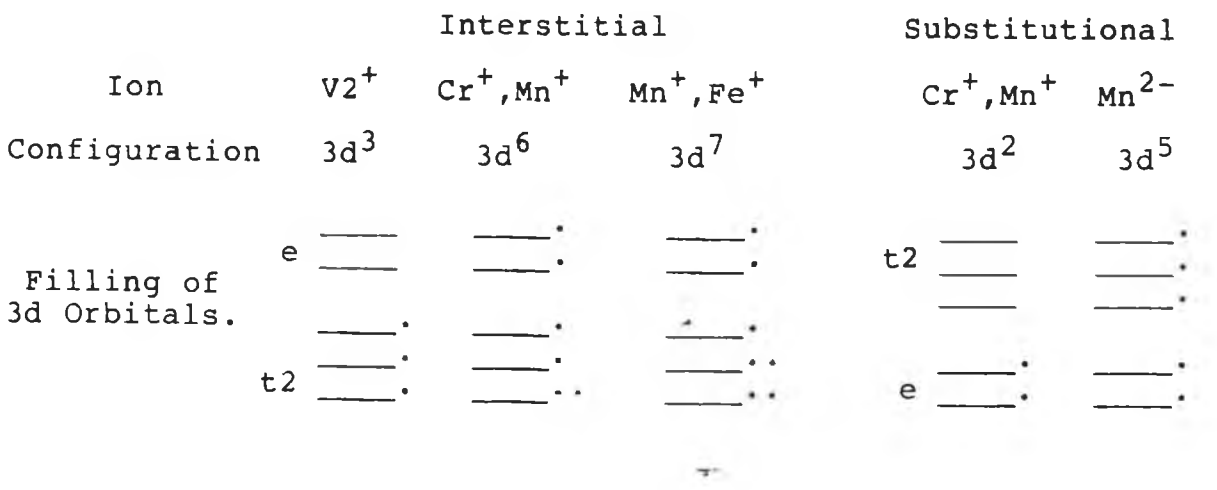

Figure 2.2, Electronic structure of 3d metal ions in silicon [25].

2.4 Photoluminescence Properties.

TM imputities such as copper (Cu), iron (Fe), and chromium (Cr) have recently been reported as responsible for the formation of isoelectronic traps in silicon, so beginning a new era in luminescing defects [24]. The observed photoluminescence (PL) is characterised by strong intensities although the concentrations of the emitting centers may be quite low. According to Sauer and Weber [24] such large intensities at low concentrations indicate internal quantum efficiencies near unity.

As stated eariler, for many of the TM impurities pairing reactions of interstitial and substitutional atoms are found to occur. Experimental evidence for such pairing has come primarily from EPR work [25]. Recently however, PL has been found to provide evidence of such pairs [30,31]. Fortunately a defect which would not be detectable by EPR due to the absence of unpaired electrons, may be detected in PL by observing the radiative recombination of excitons bound to the defect. In this study PL has been used to examine the properties of silicon doped with the deep double acceptor, zinc, and the highly mobile transition metal impurity, copper.

Table 2.1 gives three examples of impurities in silicon forming isoelectronic traps, i.e. copper,iron and chromium. This table shows the zero-phonon line energy and

the local mode energy. It can be seen from the table that as the atomic weight of the impurity atom increases the local mode energy decreases. This is so because the heavier the impurity atom the smaller the vibration it makes with the lattice and so the smaller it's local mode energy.

Table 2.1 Parameters of PL lines.

	Cu-Cu	Fe-B	Cr-B
PL line position (ev)			
Zero phonon	1.0145	1.0668	0.8439
Local modes	1.0075	1.0572	0.8302
	1.0005	1.0470	0.8160
	0.9933	1.0363	
Local mode energy (mev)	7.0	9.6	13.6

2.4.1 Copper doped Silicon.

Most of the TM's are known to be fast diffusing elements in a silicon lattice at elevated temperature, in particular copper, making it a suitable element to study. For the characteristic photoluminescence spectrum shown in figure 2.3 below it has been conclusively proven, by isotope line shifts, that copper is in fact responsible for the defect, and the spectrum is assigned to isoelectronic Cu-Cu pairs in a [111] configuration [31].

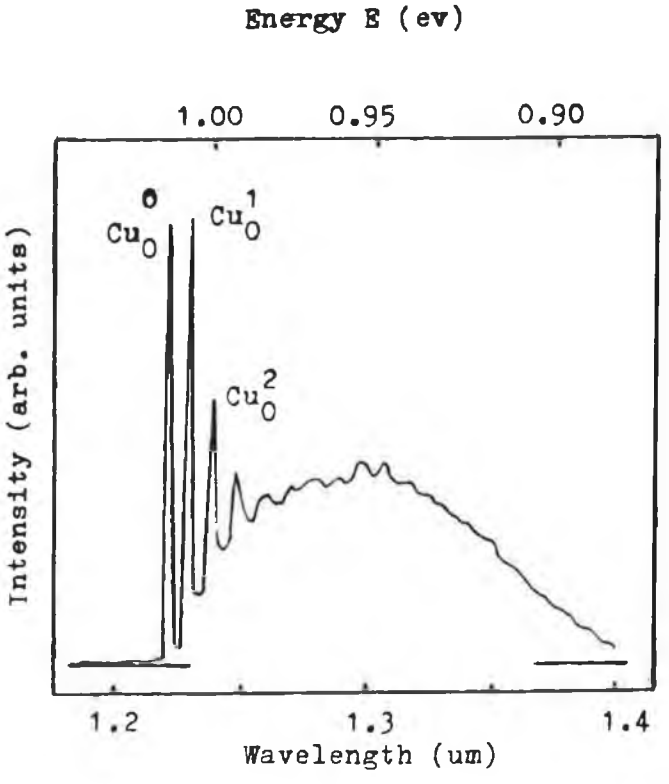

Figure 2.3, Spectrum of Cu-Cu pair luminescence with local mode sideband structure (Cu_O^O, ...)

The low temperature PL spectrum reveals a series of sharp satellites accompanying the no-phonon (NP) line. This ground state to ground state transition is accompanyed by up to twelve Stokes satellites at successive line spacings of 7.0ev. Special features observed at higher temperatures were identified as anti-Stokes replicas as well as transitions originating in electronic states at E_o = 0.15mev, E_1 = 1.9mev and E_2 = 9.6mev above the upper defect electronic ground state at E_o. The observed spectroscopic spacings from the NP line of these excited states are consistant with the quantitative analysis of the temperature dependence of the NP line intensity. The large background phonon sideband which accompanys the sharp vibrational modes (Cu_o^o ,...) is due to the coupling of the low energy acoustic lattice modes and increases dramatically at higher temperatures. Because the thermal dissociation energy of the exciton and the spectroscopic localisation energy differ so much, a description in terms of a isoelectronic donor or acceptor can be made. In this way the binding energy of the more tightly bound particle can be calculated and this energy reflects deep donor or acceptor binding properties. A number of recently detected line systems have been ascribed to complexes containing other transition metal ions [24,30,31]. Electrical data for TM's in silicon are described in several hundred publications, most of which are reviewed by Chen and Milnes [37]. Conclusive identification and energy levels are, however not available in general.

2.4.2 Zinc doped Silicon.

If the impurity zinc only, is incorporated into the silicon lattice then three acceptor levels may be formed in the band gap (33). Two donor levels appear as a result of precipation of the zinc - silicon solid solution and are attributed to interstial zinc. The high diffusion coefficient found for zinc in silicon suggests that the flow of zinc at high temperatures is mainly interstitial.

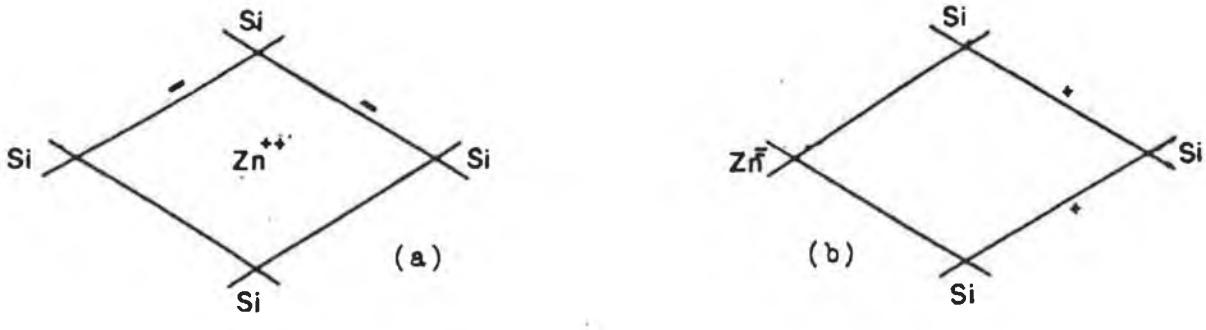

Figure 2.4, Substitutional & Interstitial Zinc in silicon.

Figure 2.4 (a) above illustrates an interstitial zinc atom which would be expected to introduce two donor levels into silicon. Since at low temperatures zinc is found to introduce

acceptor levels, it is assumed that interstitial zinc reacts with lattice vacancies at high temperatures to produce substitutional zinc. Figure 2.4 (b) shows a substitutional zinc atom which might be expected to introduce two acceptor levels. Thus zinc can conceivably introduce both donors and acceptors into pure silicon. Zinc diffusion into doped silicon may however produce ion pairs and complexes. The compounds will have empty orbitals and so may act as acceptors. Zinc was found to migrate in the form of positive doubly charged ions in silicon in the temperature range 980-1270°C by using the p-n junction technique [34]. Investigations by Glinchuk [35] and Kornilov [36] suggest that zinc, based on its multiply charged energy states may be an effective recombination centre and so be of primary importance in minority carrier silicon devices. Work has been done by various authors but in particular Sclar [37], in which the suitability of zinc doped Silicon as an infrared detector was investigated. It was found that the spectral response of a Si:Zn system was in the band 2.5um and 3.3um at a working temperature of 112K. This response is similar to that of the lead sulphide (PbS) intrinsic detector and its detectivity approaches competitive values.

2.3 Conclusion.

A brief review has been given on transition metal impurities in silicon, with particular reference to the Ludwig & Woodbury model which helps to explain EPR spectra of

transition metal doped silicon. A brief discussion on the diffusivity and solubility properties of such impurities in silicon has also been given. A summary of known TM related photoluminescence bands, and a discussion of the properties of Si:Cu and Si:Zn have also been included. The research which is described in this thesis concerns a new photoluminesence band associated with both Copper and Zinc. Before presenting detailed results of the photoluminescence measurements, the experimental techniques employed are described in the next chapter.

CHAPTER 3. PAGE.

Experimental Methods.

CHAPTER 3. Experimental Methods.

3.1 Introduction.

When Silicon is doped with the transition metals copper and zinc, a broad luminescent band appears in the spectrum corresponding to transitions lying in the infra-red region of the electromagnetic spectrum. Because the efficiency of luminescence is small at room temperature, the samples must be cooled to low temperatures.

There are two bands associated with this particular defect in silicon at low temperatures the first of which has been studied in detail by various authors [30,31] and the second which will be described in this thesis.

(1) A band ranging from 1.2 microns to 1.4 microns which has been identified with a copper-copper pair defect.

and

(2) A second band ranging from 1.3 microns to 1.7 microns.

It is this second region which is of most interest as it is only observed when both copper and zinc are diffused into silicon. The presence of water vapour absorption in the region of interest complicates the spectra considerably and so an algorithm was written to correct for this.

The experimental system and signal processing developed to record the spectra and to overcome these problems are discussed in detail in the following sections.

3.2 Experimental System.

Luminescence spectra of P-type silicon doped with copper and zinc were recorded at temperatures ranging from 4.2K to 125K. The excitation source used was a 150W xenon arc lamp, whose output was focussed down into a 0.25m spectrometer (600 lines/mm) and the relevant exciting wavelength was focussed down onto the sample. The luminescence was collected by an aspheric lens and focussed into a Spex one metre focal length Spectrometer (600 lines/mm). The detection was through a North Coast germanium pin-diode, which was interfaced to a BBC microcomputer via an analogue -to - digital converter for signal processing.

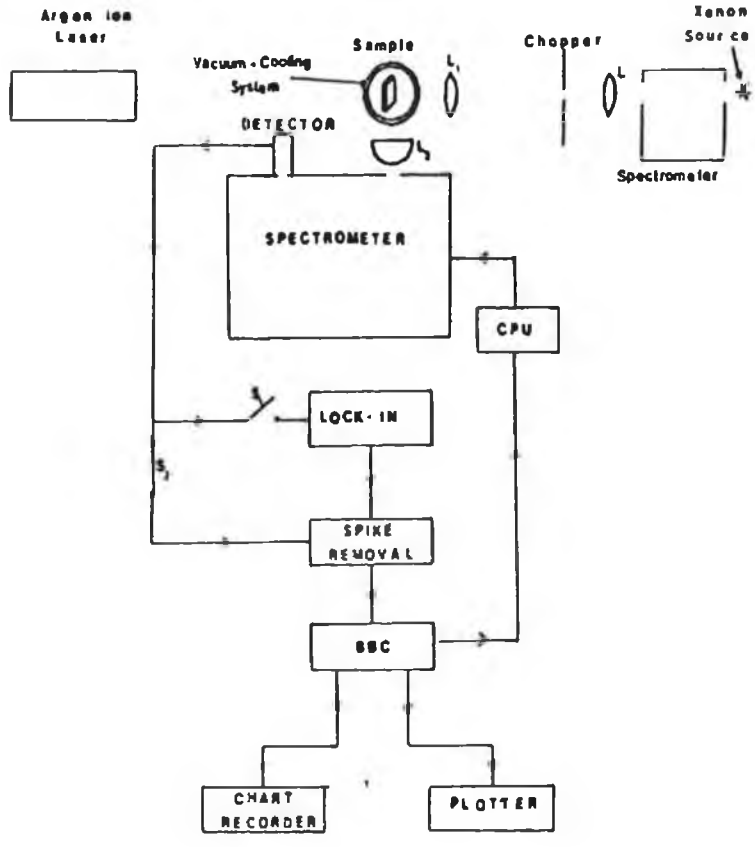

Figure 3.1, Experimental Apparatus.

3.2.1 Sample preparation and cooling.

Samples were prepared by taking equal amounts (2 grams) of copper (99.99%) and zinc (99.99%) and placing them along with P-type Hoboken float-zone refined silicon into an evacuated quartz tube. After sealing, the tube was placed into the furnace heated to 1100^{o}C and left for sixteen hours to ensure complete diffusion of both impurities. It was necessary to perform the diffusion in a helium atmosphere so as to minimise unwanted impurities, such as oxygen from entering the silicon lattice at such high temperatures. On completion of diffusion the samples were quenched in vacuum oil and then thoroughly cleaned following the procedure given in table 3.1 below.

Table 3.1 Cleaning Procedure.

1. Rinse in methanol.
2. Boil in methanol.
3. Boil in trichorethylene.
4. Rinse in methanol.
5. Rinse in de-ionized water.
6. Rinse in 10% solution of HF in HNO_3.
7. Rinse in de-ionized water.
8. Allow to dry.

This procedure enabled good surfaces to be obtained so that efficient luminescence was produced.

As stated above the samples must be cooled to low temperatures. This was achieved by an Air Products compressor - expander module (CS202W), which took the temperature down to 15K. During operation the compressor draws low pressure helium from the system return line, compresses, cools, cleans it and then delivers it through the system supply line to the expander line. On leaving the compressor, the helium gas contains heat and some lubricant which have to be got rid of. The water return system cools the gas while the oil seperator and the adsorber clear any oil particles which may be in the gas. From the adsorber the gas is passed to the expander module where on entry it is further cooled on its way to the heat station. The heat station temperature is thus reduced providing refrigeration at cryogenic temperatures. Because of radiation losses and the fact that cryo grease was used to mount the samples onto the sample holder the lower limit of the temperature was 15K.

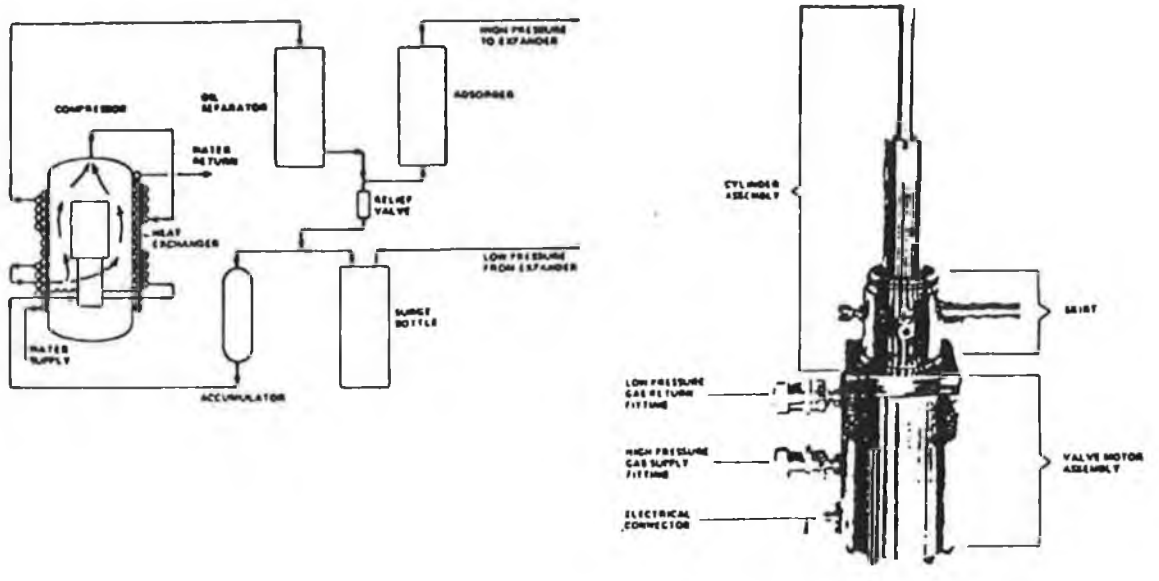

Figure 3.2, (a) Compressor and (b) Expander modules.

In addition to the expander module, there is also included a sample holder connected to a second stage heat station, a radiation shield connected to the first stage heat station and a vacuum shroud connected to the skirt.(figure 3.2). Both the radiation shield and the vacuum shroud are designed so as to allow incoming light to illuminate the sample and allow the luminescence to be collected by the aspheric lens L2. The sample holder is made from pure copper which needs to be able to hold the sample securely, this was achieved by using cryo grease because of its good conductivity at low temperatures. Incorporated into the cyclinder assembly is a thermocouple (Au Fe/Chromel) and a heater, both of which were connected to a control unit. In this way good control of the temperature of the sample could be maintained.

As the lower temperature obtained with this procedure was 15K a Thor helium flow cryostat (C584) was employed to work at liquid - helium temperatures. Figure 3.4 shows a schematic diagram of the system used.

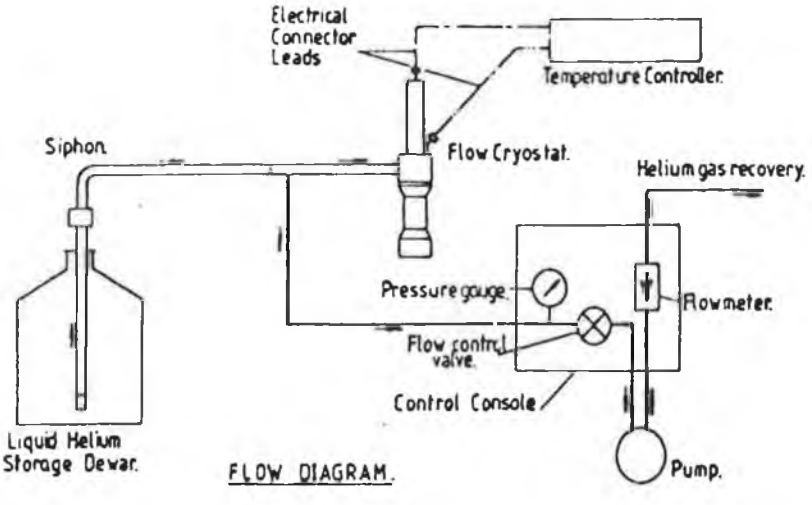

Figure 3.3, Liquid Helium Flow Cryostat.

The system consists of a flow cryostat, siphon, sample stick, gas flow regulator system, pump and liquid helium storage can. Electrical connections on the sample stick enable temperatures to be read off easily. The sample is cooled by conduction as the liquid helium is admitted into the cryostat by means of a pump but does not come in contact with the sample. The sample makes thermal contact with the liquid helium by means of helium gas admitted into the sample space at atmospheric pressure and so the sample is cooled by conduction.

3.2.2 Optics and detection system.

The excitation sources used were a xenon arc lamp (150w) and an argon ion laser (Coherent model 52). In the case of the xenon arc lamp the light was first focussed into a 0.25m spectrometer whose grating was ruled at 600 lines/mm and blazed at 1.0 microns. This infra-red grating allows wavelengths just above the bandgap of silicon to be used which were found to give efficient luminescence. The xenon arc lamp gave strong output between the wavelengths 800nm and 1000nm which was particularly suitable for the experiments undertaken here. However when using the laser there was no need for this spectrometer as the required wavelengths could be tuned in as needed. The incident light was then focussed down onto the sample and the luminescence was directed into the 1m SPEX spectrometer (model 1704) by means of an aspheric lens. The SPEX 1704 1m Czerney - Turner spectrometer was

fitted with a grating ruled at 600 line/mm and blazed for 1.2 microns. Control of the grating motors was by a compudrive CD2 microprocessor system which in turn was controlled by a BBC microcomputer. An external pulse provided by the microcomputer moved the grating a predetermined increment and this would repeat until the wavelength range was completed. In this manner a complete spectrum could be obtained.

Detection of the luminescent features was made using a North Coast EO-187 liquid nitrogen cooled detector. When the detecting element and the electronics reached thermal equilibrium (77K), a quiescent voltage of approximately -0.95 Volts appears on the output. Illumination of the diode with infra-red radiation results in a positive signal being added to this quiescent level. Because of this level a 'back off' circuit was employed which resulted in the voltage varying from 0 volts to some positive voltage value. The detector was so sensitive that cosmic radiation caused large spikes to appear on the output and so distort the true output. An electronic spike removal unit was built to overcome this problem. When a spike appeared on the output of the detector, a large differentiated signal was produced causing a sample & hold circuit to come into effect. In this way cosmic spikes were eliminated from the spectra. Although the circuit usually operated satisfactorily small spikes were recorded at high gain settings. In these circumstances software was used to eliminate the spikes which is explained in the next section. After passing through the spike removal unit the signal was amplified and then passed through a 12 bit

analogue-digital converter. From there the signal was transferred to the BBC microcomputer where the necessary processing and analysing was performed.

3.3 Signal Processing.

The spectral region in which the luminescence of interest lies, is a region in which there is strong atmospheric water vapour absorption. This absorption consists of large 'dips' in the luminescence signal giving strange features in the spectra. It was decided in order to obtain reasonable spectra, that these anomalies would have to be eliminated. This was achieved by software in the following manner.

A standard light source was used in which the spectral response was known. This source (Optronics 200W tungsten filament lamp) was passed through the same optical path as the luminescence, and the output monitored by computer. As the true spectral response was known irregularties caused by water absorption over a given wavelength range can be measured. This water vapour spectrum was then divided into all observed luminescence spectra over the same wavelength region. In theory therefore the water vapour effect could be removed from the spectra but because of changing humidity, the affect of the absorption on the luminescence changes and so the computer will adjust incorrectly. Another problem inherent in the system is the

reproducability of the spectrometer in taking two seperate spectra. As the vapour lines are narrow (FWHM =2mev) then any deviation of the spectrometer would cause non-cancellation of the water vapour feature and introduce small positive and negative going signals.

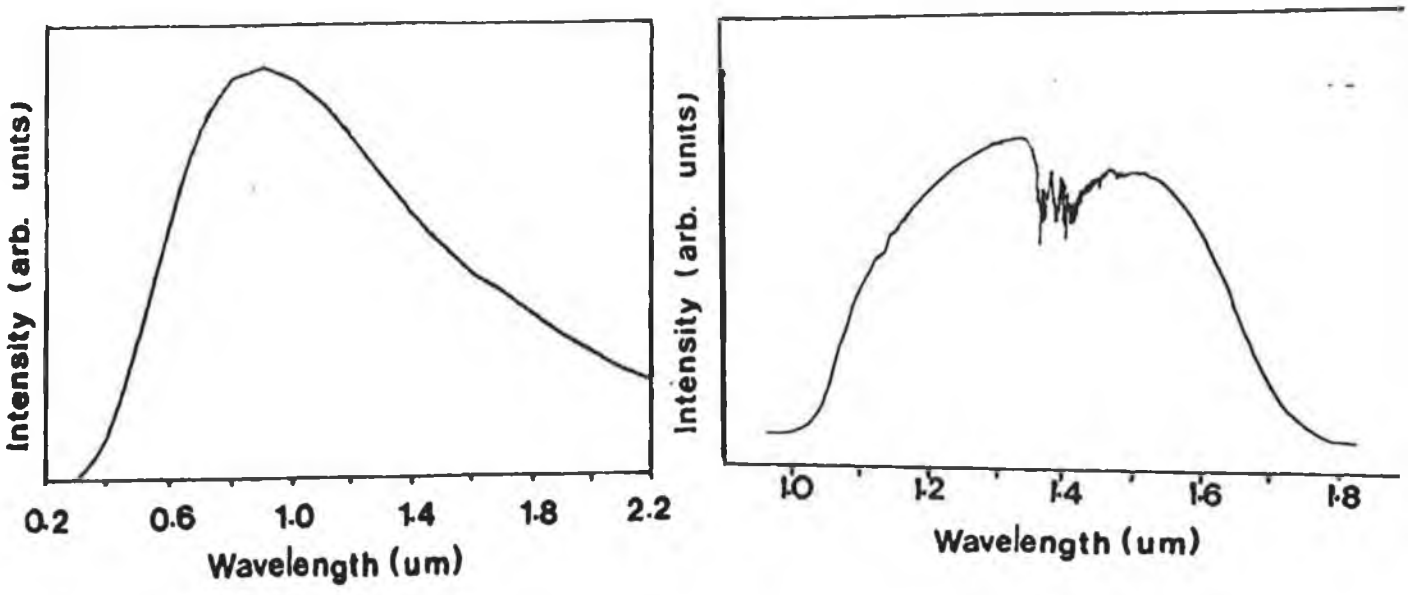

Figure 3.4, Spectral and Experimental response of a tungsten lamp.

It is evident from figure 3.4 (a) & (b) that the ideal response of the lamp as given by the manufacturers is different from that obtained experimentally. The difference being due to the detector and grating response over the specified wavelength range. This anomaly was eliminated by the following simple technique. The ideal response curve was normalised with respect to its maximium level and percentage

drop in intensity at various wavelengths obtained. These values were then compared to the percentage drop in intensity of the experimental response at the same wavelength readings.

The Germanium detector used had a DC and an AC facility and it was found while recording spectra in DC a small drift in the output signal was obtained. This error was easily remedied by taking the slope of the line joining the first and last points of the spectrum and adjusting accordingly. However, for a region where there is a large band structure this may not be possible. In this situation AC techniques are best employed as there is no drift component but it has the disadvantage of reducing the signal level by 1/2.

Using the AC technique the excitation light is chopped at a known frequency and the AC component of the luminescence is fed into a lock-in amplifier along with the reference signal usually obtained from the chopper. The lock-in amplifier works on the principle that any signal which is of the same frequency as the reference signal will be enhanced while all other signals of different frequency will be neglected. The output of the lock-in is a DC signal which is proportional to the amplitude of the AC input component.

Because luminescence from inequivalent centres will have different decay rates this difference may be used to distinguish between different luminescence features. This is achieved simply by using 'phase sensitive' techniques. The amplitude of the pumping light is square wave modulated by a

chopper, and as a result, the luminescent output is partially modulated at the chopping frequency and the modulated output is detected by lock-in techniques. The broken curves V1 and V2 in figure 3.5 show the sine wave components which are detected by the lock-in. The luminescent output is obtained by 'beating' it against a reference signal V_r derived from the chopper. It is clearly seen that a maximium signal is obtained when both the phase of the reference and that of the luminescence coincides. If it is supposed that two luminescent outputs from different centres occur, having different decay rates, then their sine wave components will be out of phase with each other as ϕ below. In this situation the signal from

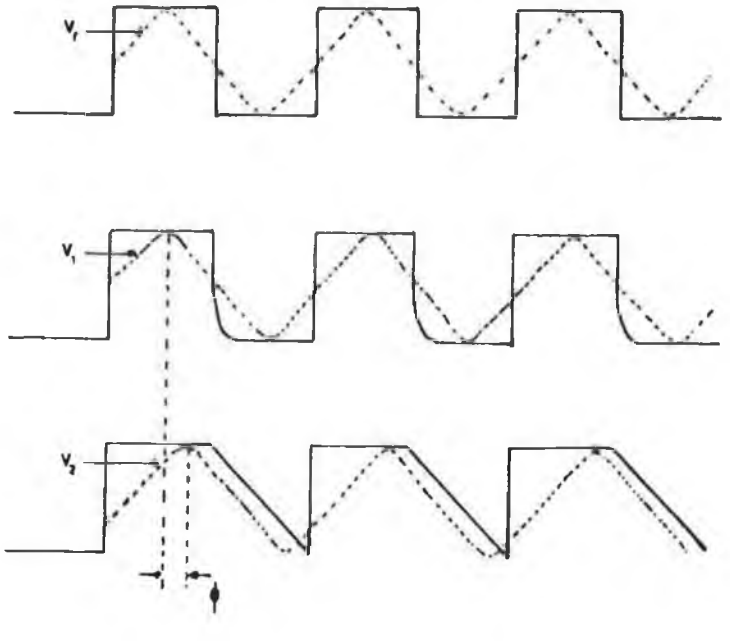

Figure 3.5, Luminescence patterns from fast and slow decay.

V2 is below its maximium and if the phase is adjusted so that V1 is nulled then the only signal from the lock-in will be due to V2. In this way signal contribution from different luminescent centers can be eliminated and only one center be examined. Figure 3.6(a) shows a complete spectrum from 1.1 to 1.7 showing the now familiar Copper pair spectrum along with new system. From various articles [24,25] it was found that the lifetime component for the Cu-Cu pair varied between 460 and 670 microsec. Therefore by nulling this signal one can see the contribution from the Cu-Zn system only. Figure 3.6(b) shows this very well.

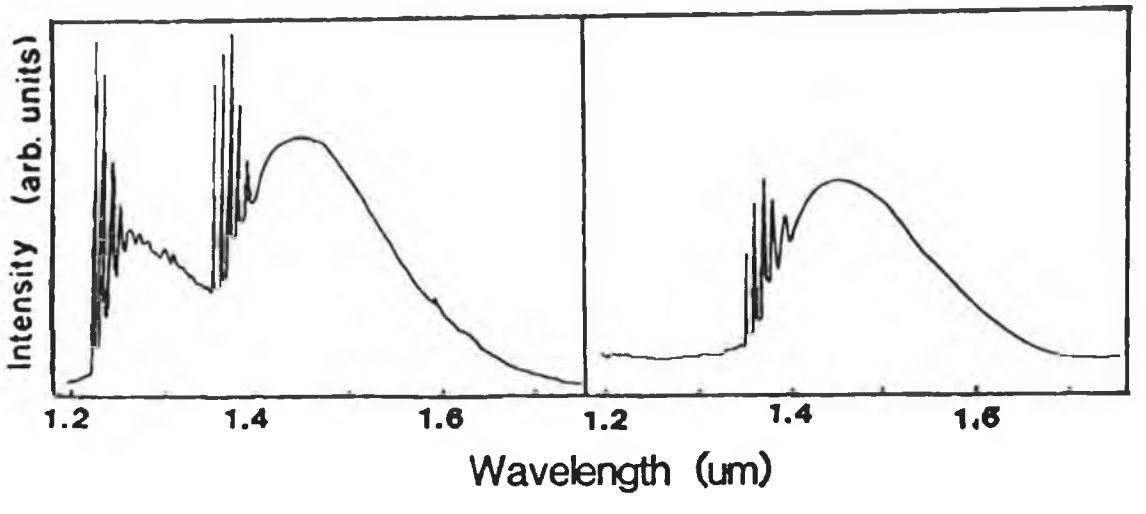

Figure 3.6, The effect of lock-in techniques.

As was stated above cosmic ray spikes were detected by this particular type of detector and caused sharp spikes to appear in the spectra. This situation was remedied to some extent while working in DC by the spike eliminator, which got rid of most of the pulses. However while working in AC the suitation was complicated by the fact that spikes which were out of phase with the signal appeared as negative pulses. The spike removal unit was not able to handle such pulses so software techniques were employed. By finding the full width half maximum (FWHM) of the sharpest known luminescent line then one is able to compare this FWHM with that of all other lines. As the spikes encountered were very sharp their FWHM was less than the luminescence features and in this way unwanted spikes were eliminated.

Figure 3.7 shows a spectrum of the system in question in the region 1.34 microns to 1.45 microns, showing the elimination of water vapour absorption (b), and cosmic ray spikes (c).

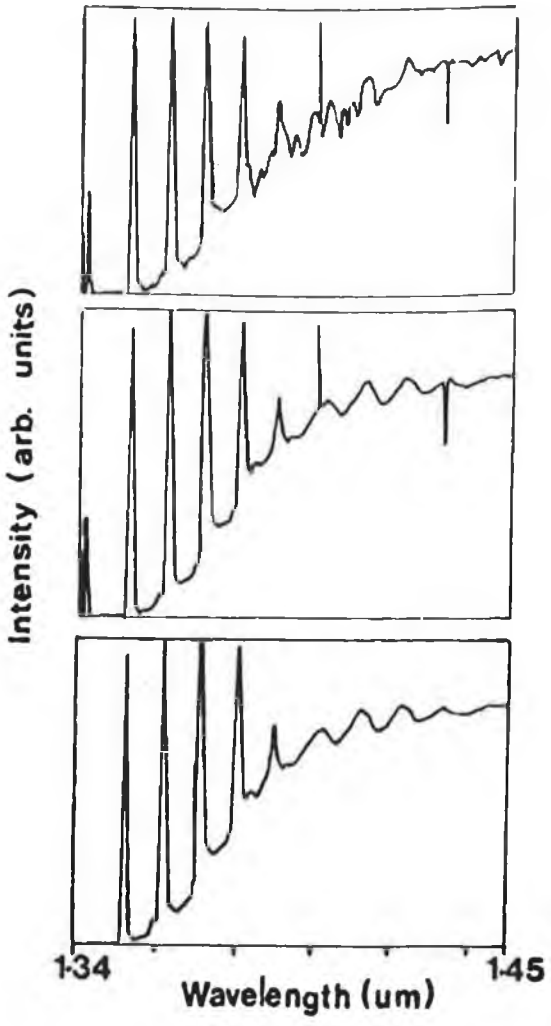

Figure 3.7, Spectra showing (a) water vapour absorption effects, (b) cosmic spikes effects and (c) elimination of such effects.

3.4 Signal Analysis.

Having obtained the various spectra which were processed as in section 3.3, it was then necessary to analyse the data now acquired. Use was made of a BBC microcomputer and a VAX system for such analysis, which principally took the form of finding lifetime components of the centre in question. In finding the decay kinetics of the system use was made of a chopper configuration as shown in figure 3.8 below.

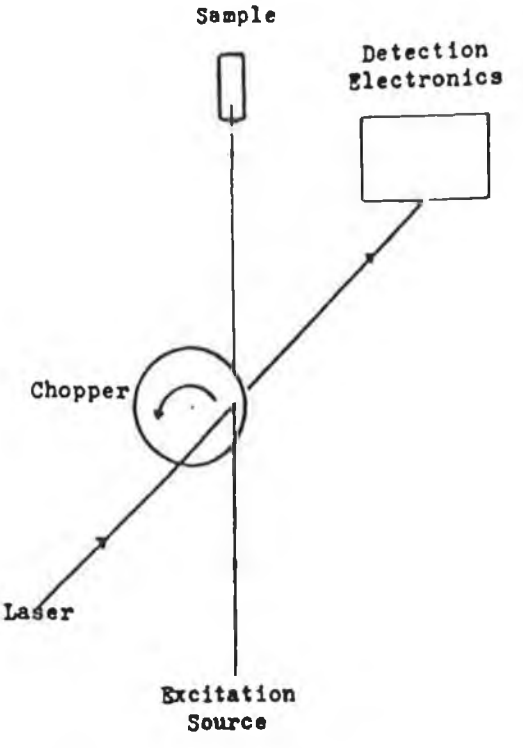

Figure 3.8, Chopper arragement.

The excitation source (xenon arc lamp) was passed through the chopper, whose aperature was 3mm in diameter. At the same time a helium neon laser beam was passed through this same aperature, and whose spot could be positioned easily for the detection electronics (figure 3.9). With this arrangement, when the excitation light was chopped off the sample, a pulse was sent from the detection electronics which triggered the microcomputer. The microcomputer then read the detector via an analogue to digital converter. In this way a series of lifetime measurements could be made over time scales ranging from 16msec to 400msec depending on software.

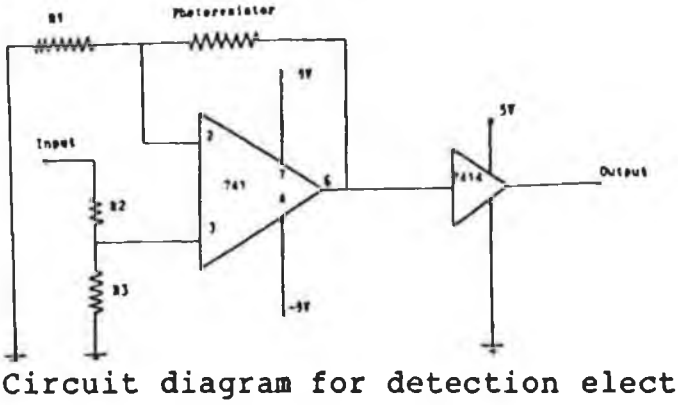

Figure 3.9, Circuit diagram for detection electronics.

Having obtained the relevant decay curves it was then necessary to extract the various lifetime components from this data. From semi-log plots of $Ln(I/I_{max})$ vs Time, it was clear that there were three components present in the data. Subsequently by fitting an exponential to the long lived portion (τ_3) and subtracting this fit from the original data one was able to retrieve a second component (τ_2) which when subtracted from the now new generated data revealed the third component (τ_1). In this way the various components could be extracted, giving an equation describing their behaviour given by equation 3.1.

$$f(t) = A \exp(-t/\tau_1) + B \exp(-t/\tau_2) + C \exp(-t/\tau_3) \quad -- \quad 3.1$$

where A,B,C are preexponential constants, t is time and τ_1, τ_2, τ_3 are the lifetime components obtained as above. The response of the system was also measured in the same way and it was found that it also had three components associated with it. Because of its complexity no discernible results could be taken from the actual decay curves and their log plots as the system was imposing a large contributon.

It was therefore necessary to deconvolute the contribution of the system out of the actual decay curves and so obtain the true response of the sample. If S(t) defines the observed sample response and D(t) the detector response then one is required to derive the true sample impulse response i(t) i.e. the response that would be observed if the

sample was excited by a pulse of zero duration but of finite energy. If D(t) is approximated by a string of impulses and a functional form assumed for i(t) then a series of values of S(t) can be obtained at different times as a simple summation of the contributions from all previous impulses. It will be shown how any continuous D(t) can be decomposed into a string of impulses and a summation over finite time evaluated, resulting in what is known as the convolution integral. This idea can be understood by examining figure 3.10,

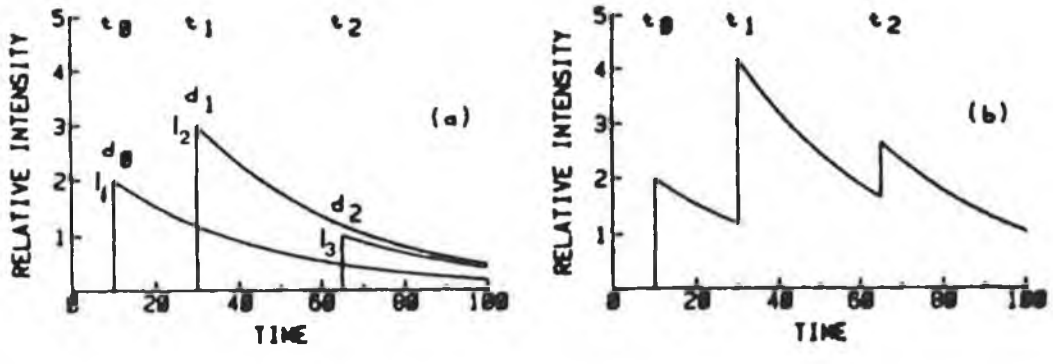

Figure 3.10, Three excitation impulse spikes of different area and occuring at times t_0, t_1, t_2; and (b) the summation of these pulses [32].

Assuming a simple exponential of the form EXP(-t/τ) for the impulse function then the observed decay S(t) will be the sum of the contributions from the three impulses at t_0, t_1 and t_2.

i.e. $S(t) = D_0 + D_1 + D_2 \qquad t_2 <= t$

$S(t) = D_0 + D_1 \qquad t_1 < t < t_2$

$$S(t) = D_0 \qquad t_0 < t < t_1$$

$$S(t) = 0 \qquad t_0 > t$$

where $D_0 = I_1 \text{ EXP } [-(t-t_0)/\tau]$

$D_1 = I_2 \text{ EXP } [-(t-t_1)/\tau]$

$D_2 = I_3 \text{ EXP } [-(t-t_2)/\tau]$

where D_0, D_1 and D_2 are the responses of the sample to only the excitation pulses at t_0, t_1 and t_2. From this analysis therefore if there are a number of impulses at times t_j and each excitation impulse has a weighting factor of D_j then

$$S(t) = \sum_{0}^{p} D_j \, i(t-t_j)$$

where p assumes the largest value such that $t_p <= t$. As stated above the equations just described confront the problem of a discrete form for D(t). However in most cases D(t) is given by a continuous function and needs to be decomposed into a series of impulses.

Each D(t) between $t_j-\Delta t/2$ and $t_j+\Delta t/2$ is replaced with an impulse at t_j where Δt is the separation in time between points. As Δt becomes small then

$$Dj = D(t_j)*\Delta t$$

therefore

$$S(t) = \sum D(t_j)\ i(t-t_j)\ \Delta t$$

for small enough Δt this equation approaches the integral

$$S(t) = \int_0^t D(x)\ i(t-x)\ dx = \int_0^t i(x)\ D(t-x)\ dx \text{ ---} \quad 3.2$$

$$S(t) = D(t) * i(t)$$

where i(t) represents the true response of the sample and '*' denotes convolution. From equation 3.2 it can be easily seen that if a functional form for the true response i(t) is assumed i.e. a single or double exponential, then the integral can be evaluated and expressions for S(t) can be obtained. This calculated form of S(t), denoted Scal(t), is then compared to the actual set of S(t), denoted Sexp(t), obtained experimentally and a good fit is got via software using least square reduction methods. The results obtained by this method are given in the following chapter.

3.4.1 Software Analysis.

The structure of the programming was such that memory space was conserved at all times. The programes were written in Basic, and in Assembler when data needed to be read into the computer quickly (program A2.2 appendix 1). The program structure was as that shown in figure 3.11 below, i.e. broken up into four main sections, acquisition, processing, analysing and displaying of data.

Flow chart of program structure.

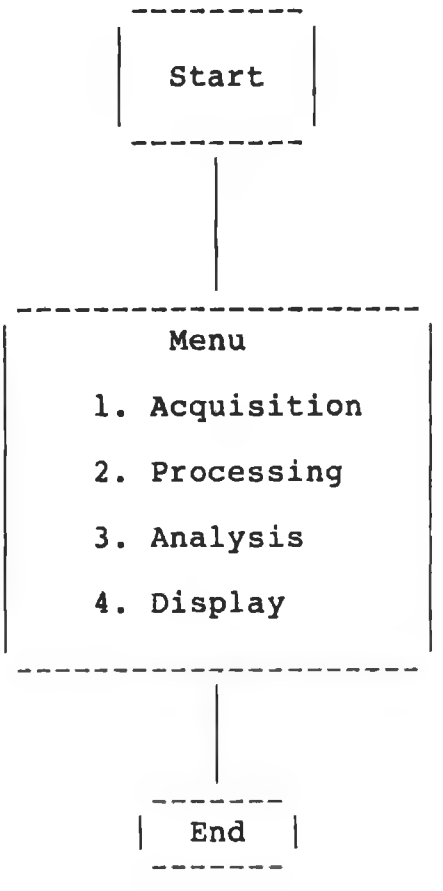

Figure 3.11, Schematic diagram of program structure.

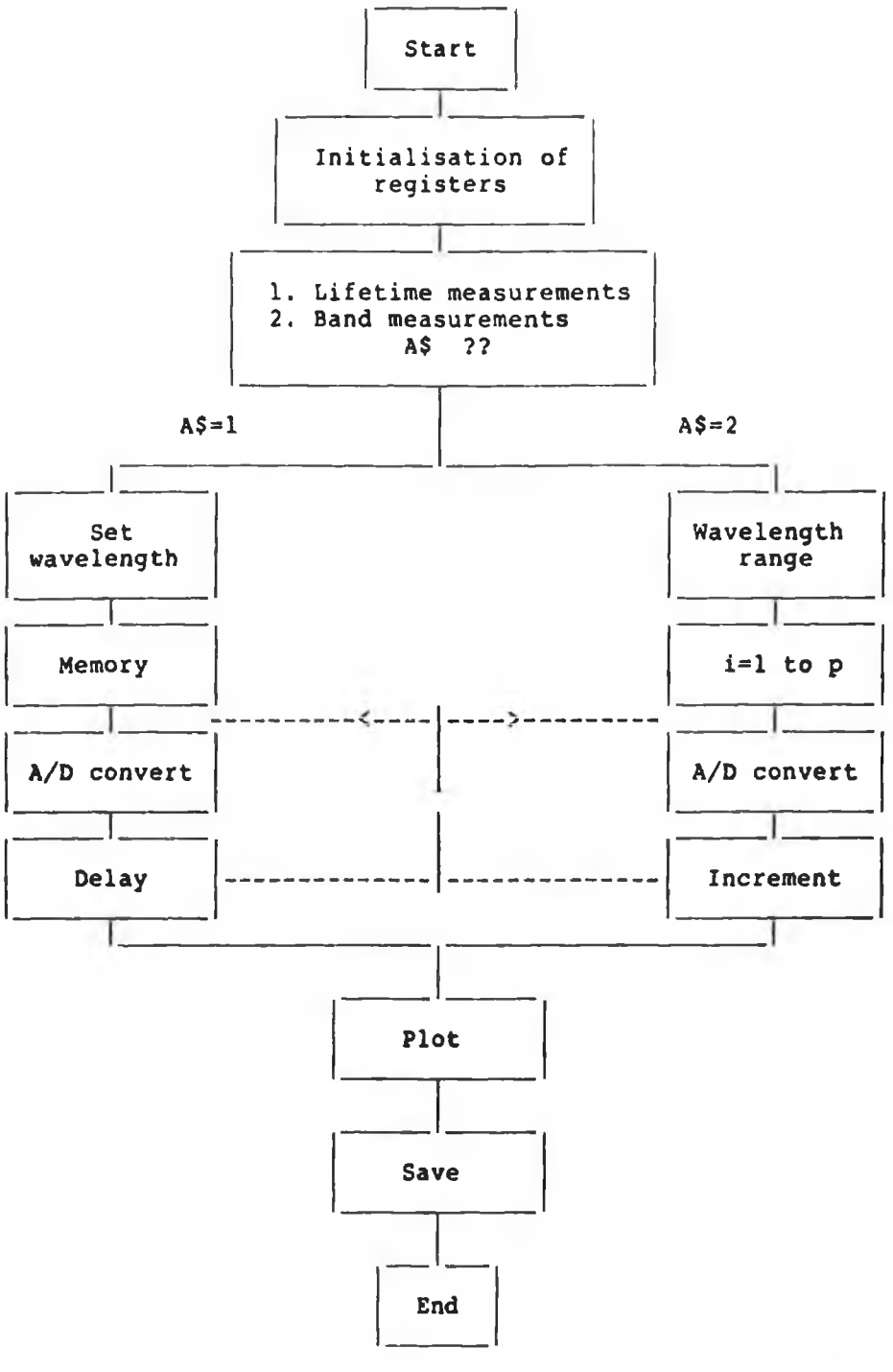

Figure 3.12, Flow chart of ' Data Acquisition '.

These programs interface the BBC microcomputer with external peripherals via the analogue to digital converter so enabling the operator to control the grating motors, to sample the detector at specific time intervals or over a specific wavelength range and to control a chopper mechanism as described in section 3.4.

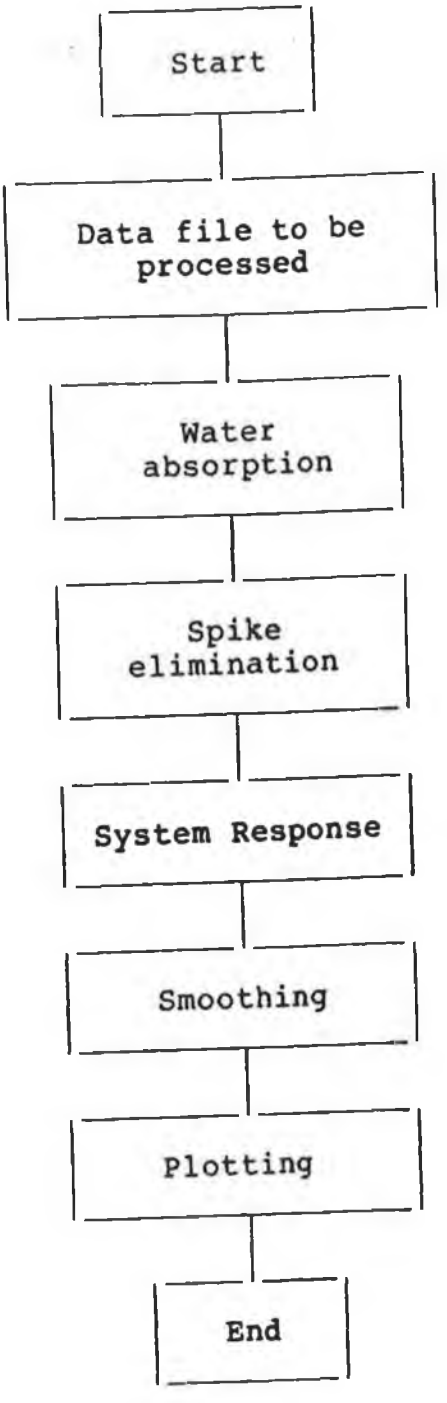

Figure 3.13, Flow chart of ' Data Processing '.

This program corrects spectra for system response, water vapour absorption and for the presence of cosmic ray spikes, all of which have been described earlier.

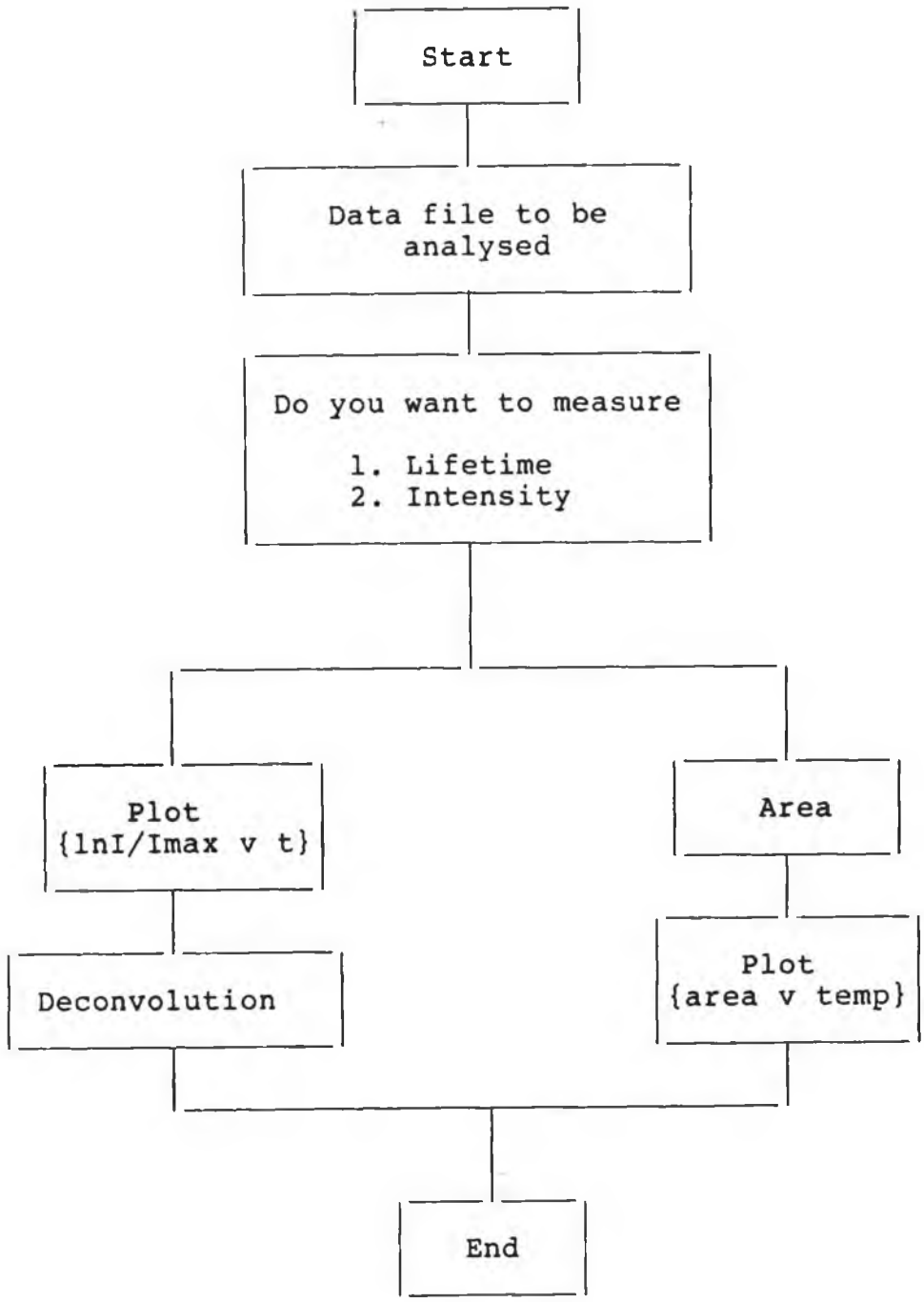

Figure 3.14, Flow chart of ' Data Analysis '.

This set of programs allow lifetime measurements to be made using two methods, semi log plots of $Ln(I/I_{max})$ vs Time and deconvolution, each of which has been explained in the text. Programs give 'hard' copies of the various spectra which were obtained during experiments.

3.5 Conclusion.

The above chapter clearly explains the experimental system used throughout the project, the sample preparation, and the detection procedure both hardware and software. It was stated that low temperatures were needed in order to detect the luminescence coming from the samples. In this work the luminescence was dispersed by a SPEX 1m spectrometer and detected by a liquid nitrogen germanium detector. Software processing of spectra allowed the suppression of cosmic spikes as well as eliminating the effects of both water vapour absorption and the system response.

CHAPTER 4. PAGE.

Results and Discussion.

Chapter 4: Results and Analysis.

4.1 Introduction.

The electrical properties of silicon can be influenced by the presence of impurities in its crystalline lattice and consequently a great amount of effort has been directed at understanding the behaviour of such defects. The normal procedure has been to first try and identify the defects present and then understand the mechanisms involved in their incorporation into the lattice. These microscopic descriptions of the individual defects will then provide insight into their influence on the macroscopic properties of the host lattice.

In the following paragraphs, the luminescence properties of the centre will be considered as well as how the centre is affected by being part of a crystal lattice which can undergo both static and dynamic distortions. These dynamic changes are brought about by atoms vibrating about some average position. Because of these distortions the electronic states of the impurity atom can be severely affected. In addition the environment may be affected by changes in the electronic state of the impurity. It is

therefore clear that in order to describe optical transitions both the impurity state as well as the lattice state should be considered.

Spectra relating to transition metal impurities in silicon show strong phonon side bands which are due to the excitation of lattice phonons and localized vibrations during the optical transitions. The localized vibrations are often sufficiently described in a configurational co-ordinate diagram, as shown in figure 4.1.

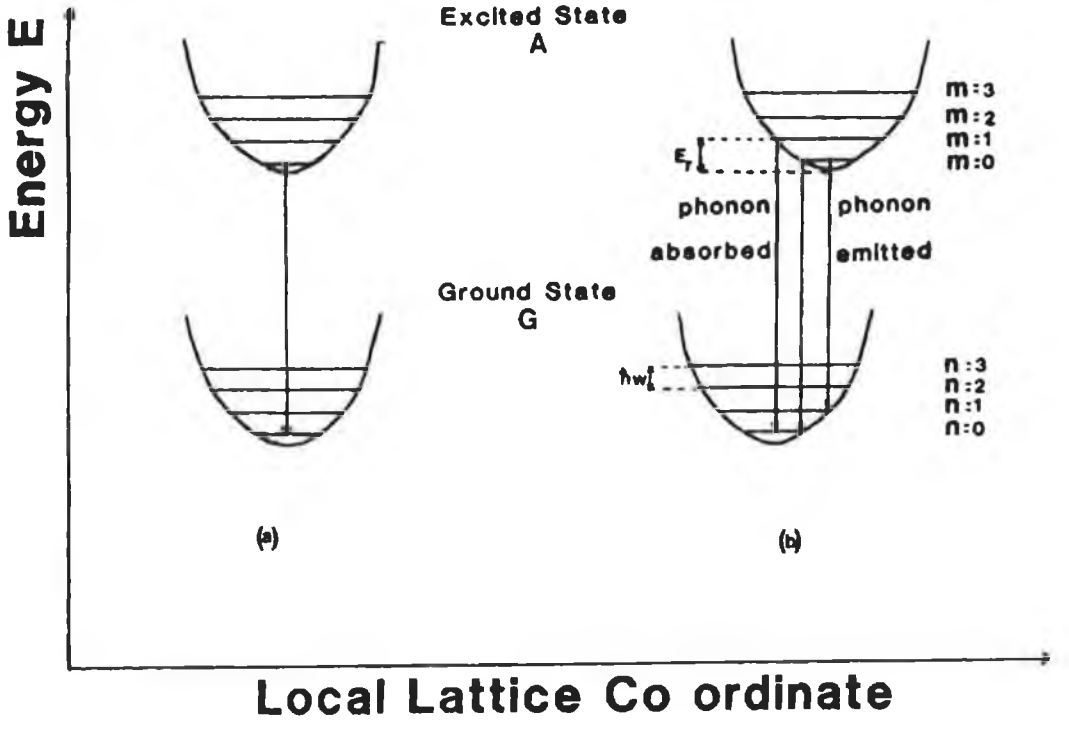

Figure 4.1, Co-ordinate diagram showing (a) weak coupling and (b) strong coupling.

Figure 4.1 shows such a diagram for one vibrational mode with energy $\hbar\omega$. The ground state (G) and the excited state (A) are shown. It is assumed that there exists discrete quantum states of the lattice, these are denoted n=0, n=1, ..., when

the electronic system is in the ground state and m=0, m=1, ..., when the electronic system is in the excited state. Physically one assumes that the electrons move in a potential well determined by the actual positions of the neighbouring atoms and so the energies of the electronic defect states are affected by the atomic position. On the other hand the equilibrium positions and vibrational states of the nuclei are determined by the average positions of the electrons and so depend only upon the electronic state. Excitation or recombination between defect states therefore causes rearrangements of the atoms in the defect surroundings.

The solutions to the harmonic oscillator equation

$$E_n = (n+1/2)\hbar w \qquad \ldots\ldots\ldots \quad 4.1$$

form a ladder of states with the energy separation $\hbar w$, and each such quantum of energy is known as a phonon. The new equilibrium position in the excited state causes an energy relaxation

$$E_r = S\hbar w \qquad \ldots\ldots\ldots \quad 4.2$$

where S is the Huang Rhys factor and is a measure of the coupling coordinate displacement between the ground state and the excited state. For large values of S - strong phonon coupling - the energies of the electronic state are strongly affected by the lattice relaxation. In luminescence at low temperature ($KT << \hbar w$) one observes transitions from the

lowest excited state (m=0) into the different ground states n=0, n=1, ...This explains the equidistant line systems shown in the following sections.

The positions of the electronic levels depend on the value of the crystal field, as does the frequency of the radiation emitted. Because of lattice vibrations the crystal field is being modulated and this modulates the frequency of the emitted radiation. When the crystal field modulation is weak the associated side bands which are produced in optical studies are weak and the spectra are dominated by sharp lines. However when the field modulation is strong, the side bands become more broad and the sharp lines reduce in intensity. According to crystal field modulation theory, the energy of the no-phonon line should be determined by the static crystal field of the atoms in their average positions, and it should be exceedingly sharp. However in practice the lines are much broader than predicted by theory. The reason being that strains and defects in the structure of the crystal cause the average seperation between neighbours to vary from place to place. This causes a range of values for the energy of the no-phonon line from atoms in different parts of the crystal. When the light is from a macroscopic volume of crystal, the no-phonon line is a composite of very sharp no-phonon lines from different microscopic sections of this volume, each with a slightly different energy. This inhomogeneous broading causes the finite width of the observed no-phonon line.

4.2 The copper-zinc system in Silicon.

Having established the experimental and signal analysis techniques in the preceeding chapter, there now follows a review of the results obtained during the experimental work carried out in the N.I.H.E. Dublin. As was stated eariler in this thesis, the incorporation of both copper and zinc reveals a spectrum as shown in figure 4.2.

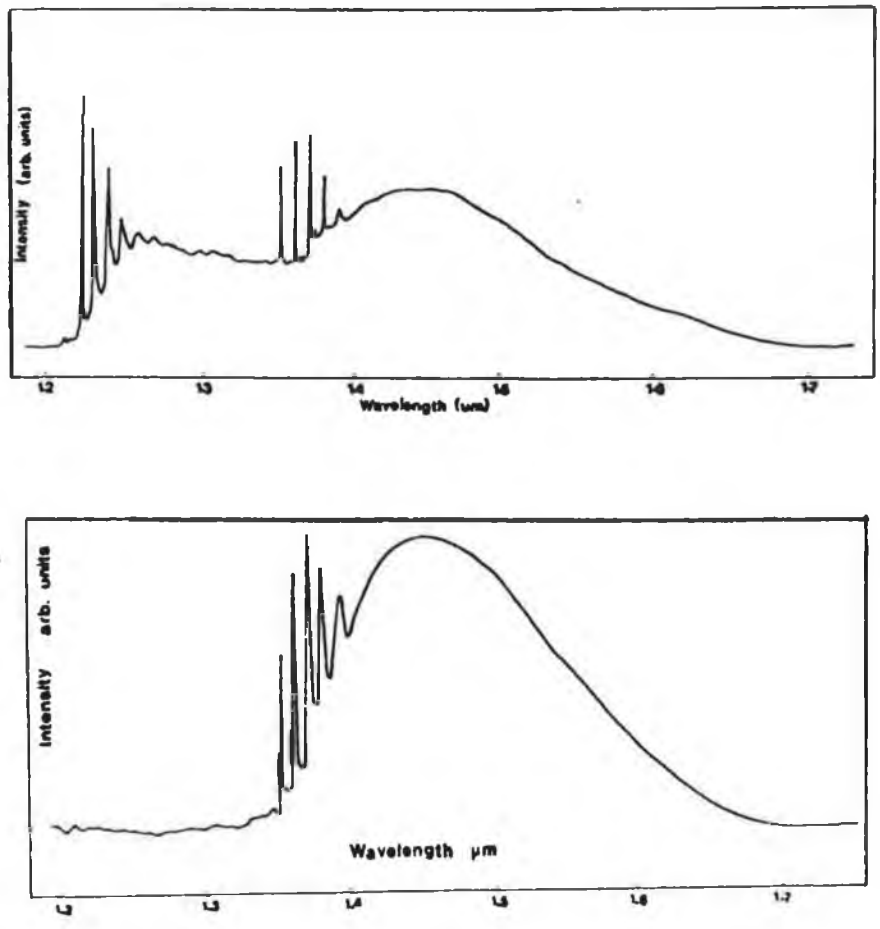

Figure 4.2, Low temperature (T=14.5K) spectra of (a) CuZn luminescence and (b) with Cu phased out.

Figure 4.2 contains the characteristic copper band which is associated with a copper-copper pair, as well as the new band associated with the presence of copper and zinc. This new band ranges from 1.3 um (956.1mev) to 1.7 um (731.2mev). Watkins et.al.(39)detected the copper associated luminescence in copper doped samples and measured lifetimes (480 - 670 microsec) in the temperature range 1.3K to 13K. Luminescence transitions from different centres will generally have different lifetimes. It is then possible to distinguish between the two bands using lock-in techniques, if the detector response is faster than at least one of the luminescence decay times. Figure 4.2 shows the result when the copper band is phased out leaving only the contribution due to the copper-zinc band.

4.2.1 Intensity Analysis.

The low temperature PL spectra of a silicon sample (p-type) doped with copper and zinc is shown in figure 4.3. The 4.2K spectrum is dominated by the lines $CuZn_o^o$, $CuZn_o^1$,..., and also by a broad background signal. The line labelled $CuZn_o^o$ is a NP line located at 919.56mev $\pm$ 0.1mev and the various phonon replicas $CuZn_o^1$,... are seperated by 6.3mev. The labelling $CuZn_i^j$ is indicative of how such systems are commonly described. Upper indices characterise the number of emitted phonons (positive integer) or absorbed phonons (negative integer), while the lower indices refer to electronic excitations in the upper defect state. The Stokes

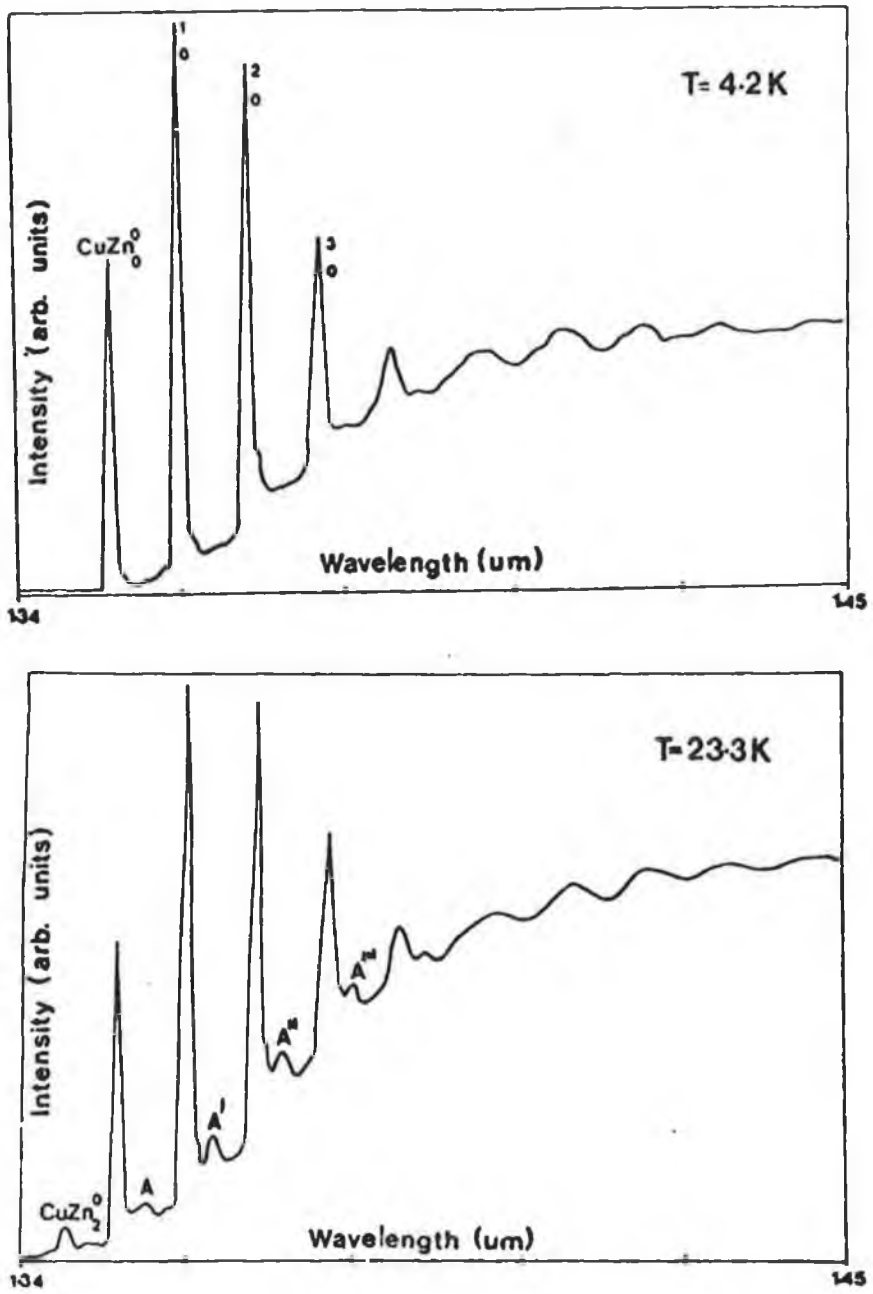

Figure 4.3, Spectra of CuZn luminescence with local mode sideband structure, for T=4.2K and T=23.3K.

vibrational mode satellites $CuZn'_{o}$,.... are replicated at higher temperatures as anti-Stokes satellites $CuZn'_{o}$, while new lines appear also seperated by 6.3mev and are labelled A, A',A'' ,... . The general complexity of the sideband as a whole is indicative of coupling to a wide spectrum of phonons by the centre from which the luminescence originates. Table 4.1 gives both the energy and wavelength positions of all the lines seen in the spectra.

It is suggested that the line labelled $CuZn^{o}_{2}$, is replicated as a Stokes vibrational mode satellite with a phonon energy equal to 6.3 mev. This is clearly shown in figure 4.4 where the first phonon replica is partially lost under the no-phonon line $CuZn^{o}_{o}$, and the subsequent phonon replicas are too weak to be detected.

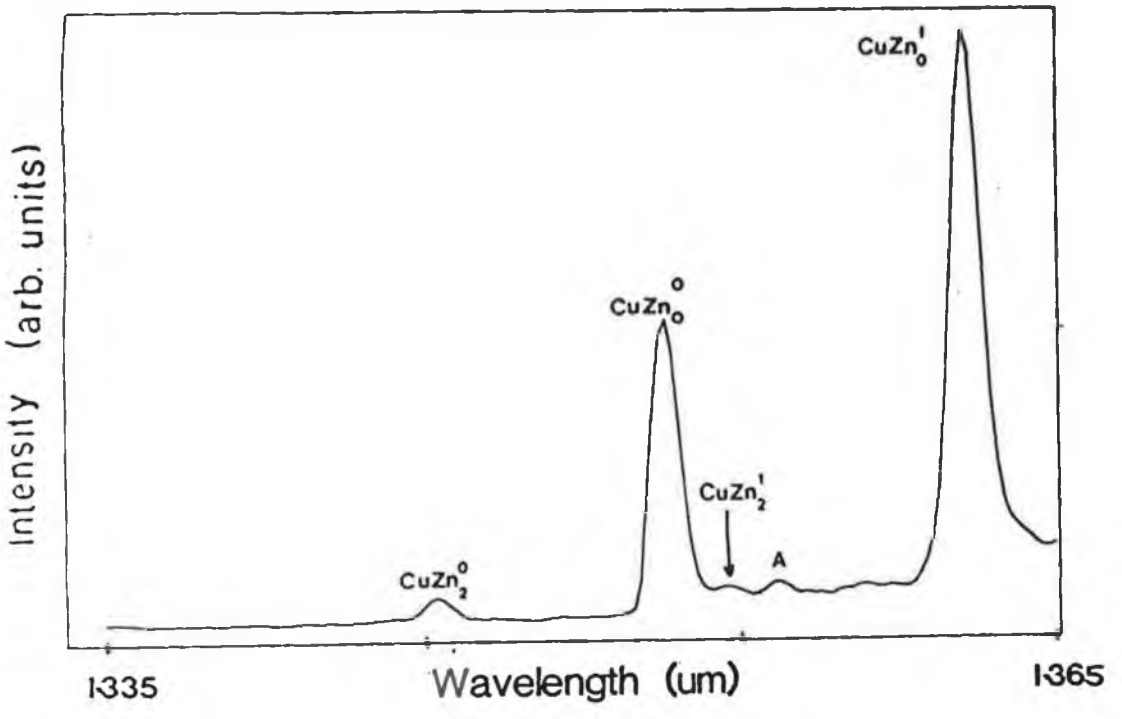

Figure 4.4, Detailed diagram of stucture around the no-phonon line located at 919.5 mev (I_o) showing the replica of the $CuZn^{o}_{2}$ line (I_1) at T=20K.

The relative intensity of the lines I_o and I_1 as a function of temperature is shown in figure 4.7. A comparison of the spectroscopic energy separation and the activation energy obtained from the slope of the graph of $\ln(I_1/I_o)$ versus 1/temperature, indicates a common ground state for the transition. In order to show how this is so, consider the following diagram representing an energy level diagram for some semiconductor. Both levels are decaying to a common level and their population densities are as shown. It is assumed that the degeneracies in both cases are equal.

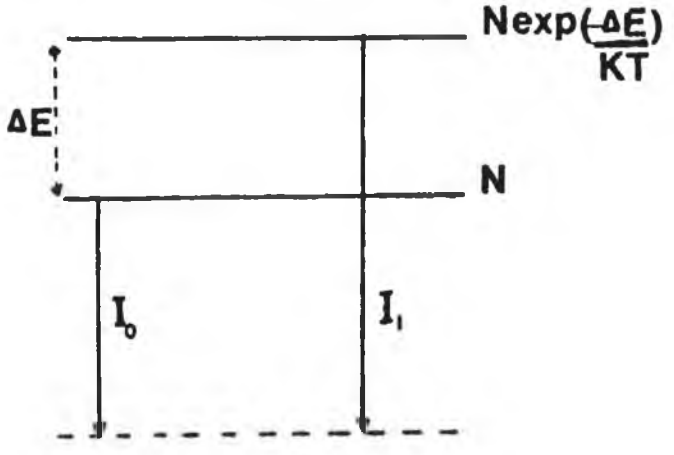

Figure 4.5, Energy level diagram.

If I_o indicates the intensity of the low lying level then $I_o=f_o$ N where fo is the transition probability for that level and N is the population of that level. By the same token the intensity $I_1=f_1$ N exp(-ΔE/KT).

Therefore

$$\frac{I_1}{I_o} = \frac{f_1}{f_o}\exp(-\Delta E/KT)$$

Taking LOG_e of both sides of the equation reveals

$$LOG_e \frac{I_1}{I_o} = LOG_e \frac{f_1}{f_o} - \Delta E/KT \quad .... \ 4.3$$

Therefore a plot of $LOG_e(I_1/I_o)$ vs $1/T$ gives a slope of $-\Delta E/K$ and an intercept of $LOG_e(f_1/f_o)$.

To verify that this thermalization obeys Maxwell-Boltzman statistics, a careful study of the temperature dependent line intensities was undertaken. Care must be taken at low temperatures in order not to heat the sample with the excitation source. To overcome this problem a defocussed beam was used and so the thermocouple reading would accurately reflect the sample temperature.

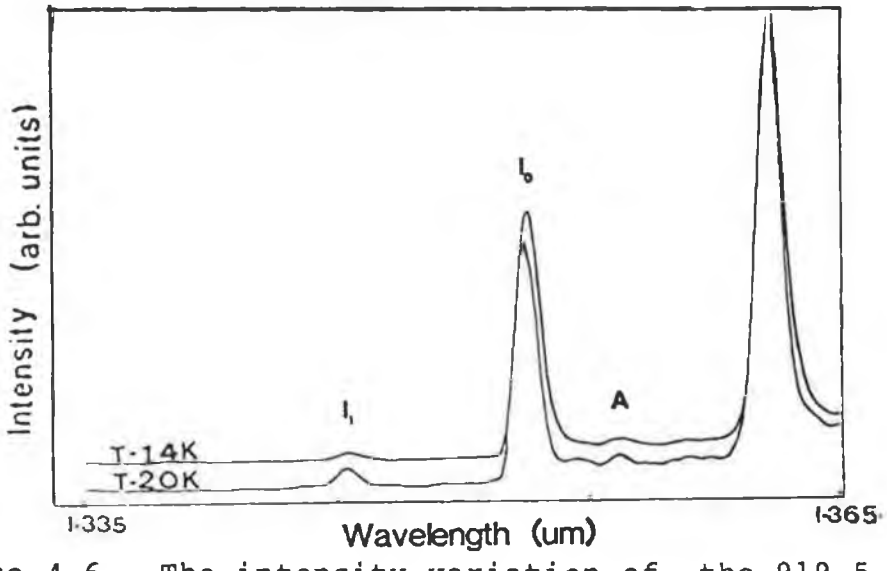

Figure 4.6, The intensity variation of the 919.5 mev (I_o) 924 mev (I_1) lines.

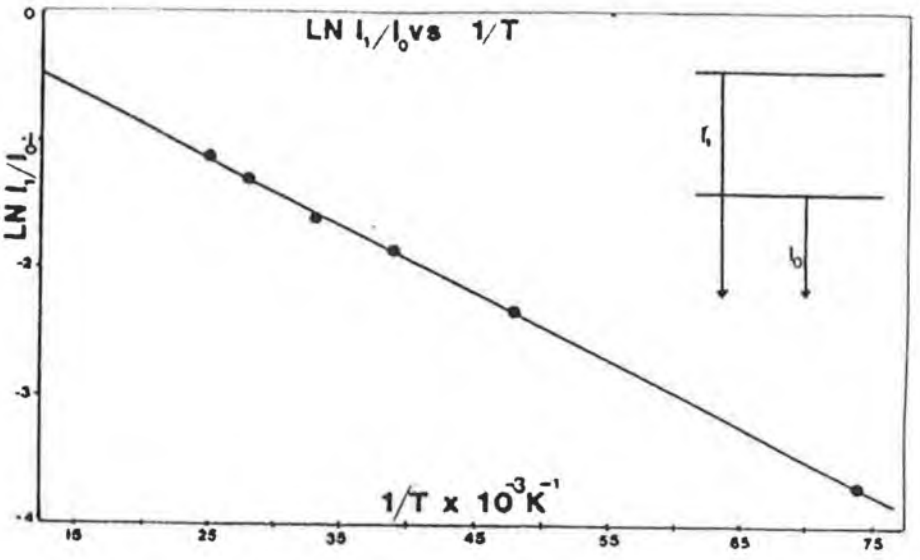

Figure 4.7, The thermalization of I_o and I_1 lines.

The truly LOG behaviour of intensity of the lines I_o and I_1 is shown clearly in figure 4.7 above. The activation energy (4.6 $\pm$ 0.1 mev) obtained from the slope of the graph is consistent with the spectroscopic separation, within experimental error,(Slope = - $\Delta E/k$, k = Boltzman's constant). The intensity of the zero phonon line (919.5 mev) will decrease with increasing temperature as the transitions involving thermally stimulated emission of phonons become more probable. Therefore the strength of the zero phonon line is affected by the strength of that transition's coupling to the lattice. By extrapolation of data on figure 4.7 to infinite temperature, one may obtain the ratio of the transition probability of the zero phonon line to that of the excited level, assuming equal phonon coupling for the states. The ratio obtained in experiment suggested that both lines I_o and I_1 were equally probable,

i.e. $f_1/f_o = 1.$

From the high temperature spectrum of figure 4.3

(b), it is clear that a new set of lines emerges labelled A, A', A'', .. Since we observe line A only in higher temperature spectra, it's initial state must lie higher in energy than the initial state of $CuZn^{o}_{o}$. Since the position of line A is lower in energy than $CuZn^{o}_{o}$, this implies a schematic energy level system as shown in figure 4.8 for these two lines.

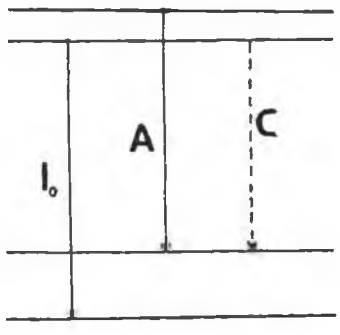

Figure 4.8, A split ground state configuration.

We do not find any evidence to support this model. Specifically the transition marked C in figure 4.8 would be expected to produce a line in the spectrum, unless totally forbidden by selection rules. Given the strong phonon coupling which this centre experiences, a totally forbidden transition is very unlikely. Furthermore all isoelectronic centres reported to date for silicon produce a singlet ground state. A careful study of the thermalisation behaviour of the line marked A suggests an alternative explanation. The results of these measurements are shown in figure 4.9. This data indicates that the initial state for line A lies 3.2 $\pm$ 0.1 mev above the initial state of $CuZn^{o}_{o}$. The separation of $CuZn^{o}_{o}$ and A is 3.0 $\pm$ 0.1 mev. Note that the sum of these quantities (6.2 $\pm$ 0.2 mev) agrees within experimental error with the energy of the strong local mode phonon which

dominates the spectrum. All of these facts are reconciled if we assume that the line A observed in the spectra is the first phonon replica of a (weak) zero phonon line which lies 3.2 mev above $CuZn^{o}_{o}$. We have examined the spectra carefully for such a line, but without success. In the absence of any direct evidence to support this second model, we examine in detail the structure of the phonon sideband.

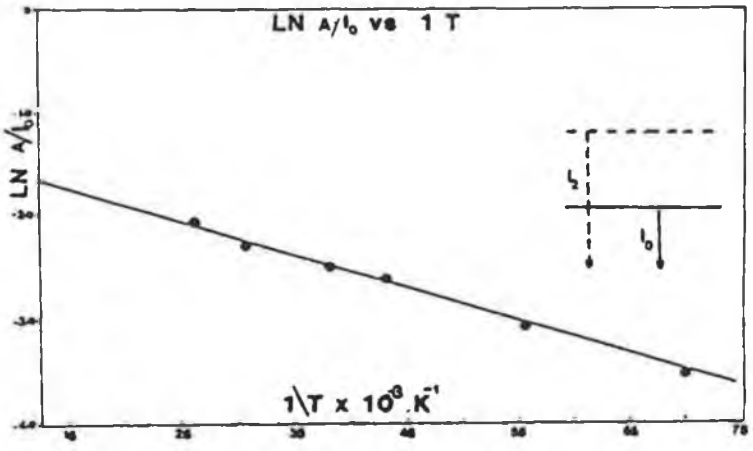

Figure 4.9, The thermalization of the Io and A lines.

As stated in section 4.1 the relative intensities of the various lines in the spectrum is largely dependent on the coupling with the lattice. This coupling is characterisied by a factor known as the Huang Rhys factor (S). The relationship for the intensities is given by [47]

$$\frac{I_n}{I_o} = \frac{S^n}{n!} \qquad \ldots\ldots\ldots 4.4$$

Where I_n is the intensity on the n^{th} phonon and I_o the intensity of the no-phonon line. Using this equation and the fact that the local mode energy is known to be 6.3 mev, then

a series of spectra can be computed numerically to replicate the experimentally obtained spectra. Figure 4.10 shows a series of spectra obtained numerically for the three system $CuZn_o$, A, and $CuZn_2$. Adding these three line systems together and introducing a background band reveals figure 4.11. When compared to the experimentally obtained spectrum figure 4.11 (b), then there is good aggreement at high energies for S=1.78, but at low energies the computed spectrum differs from that of the experimental spectrum. It should be noted that at these low energies water vapour absorption, which was discussed in chapter 3, strongly affects the spectra. It is therefore impossible to state with much certainity these lines are as strong as they seem to appear in the spectra.

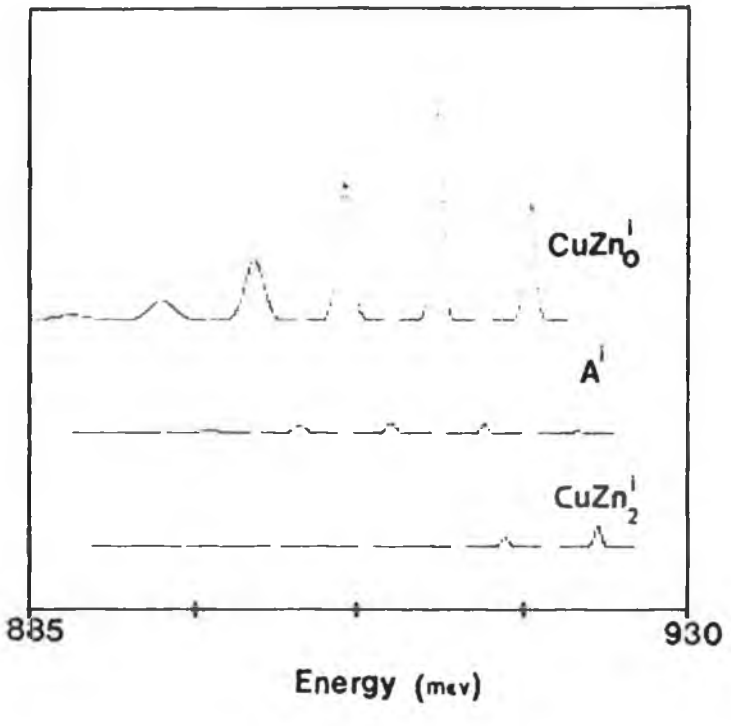

Figure 4.10, Numerically computed line systems for the $CuZn_o^o$ A, and $CuZn_2^o$ systems.

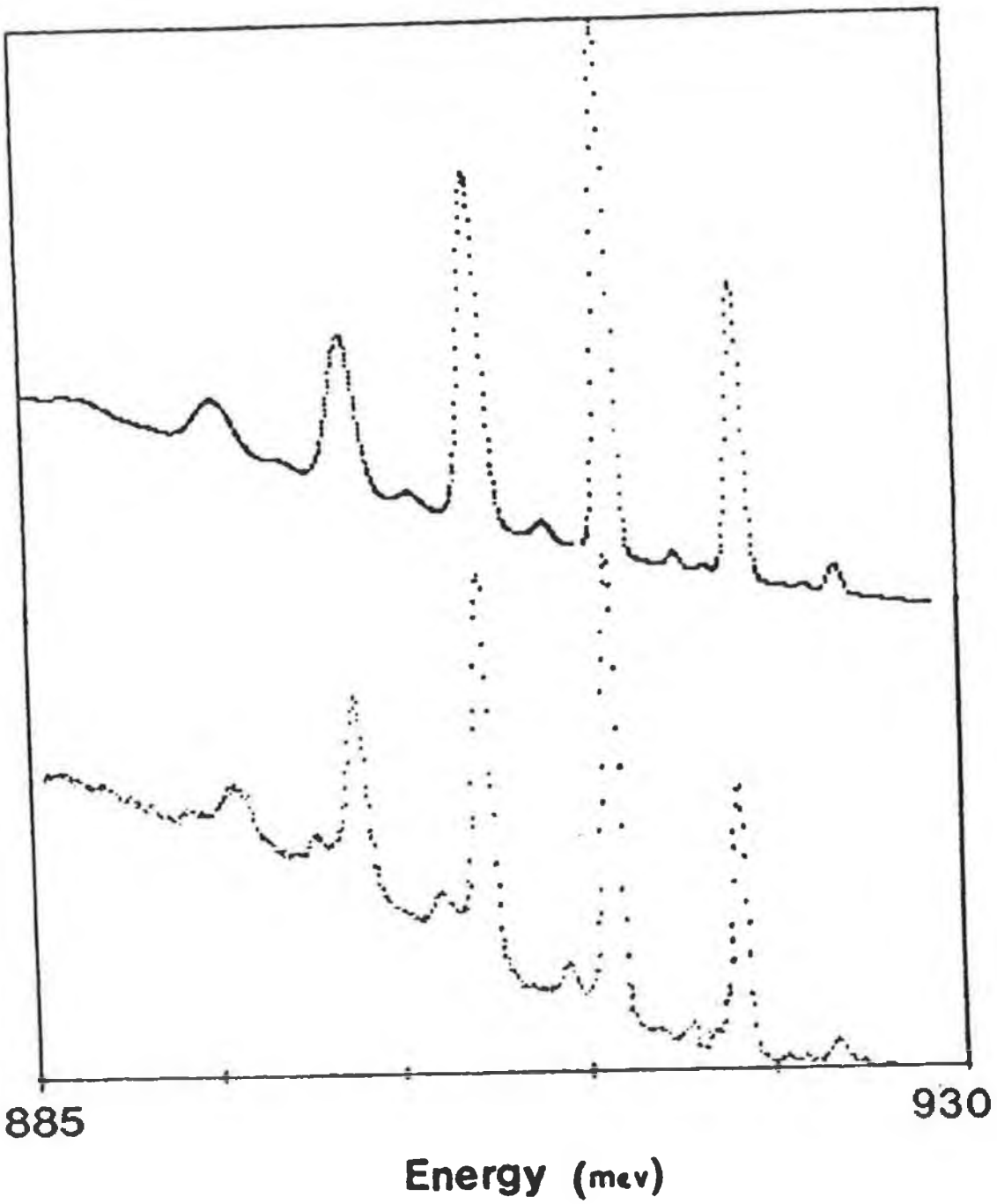

Figure 4.11, Theoretical and Experimental obtained spectra.

Table 4.1 , Energy and Wavelength positions of lines.

Line :		Energy : (mev) ± 0.05	Wavelength : (Angs) ± 5
$CuZn_o^{-1}$		925.47	13431
$CuZn_2^o$		924.22	13452
$CuZn_o^o$		919.56	13517.3
$CuZn_1^{'}$	(A)	916.6	13553.2
$CuZn_o^{'}$		913.12	13615.6
$CuZn_1$	(A')	910.6	13650.5
$CuZn_o$		906.8	13707.26
$CuZn_1$	(A'')	904.5	13742.2
$CuZn_o$		900.65	13801.14
$CuZn_1$	(A''')	898.23	13838.25
$CuZn_o$		894.43	13897.2
$CuZn_1$		892.32	13929.9
$CuZn_1$		886.5	14021.6
$CuZn_1$		880.32	14119.9
$CuZn_1$		873.83	14224.7
$CuZn_1$		867.6	14327.3
$CuZn_1$		860.0	14453.9

The above analysis of the thermalisation of the various lines would suggest firstly that there is an excited state transition ($CuZn_2^o$), located 4.6mev above the no-phonon line. We also conclude on the basis of thermalisation data and the modelling of the phonon sidebands that another excited state exists at approximately 3.2 mev above $CuZn_o^o$. Based on these conclusions we propose the energy level diagram shown in figure 4.12 for the centre.

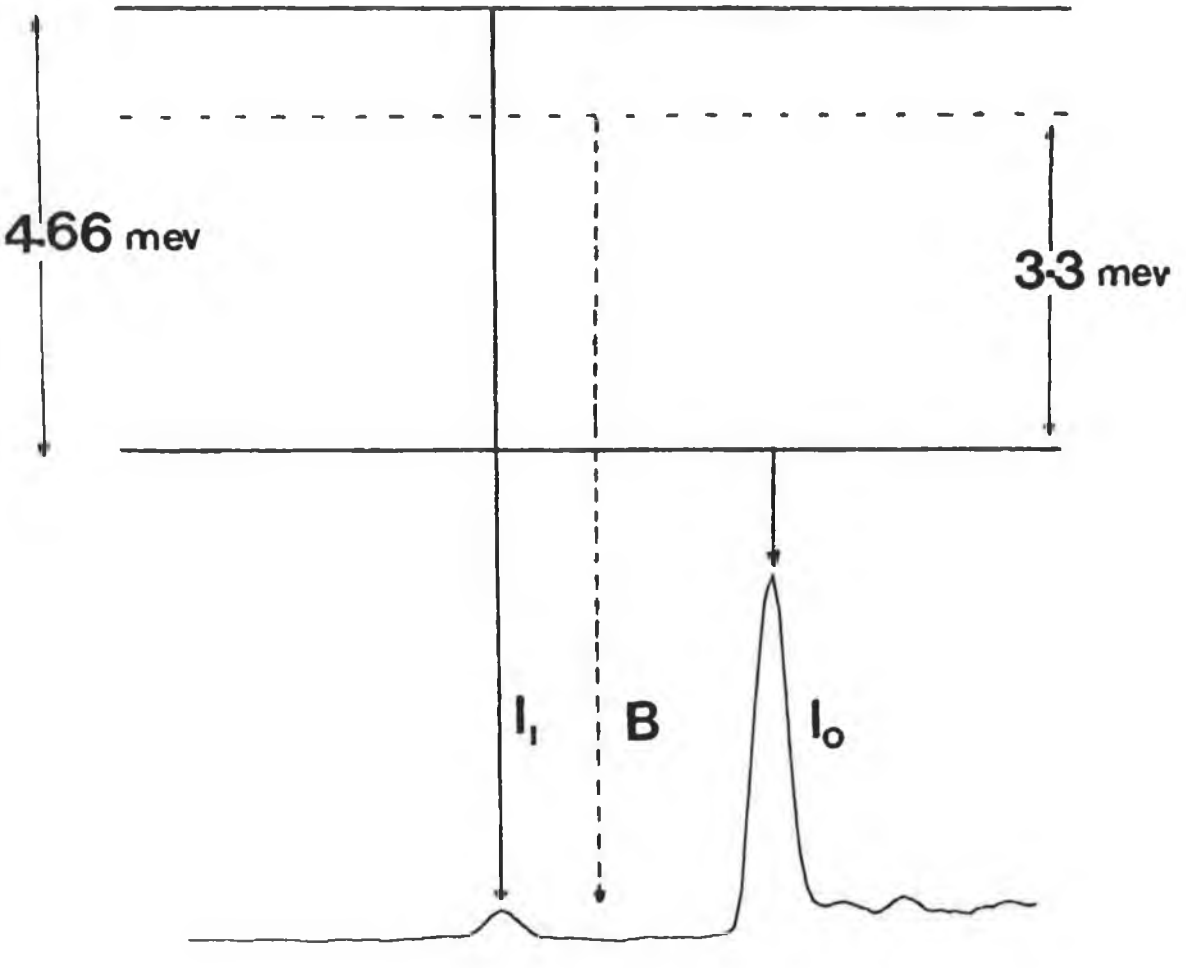

Figure 4.12,Energy level diagram for the CuZn related system.

4.3 Photoluminescence Lifetime Analysis.

PL lifetime measurements have played an important role in proving the isoelectronic nature of binding centres since the associated lines have extremely long decay times. The apparatus used in obtaining the decay kinetics of the system is explained in full in section 3.4. Because the lifetime of the system under inspection was so long, the conventional technique of collecting data using a box car single averager could not be used. (The model of averager available was a EG&G 4422 giving a maximum gate time of 20 msec). Therefore two methods were concentrated on, lock-in techniques in which the phase difference between the excitation and the luminescence is adjusted to maximise or minimise the detector response and so enable lifetimes to be calculated. The second technique involved programming a microcomputer to act as a box car averager but with a gate time that varied from 16 msec to 400 msec.

4.3.1 Lock-in Techniques.

This technique utilizes a chopped pump light source and phase sensitive detection. If the sample is optically pumped with a light source which is chopped at a frequency w, the luminescent transitions would be modulated in intensity at the chopping frequency, and there would be a phase difference between the pump light and the transition which

would be determined by the lifetime of the particular level under investigation. This phase difference could be read exactly from the lock-in detector (model EG&G 5206). An additional feature of this method is that the phase control could be set to null out any signal of a given time constant and so leaving only contributions from longer time constants. The lifetime component is obtained either from the time or phase shift between the excitation waveform and the sample emission or the degree of modulation of the emission. The equation

$$\text{Tan}\ (\phi) = wt \qquad \ldots\ldots\ldots\ 4.5$$

allows lifetimes to be easily calculated,

where ϕ = phase difference,

w = angular frequency,

t = lifetime component.

Table 4.2 Lock-in technique.

Temperature (K)	Phase (o)	Lifetime (msec)
13	53.7	10.57
20	53.2	10.38
25	52.6	10.16
30	51.6	9.80
35	48.3	8.72
40	46.1	8.07
45	43.2	7.29
50	42.4	7.09
55	40.6	6.66
60	40.0	6.52

This method however only gave a single value for the lifetime because of the fact that only one frequency was used, and so the lifetime obtained could be termed a mean lifetime.

More novel techniques such as 'quadrature frequency resolved spectroscopy' (QFRS) in which the lock-in is set in exact quadrature by observing scattered excitation light and nulling the signal, and 'in-phase FRS' in which the lock-in is set to maximise the signal are both commonly used today. A frequency sweep then gives a signal from which the lifetime can be calculated. The mathematics which describes this is explained elsewhere (41).

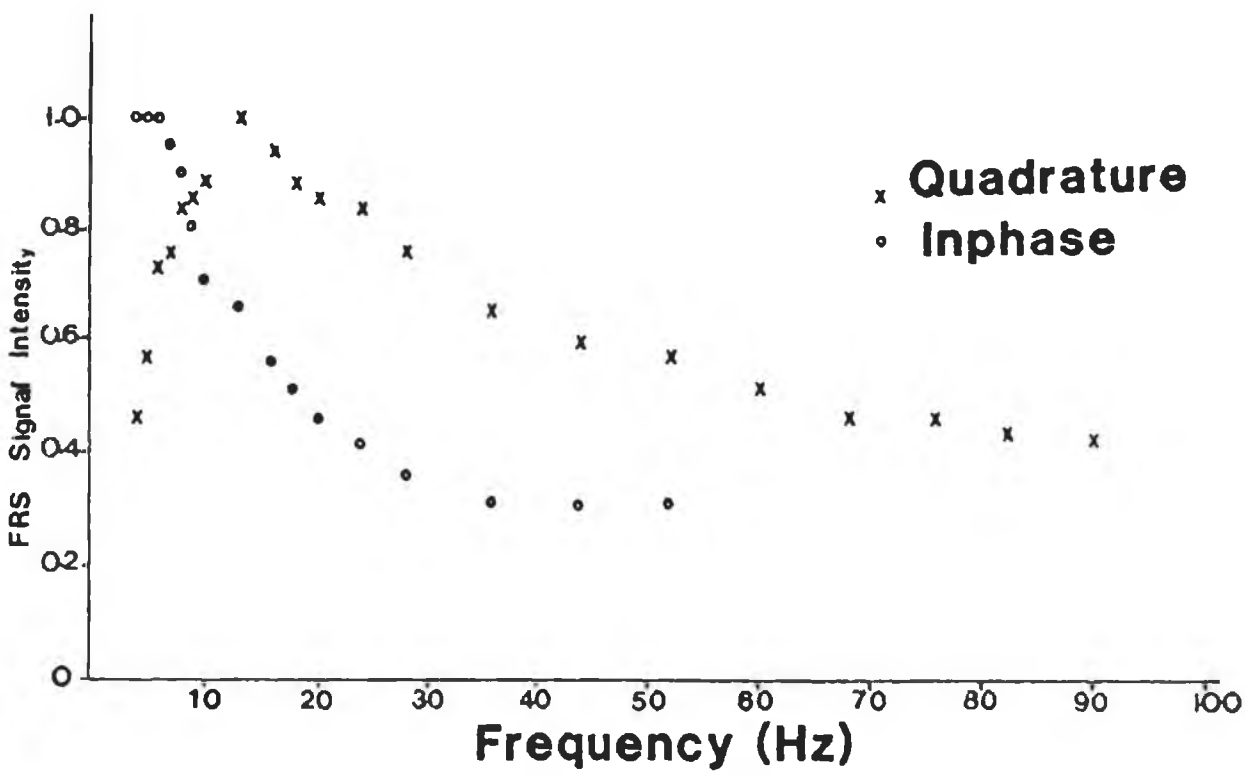

Figure 4.14, QFRS and In-phase FRS for the CuZn system.

This, however did not give conclusive results because of the long lifetimes involved which necessitated slow chopping frequencies. In order to utilise this method a frequency scan from very low frequencies to high frequencies has to be made. It was, however impossible to get accurate data at low frequency because the lock-in amplifier used was not accurate enough at these frequencies.

4.3.2. Computer Techniques.

As was stated eariler, the conventional box car averager could not be used because the lifetime components being measured were too long lived. It was therefore necessary to program a microcomputer to act as a box car but with a much longer variable gate time. The apparatus is explained in section 3.4 while the software is given in appendix 1. Figure 4.15(a) shows an Intensity versus Time plot for the detector while (b) shows the corresponding log plot. From this plot it is clearly seen that in fact the response of the detector is a highly complex function and not a simple exponentional. Using a NAG libary routine (F04JAF) a functional form for the response could be obtained. This routine confirmed that the response was a sum of three exponentials with time constants and preexponential factors given in table 4.3.

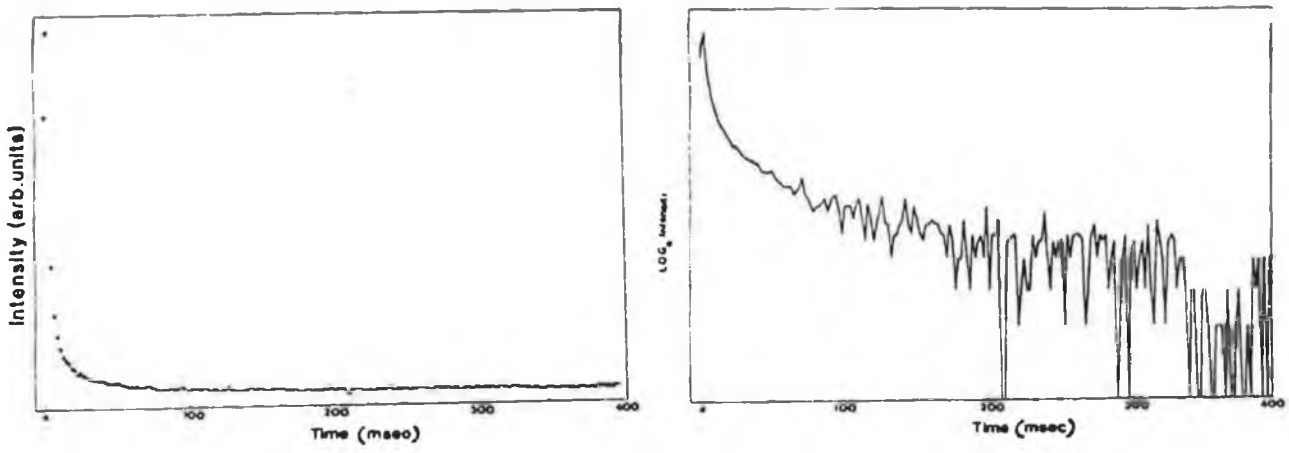

Figure 4.15, (a) Intensity vs Time,(b) Log intensity vs Time, for detector.

Table 4.3, Response function of detector.

$$D(t) = k1\exp(-t/\tau 1) + k2\exp(-t/\tau 2) + k3\exp(-t/\tau 3)$$

k1 = 11.5	1 = 2.3 msec
k2 = 205.0	2 = 14.0 msec
k3 = 619.8	3 = 72.0 msec

In order to prove the values obtained from this routine to be correct the following procedure was adopted. Assuming the response curve could be fitted to a sum of three exponentials then by fitting an exponential to the long lived portion (τ_3) and subtracting this fit from the original data one is left with contributions from the remaining two components. If this process is repeated with the second component (τ_2) now subtracted then one is left with the short lived component (τ_1). In this way verification of the three components in the detector response was made.

These same procedures were performed for the sample response and yielded table 4.4 below.

Table 4.4, Lifetime components of sample.

Temperature	Lifetime		
K	msec		
	t1	t2	t3
13.4	4.5	22.3	73.3
25.3	4.8	21.2	74.3
35.0	4.3	16.9	71.1
45.0	3.5	18.6	81.6
55.1	3.6	13.6	71.6
65.1	2.1	13.8	77.6
75.0	2.1	13.5	76.5

Figure 4.16 shows Intensity vs Time plots for the sample at T=13.4K, T=35K, T=50K and T=65K. The dotted line represents the detector response. It is clearly seen that at low temperatures the lifetime is in fact long compared to the detector response and that at high temperatures the lifetime approaches the response time of the detector.

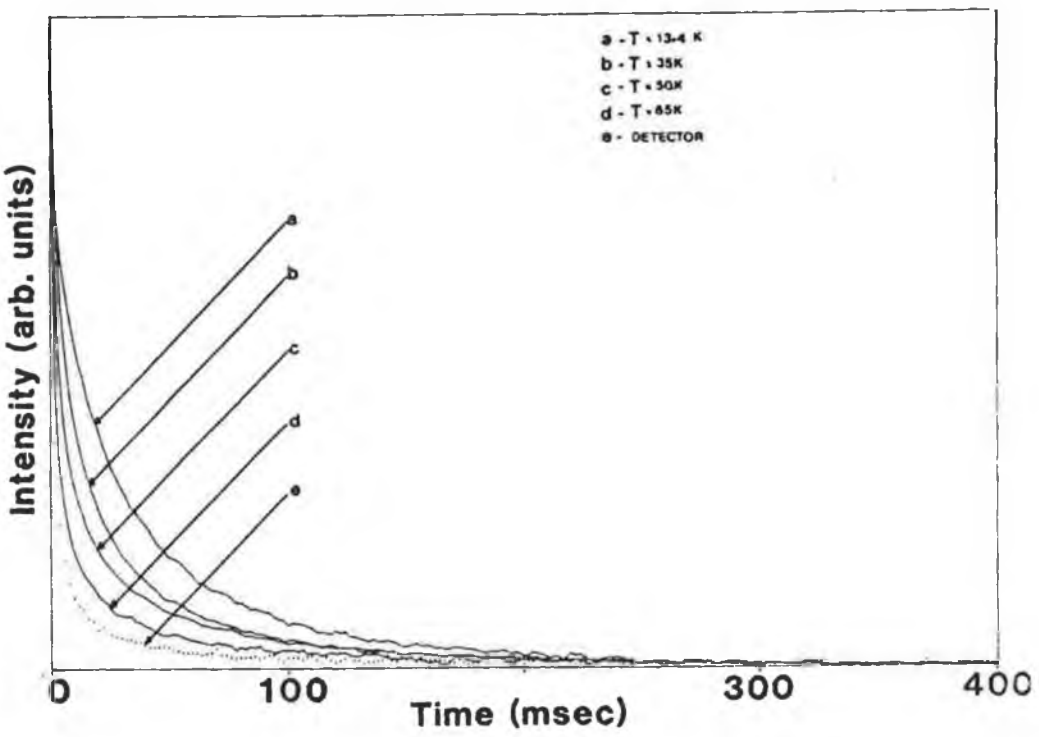

Figure 4.16, Intensity vs Time plots at (a) T=13.4K, (b) T=35K (c) T=50K and (d) T=65K.

It can be clearly seen from the above discussion that because of the complexity of the detector response the sample response was complicated and in order to obtain the 'true' response of the sample some means of eliminating the contribution of the detector from the observed response, needed to be done. The following section describes one such method, known as deconvolution.

4.3.3 Deconvolution Techniques.

As stated above the contribution from the detector needed to be considered when calculating lifetimes. Considering figure 4.17 below.

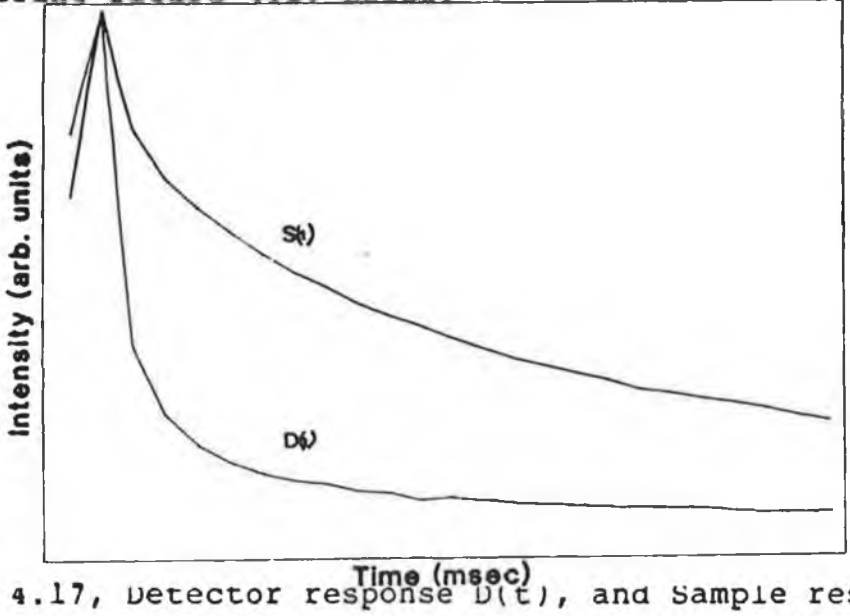

Figure 4.17, Detector response D(t), and Sample response S(t).

S(t) defines the observed sample response and D(t) the detector response then by the convolution theorem (section 3.4)

$$S(t) = \int_0^t D(t)\ i(t-x)\ dx$$

where i(t) is the true sample response.

If a single exponential for for the true response of the sample is assumed { $i(t) = k\exp(-t/\tau)$ } , then

$$S(t) = k\exp(-t/\tau) \int_0^t D(x)\ \exp(x/\tau)\ dx \quad .... \ 4.6$$

In order to solve this equation several methods ranging from Laplace and Fourier inverse transforms techniques to Least square techniques were used. It was found that the latter technique gave the most successful results as both the Laplace and Fourier methods magnified the noise element which was inherent in the data, rendering the results unusable.

On solving equation 4.6 then S(t) can be written as,

$$S(t_i) = \{ S(t_{i-1}) + k\ \Delta t D(t_{i-1}) \}\ \exp(-t/\tau) + k\ \Delta t D(t_i) \quad ..... \ 4.7$$

where $\Delta t = t_i - t_{i-1}$, k and τ are as in equation 4.6.

If on the other hand the true response of the sample is taken as an nth order exponential then the expression for S(t) becomes a sum of n terms each of the form of equation 4.6. In

this way one generates values for S(t) which are then compared to the experimentally obtained values. A mathematical comparison is then made between these values and the lifetime τ is adjusted until a good fit is obtained. To avoid having to fit the pre-exponential factor, one can normalise Scal(t) to the same peak height as Sexp(t).

The results of this method are shown in figure 4.18 in which data at T=35K,T=50K and T=65K are fitted to a single exponential impulse function.

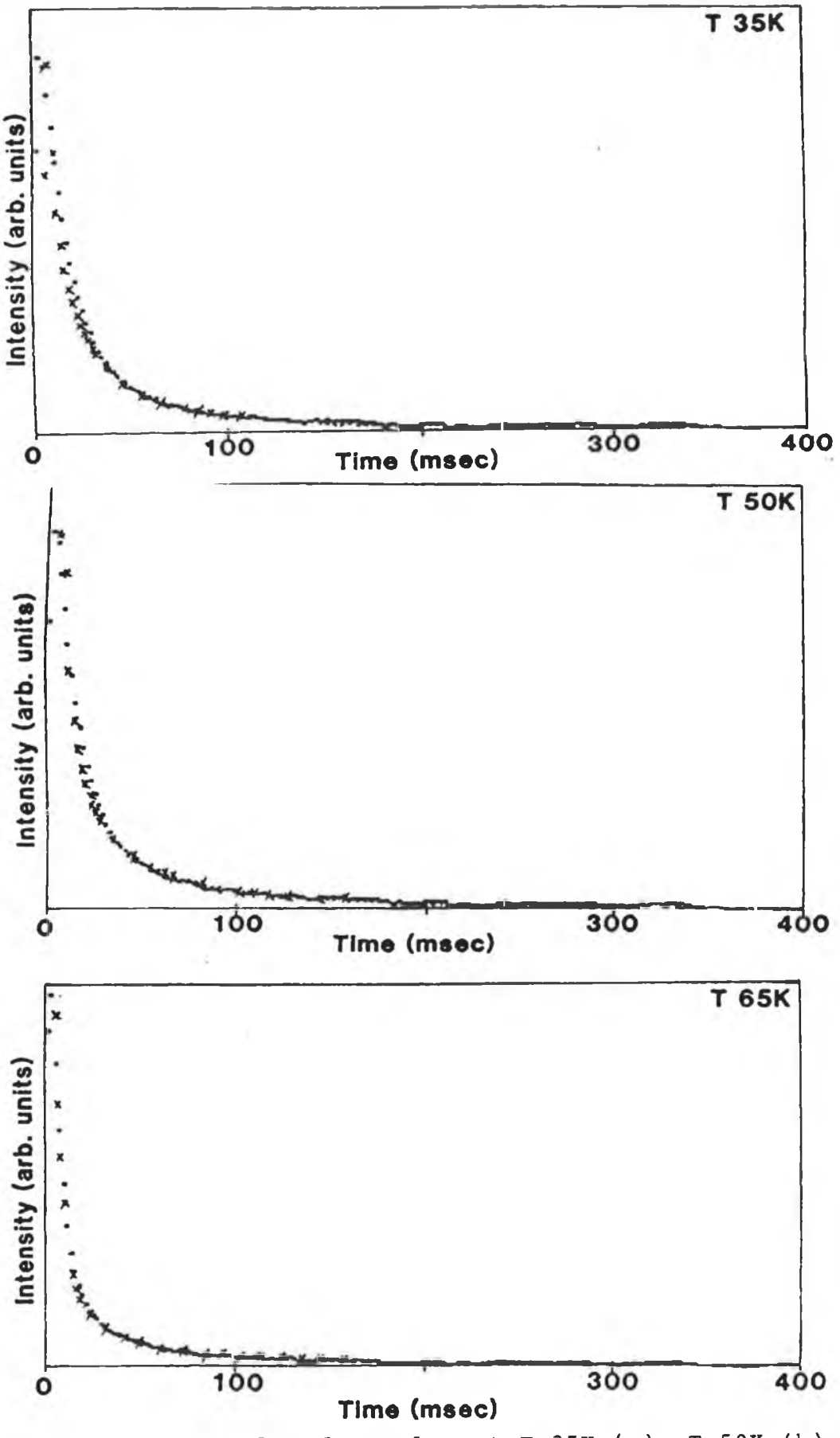

Figure 4.18, Deconvoluted results at T=35K (a), T=50K (b) and T=65K (c).

{ x - Theory, . - Experimental, }

However it was found that at low temperatures {T < 30K} that the true response was approximated by a double exponential of the form

$$i(t) = k_1 \exp(-t/\tau_1) + k_2 \exp(-t/\tau_2) \qquad \ldots\ldots 4.8$$

Solving for this in equation 4.6 gives the following results for T=13.4K and T=18.2K.

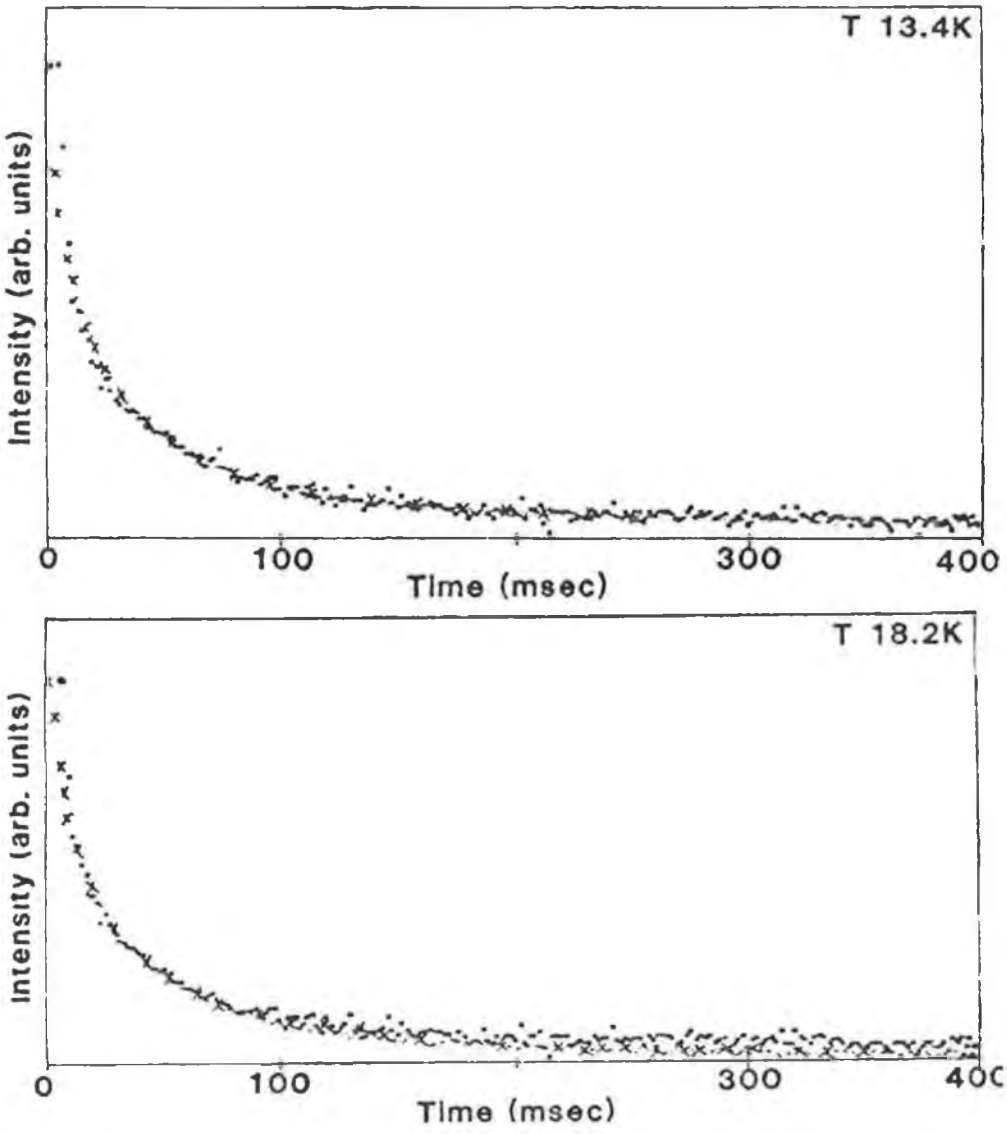

Figure 4.19, Deconvoluted results at (a) T=13.4K and (b) T=18.2K.

{ x - Theory, . - Experimental, }

From the above analysis it is evident that for temperatures below 30K, the transients consist of two components given by equation 4.8, whereas single exponential decays are observed for all temperatures above 30K. In equation 4.8 the true decay time of the luminescence is assumed to be τ_1. This term describes the decay of centres created during the excitation pulse. The 2nd term describes the decay of excited states formed by the transfer of energy into the centre from long lived traps of lifetime τ_2.

Table 4.5, Temperature and Lifetime measurements.

Temperature K	Lifetime msec	
	t_1	t_2
13.4	9.0	30.0
15.2	9.0	29.0
18.2	9.0	27.0
22.2	9.0	24.0
25.3	9.0	22.0
28.1	9.0	20.0
31.8	9.0	-
35.0	9.0	-
40.0	9.0	-
45.0	9.0	-
50.1	8.7	-
55.1	7.0	-
60.2	5.0	-
65.1	4.0	-
70.0	2.0	-
75.0	2.0	-
80.0	2.0	-
85.0	2.0	-
90.6	2.0	-

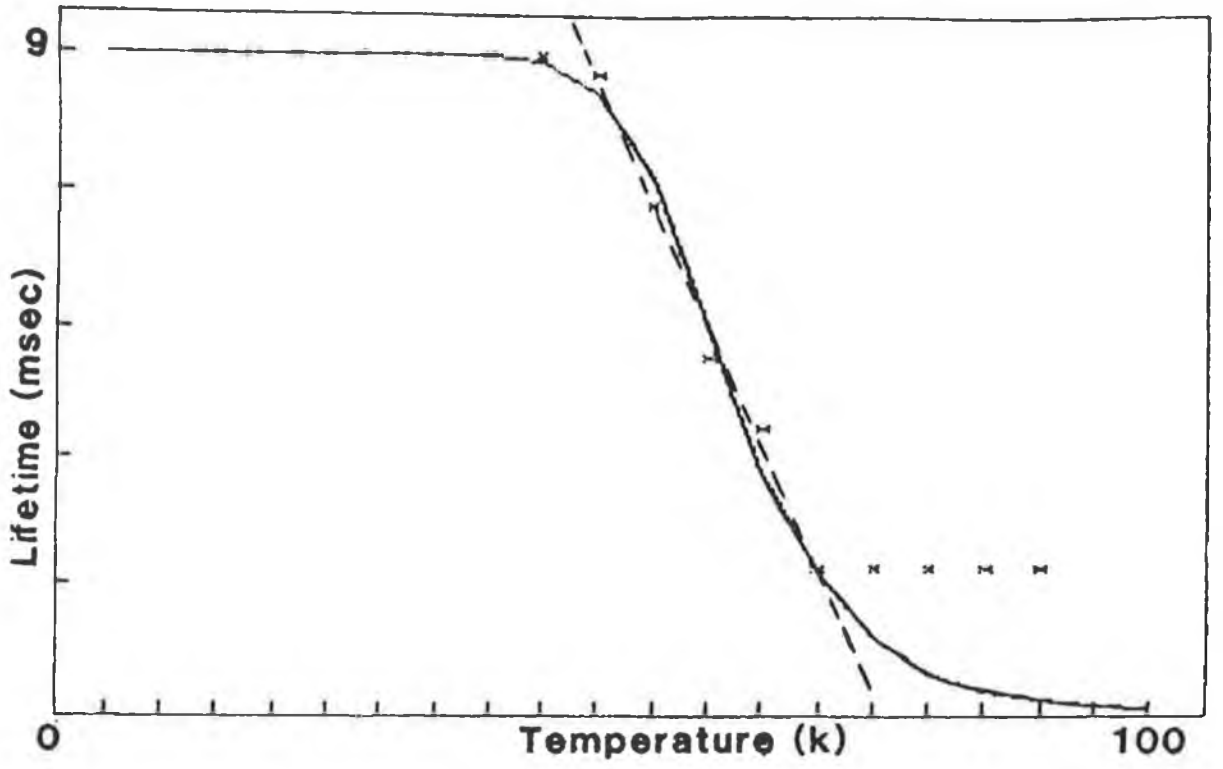

Figure 4.20, Luminescence lifetime vs temperature plot for CuZn system in silicon.

The best fit for the above data points was obtained using equation 4.9 below; the meaning of the symbols is given in figure 4.21.

$$\tau(T) = \frac{g_o+g_1\exp(-E_1/KT)+g_2\exp(-E_2/KT)+g_3\exp(-E_3/KT)}{X_o+X_1\exp(-E_1/KT)+X_2\exp(-E_2/KT)+X_3\exp(-E_3/KT)} \quad \ldots 4.9$$

where $\tau(T)$ is the experimentally determined lifetime as a function of temperature, g_i are the degeneracies of the levels and X_i are pre-exponential factors formed from the degeneracy and the transition probability of the level.

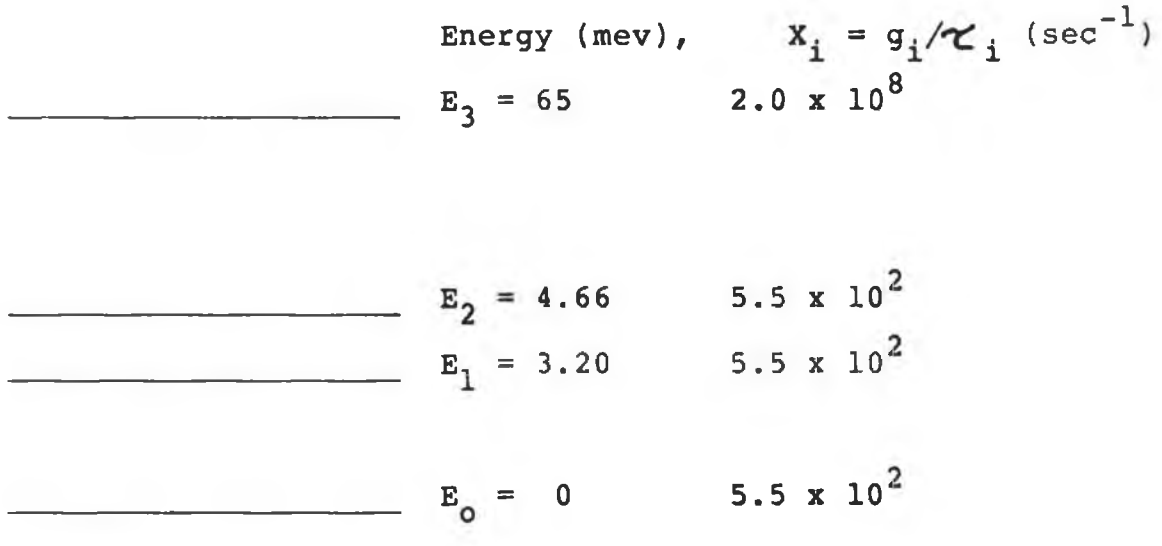

Figure 4.21, Energy level diagram for the analysis of lifetime data.

The decay process is found to have a deactivation energy equal to 65 mev (shown as the dotted line in figure 4.20). This type of temperature dependence, observed for several luminescence bands in silicon [42] indicates thermal activation of a bound electron or hole into a band. The spectroscopically obtained total binding energy was calculated to be 250 mev, leaving the binding energy of the

primary particle to be 185 mev.

It is also possible by temperature controlled PL measurements to distinguish between the weak bonding of one of the localized charge carriers and the much stronger binding energy of the remaining carrier. Figure 4.22 below shows the results of such an experiment.

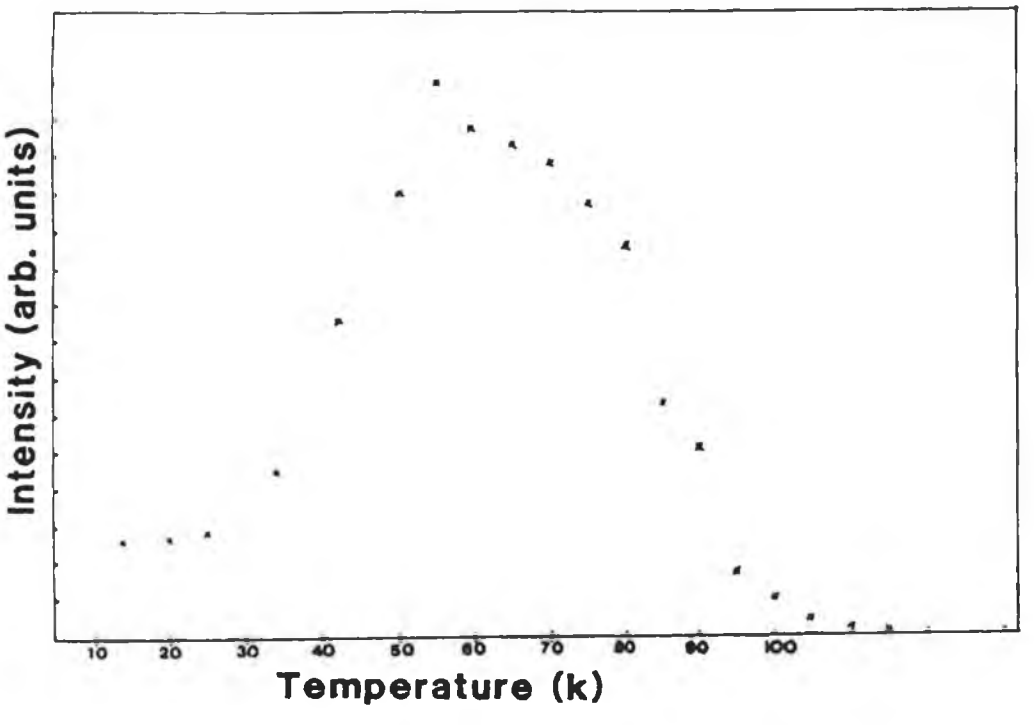

Figure 4.22, Total Intensity of Band versus Temperature.

The absolute area under the band increases dramatically between T = 10K and T = 55K. This temperature range corresponds to the filling of the optical centre whereas the temperature range T = 60K and T = 100K corresponds to the dissociation of one of the particles from the centre. A log plot of the intensity over the range T = 60K and T = 100K reveals a dissociation energy of 80 mev. Although this is different from that obtained from the decay kinetics (60 mev)

it is a quite reasonable result considering the approximations one would have to make in calculating the area under the band.

4.4 A Tentative Model.

A model which provides an approximation to the energy spacings and the relevant luminescence intensities of the lowest energy bound exciton transition for various defects in silicon , has been developed by Davies [43]. The model is based on the ideas of Morgan and Morgan developed in the early seventies [44]. The model shows how the axial nature of isoelectronic defects in silicon can be attributed to an uniaxial stress acting on the crystal's valence band and conduction band extrema. This model is only concerned with the lowest energy bound exciton states, which are assumed to be formed from a free hole taken from the k=0 valence band maximum with an angular momentum quantum number of j=3/2. The 12 electron states are formed from the conduction band minima, 2 spin states for each of the 6 minima. They form Γ_1, Γ_3 and Γ_5 orbital states when localised on a Td centre, with Γ_1 assumed to be lowest in energy and well separated from the Γ_3 and Γ_5 states. The basis states used in the calculation are therefore the products of the six hole states and the two electron states,(spin 'up' and 'down' in the $\Gamma 1$ orbital state), giving a total of twelve states. In this way the J=1 and the J=2 states are formed.

The axial nature of the isoelectronic defect is

represented by an uniform, uniaxial stress of magnitude S_t. The matrix which describes this effect is expressed in basis functions which are the twelve products of the hole wavefunctions with the electron spin states. The twelve states i=1 to 12 are ordered as follows, states i=1 to 8 are formed from the lower energy hole valence band states at k=0, and states i=9 to 12 involve the split off valence band states. The total matrix is the sum of the Hermitean matrices, M=A+B, where, A describes the valence band spin orbit coupling ζ, with elements $A_{ii}=-\zeta/3$ for i=1 to 8 and $A_{ii}=2\zeta/3$ for i=9 to 12. The spin orbit coupling (ζ)is defined to have an energy equal to 44mev for silicon [43].

B describes the electron - hole exchange energy (Δ) and the stress representing the axial nature of the defect. Morgan & Morgan [44], defined the electron - hole exchange energy as that energy which separates the J=2 states from the J=1 states. The origin of the J = 1,2 exciton states can be explained as follows. If an electron and hole are bound to a T_d centre by a potential weak compared to the spin - orbit coupling, then the lowest energy exciton states are formed from the hole j=3/2 states and the electron j=1/2 states. These states form a J=2 quintuplet and a J=1 triplet, with J=2 lower in energy by from the J=1 states.

The other parameters which appear in matrix B are related to the stress. A total of four independent parameters are used - A, B, C, S_ij. Of these A, B, C describe stress induced interactions among the P_x, P_y and P_z valence band orbital states [43]. The values of A, B and C are accurately known

for the free exciton (47). The free exciton values are adopted in this model for bound excitons on the basis that the exciton states are only slightly perturbed in going from free to bound. To include the effects of a uniaxial stress, the conventional approach of expressing the stress Hamiltonian in terms of stress tensors is adopted. The stress tensors take the form

$$S_{ij} = S_t \, \mathrm{Cos}(\hat{r}.i) \, \mathrm{Cos}(\hat{r}.j)$$

where St is the stress, $\hat{r}$ is the stress direction and i,j are crystal axis (x,y,z). The values of the S_{ij} factors can be calculated quite easily once the stress axis is known.

Matrix B is given below where,

$S_\sigma = (2S_{zz}-S_{xx}-S_{yy})B$,

$S_\epsilon = 3(S_{xx}-S_{yy})B$,

$A = 7.8\mathrm{mevGPa}^{-1}$, $B=22.6\mathrm{mevGPa}^{-1}$, $C=52.5\mathrm{mevGPa}^{-1}$

Table 4.6 Matrix B

B=	1	2	3	4	5	6	7
1	$-i\Delta - s_e$	$-\sqrt{\tfrac{1}{2}}C(s_{xz} + u_{xz})$	$-s_z - \sqrt{\tfrac{1}{2}}Cu_{xy}$	0	0	0	0
2		$-i\Delta + s_e$	0	$-s_z - \sqrt{\tfrac{1}{2}}iCs_{xy}$	$-\Delta\sqrt{3}/4$	0	0
3			$i\Delta + s_e$	$\sqrt{\tfrac{1}{2}}C(s_{xz} + u_{xz})$	0	$-i\Delta$	0
4				$i\Delta - s_e$	0	0	$-\Delta\sqrt{3}/4$
5					$i\Delta - s_e$	$-\sqrt{\tfrac{1}{2}}C(s_{xz} + u_{xz})$	$-s_z - \sqrt{\tfrac{1}{2}}iCs_{xy}$
6						$i\Delta + s_e$	0
7							$-i\Delta + s_e$
8							
9							
10							
11							
12							

8	9	10	11	12
0	$\sqrt{\tfrac{1}{2}}C(s_{xz} - u_{xz})$	$s_z\sqrt{\tfrac{1}{2}} - iCs_{xy}\sqrt{\tfrac{1}{2}}$	0	0
0	$-s_e\sqrt{\tfrac{1}{2}}$	$-\sqrt{\tfrac{1}{2}}C(s_{xz} - u_{xz})$	0	0
0	$-\sqrt{\tfrac{1}{2}}C(s_{xz} - u_{xz})$	$s_e\sqrt{\tfrac{1}{2}}$	0	0
0	$-s_z\sqrt{\tfrac{1}{2}} - iCs_{xy}\sqrt{\tfrac{1}{2}}$	$\sqrt{\tfrac{1}{2}}C(s_{xz} - u_{xz})$	0	0
0	0	0	$\sqrt{\tfrac{1}{2}}C(s_{xz} - u_{xz})$	$s_z\sqrt{\tfrac{1}{2}} - iCs_{xy}\sqrt{\tfrac{1}{2}}$
$-s_z - \sqrt{\tfrac{1}{2}}iCs_{xy}$	0	0	$-s_e\sqrt{\tfrac{1}{2}}$	$-\sqrt{\tfrac{1}{2}}C(s_{xz} - u_{xz})$
$\sqrt{\tfrac{1}{2}}C(s_{xz} - u_{xz})$	0	0	$-\sqrt{\tfrac{1}{2}}C(s_{xz} - u_{xz})$	$s_e\sqrt{\tfrac{1}{2}}$
$-i\Delta - s_e$	0	0	$-s_z\sqrt{\tfrac{1}{2}} - iCs_{xy}\sqrt{\tfrac{1}{2}}$	$\sqrt{\tfrac{1}{2}}C(s_{xz} - u_{xz})$
	$-i\Delta$	0	0	0
		$i\Delta$	$-i\Delta$	0
			$i\Delta$	0
				$-i\Delta$

(A2)

The matrices describing the effects of stress and the electron - hole exchange energy are computed and using the NAG libary routine (FO2AXF), the complete matrix is

diagonalised numerically.This technique was used by Davies [43] to explain two well known luminescence bands in silicon, the ABC band [45], and the Be related band [46], the results of which will be given discussed briefly here.

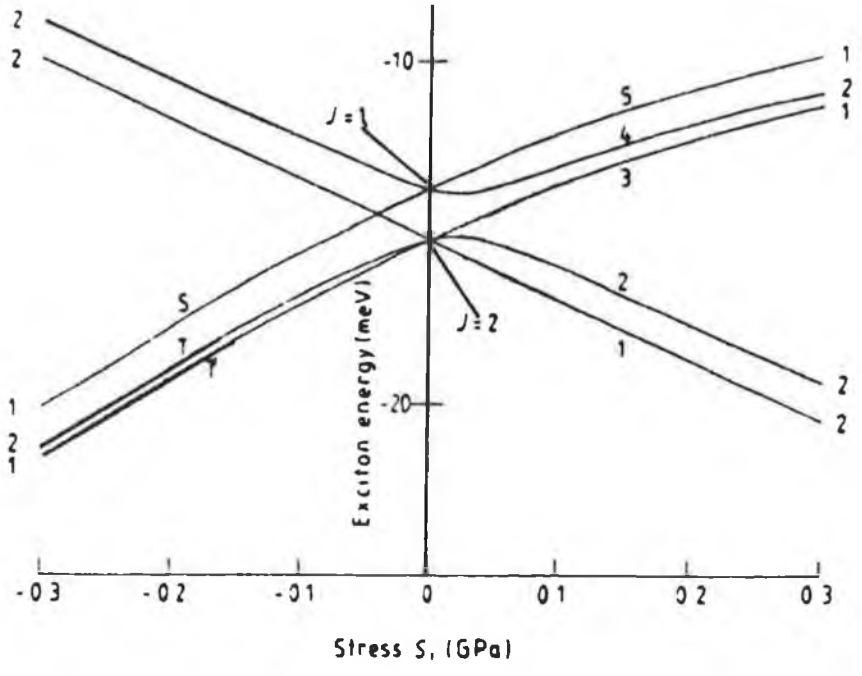

Figure 4.23, The lower energy bound exciton states as a function as stress S_t.

Considering figure 4.23, the degeneracy of each exciton state is shown in the margins. For $S_t > 0$ the energy levels are arbitarily labelled 1 to 5, and for $S_t < 0$ the states which form the triplet - singlet pair as $|S_t| \rightarrow \infty$ are labelled T & S. In fitting the ABC band and Be related band to this model it was found that the best fit was obtained with $S_t > 0$. Previous work has established that both the ABC [45] and the Be [46] related centres occur at defects with a <111> axis.

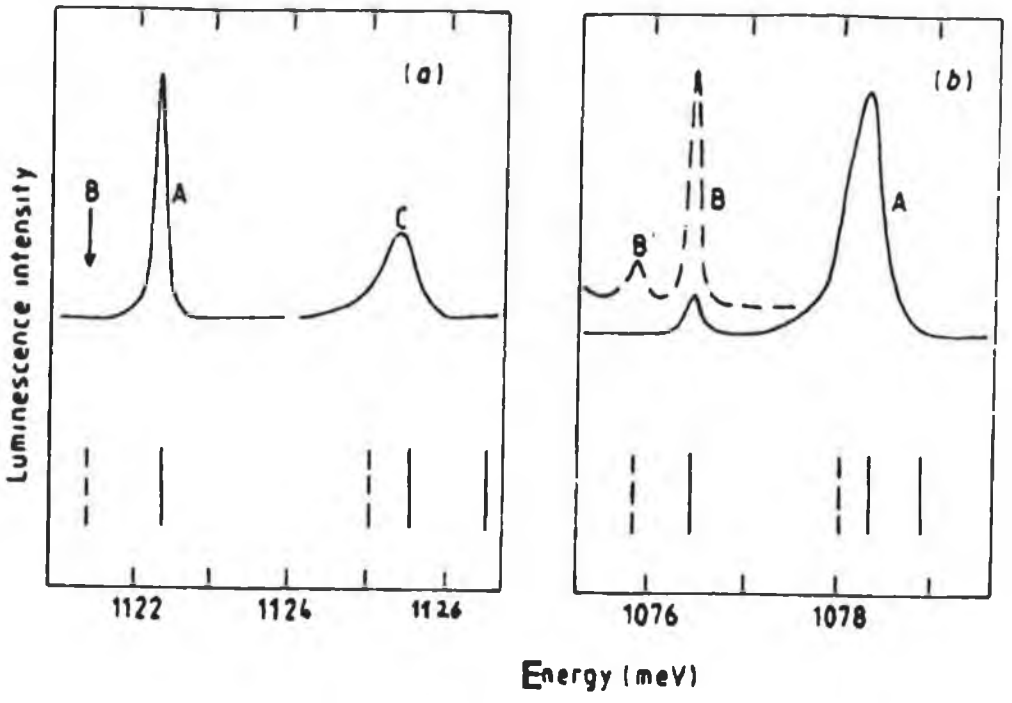

Figure 4.24, (a) The ABC no-phonon region at 30K and (b) the Be related no-phonon region at 13K and broken curve at 2K measured in luminescence. Energy spacings from the calculations are shown by the verticle lines. The forbidden transitions are shown by broken lines (43).

The model works particularly well and predicts the position of the luminescence lines. A best fit procedure can be undertaken to obtain the best fit parameters for the stress 'S_t' and the electron-hole exchange energy 'Δ'. The following table gives the results obtained from this procedure.

Table 4.7, Best fit parameters for Stress and Electron - Hole Energy [43].

Model:	Stress St (Gpa)	Electron - Hole Energy Δ (mev)
ABC	0.108 + 0.006	1.4 + 0.3
Be	0.025 + 0.002	2.18 + 0.04

Having succeeded in modelling both the ABC defect and the Be related defect, it was then attempted to fit the defect which has been stated in this thesis to be associated to both copper and zinc.

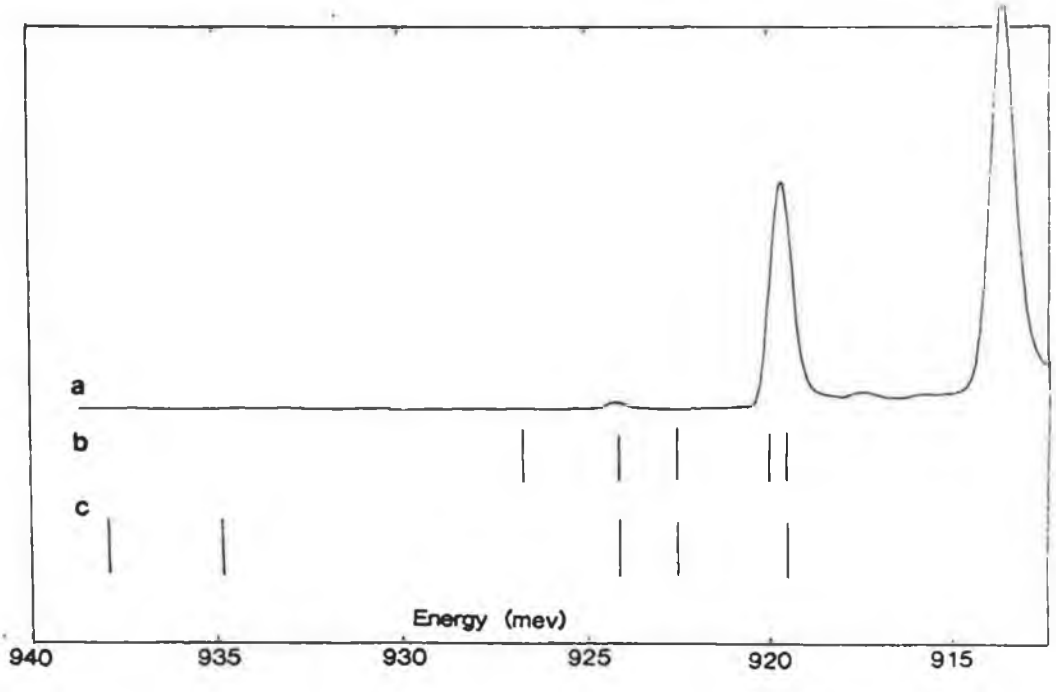

Figure 4.25, (a), The luminescence structure around the no-phonon line (919.56 mev), (b), Model prediction with Stress S_t =-0.0875 GPa and Exchange Energy Δ =4.66 mev

(c), Model prediction with Stress St = 0.140 GPa and Exchange Energy = 14.3 mev.

Figure 4.25 (a) shows the no-phonon region at 14K whereas (b)

shows the levels produced when the stress is negative. It can be seen that levels are produced 3.15 mev and 4.64 mev above the no-phonon line. These lines correspond to the lines obtained in luminescence. There is however another level produced 0.49 mev above the no-phonon line but there is no evidence of this line or it's phonon replicas in luminescence studies. According to Davies [43] this level is equally allowed as the no-phonon line and so should be seen. This would therefore seem to suggest that modelling the system with negative stress is incorrect. Figure 4.25 (c) shows another fit for which the levels produced from the model are in similar positions as those produced in luminescence. In this case there are two other levels produced 15.7 mev and 18.7 mev above the no-phonon line. These would not be expected to appear in luminescence because of their energy separation. From calculations the intensity of these lines is is predicted to be approximately 1% of the no-phonon line at 40K. It is therefore reasonable not to expect to see these lines in luminescence. This would suggest that with a positive stress and a large exchange energy the best results are obtained. Table 4.8 shows the experimentally and theoretically obtained values

Table 4.8, Theoretical values (with S_t=0.140 and Δ=14.3). Energies are normalized with respect to the no-phonon line.

LINE	ENERGY (mev)	
	Experimental :	Theoretical
excited state	3.2	3.14
excited state	4.66	4.68
	-	15.69
	-	18.74

This model very simply predicts the positions of lines found in luminescence studies, and gives a parameterisation of the properties of the lowest engery levels of excitons bound to axial isoelectronic defects in silicon. Because of its over simplification the model is expected to fit the lowest energy states best and to give an increasingly bad description to the higher energy states. Although the exciton binding energy can be related to the stress, this is by no means the only process operating to bind the exciton and so these other means should be taken into account in such a model.

This model predicts a axial defect for the copper & zinc related defect in silicon. It should be noted at this point that copper is one of the best known activators of efficient luminescence in semiconductors.The presence of both copper and zinc in a host material material has major consequences for semiconductors since the defect forms a deep lying trap in the band gap of silicon. Zinc has the configuration [Ar] $3d^{10}$ $4s^2$ while copper has [Ar] $3d^{10}$ $4s^1$,

where [Ar] represents the core electrons with the configuration of argon.

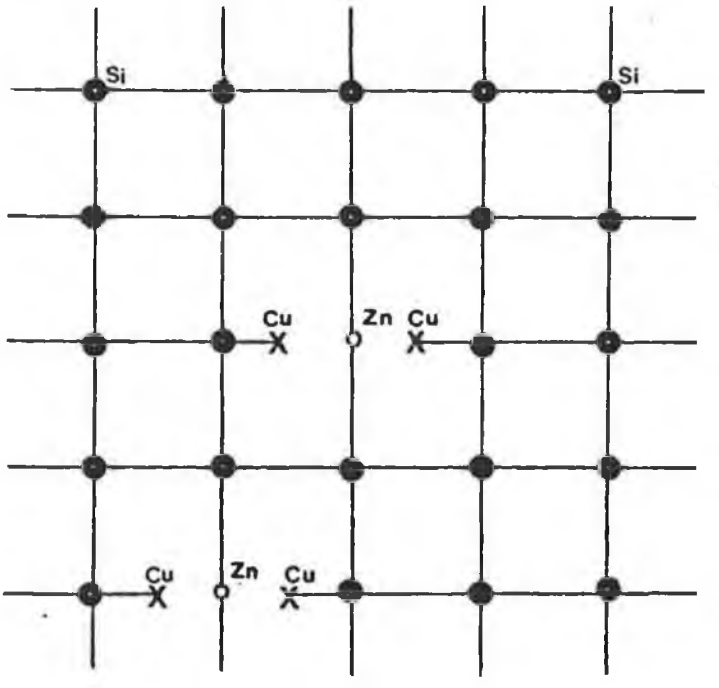

Figure 4.26, Schematic representation of the defect.

We tentatively propose that the luminescence centre is a defect with a substitutional zinc atom and two copper atoms located at interstitial sites, figure 4.26. Each copper atom provides a single electron to make up for the shortage in zinc. In this way the copper ions become Cu^{1+} $[Ar]3d^{10}$ $4s^{0}$ and the overall defect takes the form $[Cu^{1+}\ Zn^{2-}\ Cu^{1+}]^{0}$. This particular configuration is overall neutral consistent with the isoelectronic nature of the defect.

4.5 Conclusion.

In this chapter results of luminescence studies of copper-zinc doped silicon are given, revealing a no-phonon line at 919.5 mev with phonon replicas separated by 6.3 mev. Also discussed were the techniques used in obtaining lifetime measurements. These included Lock-in techniques as well as computer sampling of the signal. It is stated that in obtaining such measurements the contribution from the detector system was large and as such needed to be 'subtracted' from the data. A deconvolution technique is described and is shown to give a extremely good fit to the experimental data. The particular lifetimes obtained (Table 4.5) show that the defect is very long lived (9 msec) up to T= 45K. At higher temperatures the lifetime decreases to the response of the detector. From the graph of lifetime versus temperature the binding energy of the loosely bound particle is found to be 65mev.

The assignment of the majority of strong zero phonon line luminescence systems in silicon to exciton recombination at isoelectronic traps has relied heavily on transient luminescence decay time data, since the chemical identities of the associated defects are not yet established. It would seem from the lifetime data in figure 4.20 that suggestions to the isoelectronic nature of the defect are justified.

The modelling of the system to an uniaxial stress acting on the crystal's valence band and conduction band

extrema was achieved in section 4.4. This modelling provides an approximation to the energy spacings, and although the lowest-energy exciton states are in agreement with experimental data, the model gives a bad description to the higher energy states. It is suggested that the configuration taken up by the impurities is as follows, zinc occupys a substitutional site while two copper atoms occupy an interstitial site each, so maintaining a neutral defect and giving the defect it's isoelectronic properties.

Chapter 5.

Conclusions.

5.1 Conclusion.

The luminescence associated with exciton decay in copper-zinc doped silicon has been studied by the photoluminescence technique. The experimental findings have established that the dominant luminescence system with a no-phonon line located at 919.5 mev, is indeed due to exciton recombination at an isoelectronic centre. We tentatively suggest that a zinc atom along with two copper atoms interact to form the isoelectronic trap in silicon. We suggest that copper oxidizes into the state Cu^{1+} and that zinc forms its normal configuration in silicon i.e. Zn^{2-}. The zinc atoms reside on a substitutional site while the copper atoms reside on interstitial sites as shown in chapter 4. This particular situation gives an overall configuration of $[Cu^{+}\ Zn^{2-}\ Cu^{+}]^{0}$, which is a neutral defect. As stated earlier the chemical identity of the associated defect has not yet been conclusively established but its very long transient luminescence decay time,(9 msec up to 45K), seems to suggest recomination at a isoelectronic trap.

As reported by various authors [39], copper alone forms an isoelectronic defect in silicon and the luminescence associated with this defect is found to have a lifetime 460 usec and 670 usec in the temperature range T=1.3K to T=13K. With the introduction of an additional transition metal impurity such as zinc, the formation of a second luminescent defect occurs at lower energy. However the lifetime associated with this new defect is much longer, of the order

of 9 msec up to T=45K. A careful study of the lifetime versus temperature reveales how strongly or weakly the binding energy of the secondary particle is. Section 4.4 gives the results obtained after 'deconvoluting' the system response out of the various spectra. As was stated, this needed to be done because of the large contribution associated with the detector being present in the sample decay. An algorithm was developed and was found to work very well.

An extension of the model developed by Davies [43] shows,within experimental error,the axial nature of the defect. This simple model provides a reasonable parameterisation of the properties of the lowest energy levels of excitons bound to axial isoelectronic defects in silicon. By using two variables, the stress (St) and the electron - hole exchage energy (Δ), the energy levels can be simulated. From the analysis of the previous sections this model is sufficient at explaining the energy levels of the copper zinc related defect in silicon.

In chapter 2 it was stated that most of the transition metal impurities are known to be fast diffusing elements in silicon at elevated temperatures. Because of this fact trace contamination during processing of silicon wafers for device production is frequently observed. It is not uncommon to find associated with these impurities precipitates in the volume and on the surface of the wafer. These in turn may drastically effect the performance of the device in a number of different ways. They may cause an increase in the recombination-generation current as well as an increase in

the leakage current of reverse biased junctions [25a].

Because of the ease with which transition metals are incorporated into silicon, it is very difficult to specify exactly the impurities involved. This, however can be solved by using a technique known as isotope shift analysis. As stated in chapter 2, transition metals can have many charge states in silicon. In order to identify these charge states Zeeman analysis can be preformed.

The review material given in chapters 1 & 2 of this thesis shows that although isoelectronic traps have been studied in semiconductors, there are still some potentially rewarding areas of study, particularly in connection with transition metal impurities in silicon.

References.

(1) C. Kittel - Introduction to Solid State Physics. Published by Addison-Wesley 1985.

(2) M.A. Omar - Elementary Solid State Physics. Published by Wiley & Sons 1986.

(3) J.J. Hopfield, D.G. Thomas, R.T. Lynch, Phys. Rev. Letters 17, 312, 1966.

(4) A. Baldereschi, J.J. Hopfield, Phys. Rev. Letter 28, 171, 1972.

(5) R.A. Faulkner, Physics Rev. 175, 441, 1968.

(6) D.G. Thomas, M Gershenzen, J.J. Hopfield, Physics Rev. 131, 2397, 1963.

(7) P.J. Dean, Physics Rev. B4, 2596, 1971.

(8) M.O. Henry, E.C. Lightowlers, N. Killoran, D.J. Dunstan, B.C. Cavenett, J. Physics C14, L255, 1981.

(9) J.R. Haynes, Physics Rev Lett. 4, 361, 1960.

(10) M.A. Vouk, E.C. Lightowlers, J. Luminescence 21,329,1977

(11) G.S. Mithard, S.A. Lyon, K.R. Elliott, T.C. Gill, Solid State Commun. 29,425, 1979.

(12) D.H. Brown, S.R. Smith, J. Luminescence 21, 329, 1980.

(13) M.L.W. Twewalt, U.O. Ziemelis, R.R. Parsons, Solid State Commun. 39, 27, 1981.

(14) J. Weber, R. Sauer, P. Wagner, Proc. Int. Conf. Luminescence Berlin, 1981, ed. I. Brosser.

(15) J. Wagner, J.Weber, R. Sauer, Solid State Commun. 39, 1273, 1981.

(16) J. Weber, H. Schmidt, R.Sauer, Physics Rev. B21, 2401, 1980.

(17) J.A. Rostworowski, R.R. Parsons, Can. J. Physics, 59, 496, 1980.

(18) L. Canham, G. Davis, and E.C. Lightowlers, J. Physics C, Solid State Physics 13, L757, 1980.

(19) H.H. Woodbury, G.W. Ludwig, Phys. Rev. 117, 102, 1960.

(20) L.C. Kimerling, J.L. Benton, J.J. Rubin, Proceedings of the 11th conference on Defects & Radiation Effects in Semiconductors, edited by R.R. Hasiguti (IOP, London, 1981)

(21) J.W. Chen, A.G. Miles, Annu. Rev. Mater Sci. 10, 157 1980.

(22) F.D.M. Haldane, P.W. Anderson, Phys. Rev. B13, 255, 1976.

(23) E.R. Weber, Appl. Phys. A30, 1, 1983.

(24) R. Sauer, J. Weber, Physica 116B, 195, 1983.

(25) G.W. Ludwig, H.H. Woodbury, Solid State Phys. 13, 223, 1962.

(25a)K. Graff, Transition Metal impurities in silicon and their impact on device performance, unpublished.

(26) S.D. Brotherton, P. Bradley, A. Gill, E.R. Weber, J. Appl. Phys. 55, 952, 1984.

(27) H. Conzelmann, K. Graff, E.R. Weber, Appl. Phys. A30, 169 1983.

(28) E.R. Weber, Impurity diffusion & gettering in silicon symposium, Boston MA USA, 27-30 Nov. 1984.

(29) S.H. Malter, G.M. Tuynman, E.G. Sieverts, C.A. Ammerdaan, Phys. Rev. B25, 25, 1982.

(30) J. Weber, P. Wagner, J. Phys. Soc. Japan 49, Suppl.A,263, 1980.

(31) J. Weber, H. Bauch, R. Sauer, Phys. Rev. B24, 7688, 1982.

(32) J.N. Demas, Excited State Lifetime Measurements, - New York : Academic Press, 1983.

(32) C.B. Collins, R.O. Carlson, Phys. Rev. 108, 1409, 1957.

(33) M.K. Bakhadyikhanov, B.I. Boltaks, G.S. Kulikov, E.M. Pedyash, Fiz, Tekh. Poluprov. 4, 873, 1970.

(34) R.Sh. Malkovich, N.A. Alimbarushvili, Fiz, Tverd. Tela, 4, 2355, 1962. [Sov. Phys. Solid State 4, 1725, 1963.]

(35) K.D. Glinchuk, N.M. litovchenko, Fiz, Tverd. Tela, 5, 3003, 1963. [Sov. Phys. Solid State 5, 2197, 1964.]

(36) B.V. Kurnilov, Fiz, Teverd. Tela, 8, 201, 1966. [Sov. phys. Solid State 8, 157, 1966.]

(37) N. Sclar, Infrared Physics 17,71,1977, Pergamon Press.

(38) R. Sauer, J. Weber, Solod State Communications 49, 833, 1984.

(39) S.P. Watkins, H.O. Ziemelis, M.L.W. Thewalt, R.H. Parsons Solid State Communications 43, 687, 1982.

(40) N.S. Minaev, A.V. Mudryi, V.D. Tkachev, Sov. Physics, Semi. Cond. 13, 233,1977.

(41) S.P. Depinna, D.J. Dunstan, Philosophical Mag. B50, 579,1984.

(42) M.L.W. Thewalt, S.P. Watkins, U.O. Ziemeils, E.C. Lightowlers, M.O.Henry, Solid State Commun. 44, 573, 1982.

(43) G. Davies, J Phys. C, Solid State Phys., 17, 6331, 1984.

(44) J van W Morgan, T.N. Morgan, Phys. Rev., B1, 739, 1970.

(45) J Weber, W. Schmid, R. Sauer, Phys. Rev., B21, 2401, 1982.

(46) M.O. Henry, K.A. Moloney, J. Treacy, F.J. Mulligan, E.C. Lightowlers, J. Phys. C, Solid State Phys., 17, 1984.

APPENDIX 1 SOFTWARE. PAGE.

```
 10 REM ************************************
 20 REM *****                          *****
 30 REM *****       LINK PROGRAM       *****
 40 REM *****                          *****
 50 REM ************************************
 60 REM
 70 REM
 80 REM
 90 MODE0
100 PRINTTAB(20)"Linking program "
110 PRINTTAB(20)"_______________ "
120 PRINT:PRINT
130 PRINTTAB(20,5) "1.    Data Acquisition "
140 PRINTTAB(20,7) "2.    Data Processing  "
150 PRINTTAB(20,9) "3.    Data Analysis    "
160 PRINTTAB(20,11)"4.    Data display    "
170 PRINT:PRINT:PRINT
180 INPUT "Choice ",C$
190 IF C$="1" THEN PROCAcquisation
200 IF C$="2" THEN CHAIN "CORRECT"
210 IF C$="3" THEN CHAIN "ANALY"
220 IF C$="4" THEN CHAIN "PLOT"
230 GOTO180
240 DEF PROCAcquisition
250 CLS
260 PRINTTAB(20)  " Data   Acquisition  "
270 PRINTTAB(20)  " ___________________ "
280 PRINT:PRINT
290 PRINTTAB(20,7)  "a.  Lifetime  measurements "
300 PRINTTAB(20,9)  "b.  Intensity scan          "
310 PRINTTAB(20,11) "c.  Water vapour scan       "
320 PRINT:PRINT:PRINT
330 INPUT "Choice ",C$
340 IF C$="A" THEN CHAIN "DECAY"
350 IF C$="B" THEN CHAIN "SAMPLE"
360 IF C$="C" THEN CHAIN "VAPOUR"
370 GOTO 330
380 ENDPROC
```

```
 10 REM ********************************************************
 20 REM ****** Program to sample analogue to digital   ******
 30 REM ******  converter over a specific wavelength   ******
 40 REM ******              range.                     ******
 50 REM ********************************************************
 60 REM
 70 REM
 80 REM
 90 REM
100 REM *********************************
110 REM ***  Check for background   ***
120 REM ***          signal.        ***
130 REM *********************************
140 CLOSE$0:MODE3:A=&FCF0
150 ?(A+11)=&C0:?(A+2)=&70:?(A+4)=6:?(A+5)=0
160 C=0:PRINTTAB(5,5)" CHECK TO SEE IF SLIT IS CLOSED":K=GET
170 FOR T=1 TO 10:?A=0:?(A+12)=&0C:?(A+12)=&0E
180 a=(?(A+1))*16+(?(A))MOD16
190 C=C+a:PRINTa:NEXT :B=C DIV 10
200 PRINTTAB(5,15)"BACKGROUND D.C. SIGNAL ="B:K=GET:CLS
210 PRINTTAB(5,5) "ADJUST FOR MAX SIGNAL"
220 PRINTTAB(5,10)"TYPE R TO CONTINUE"
230 K=GET:?(A+12)=&0C:?(A+12)=&0E
240 IN=?(A+1)*16+?(A)MOD16
250 PRINTTAB(5,15)"MAX SIGNAL ="B-IN
260 IF K<>69 AND K<>82 THEN 230
270 IF K=69 THEN 230
280 REM ********************************************************
290 PRINT:PRINT:PRINT:CLS:*DRIVE0
300 PRINT:PRINT"Sample spectrum"
310 a=OPENIN"START":INPUT$a,Start
320 b=OPENIN"END":INPUT$b,End
330 c=OPENIN"Inc":INPUT$c,Inc
340 CLOSE$0
350 CLS
360 PRINT:PRINT:PRINT"Starting  wavelength "Start
370 PRINT:PRINT"Finishing wavelength "End
380 PRINT:PRINT"Incremental rate     "Inc
390 P=(End-Start)/Inc+1
400 INPUT"Do you want to change wavelength range      y/n"
410 IF GET$="Y" THEN PROCINITIAL
420 PRINT:PRINT:INPUT"Temperature of sample ",Temp
430 MODE4:DIM Y(P)
440 PROCADC:PROCDATA:PROCSAVE:PROCREPEAT:CHAIN"LINK"
450 END
460 DEF PROCINITIAL
470 CLS
480 PRINT:INPUT"Starting wavelength ",Start
490 PRINT:INPUT"Finish wavelength   ",End
500 PRINT:INPUT"Incremental rate / sec ",Inc
510 P=(End-Start)/Inc+1
520 PROCwave:ENDPROC
530 REM ********************************************************
535 REM
536 REM
```

```
540 REM ********************************
550 REM ***   Data points stored    ***
560 REM ***      in array Y(D).     ***
570 REM ********************************
580 DEF PROCDATA
590 X=0:Al=Start:CLS:M=1
600 FOR D=1 TO P
610 ?A=0:?(A+12)=&EC:FOR I=1 TO 200 :NEXT
620 ?(A+12)=&CE:Y(D)=B-(?(A+1)*16+?(A)MOD16):PRINTTAB(5,5)Al
630 MOVE X,Y(D)/2:DRAW X,Y(D)/2:X=X+1200/P:Al=Al+Inc
                              NEXT:ENDPROC
640 DEF PROCADC
650 A=&FCF0:?(A+11)=&C0:?(A+2)=&70:?(A+4)=6:?(A+5)=0:ENDPROC
660 REM ********************************************************
670 DEF PROCSAVE
680 INPUT"Do you want to save y/n"
690 IF GET$="N"  THEN ENDPROC
695 PRINT:PRINT
700 INPUT "Name of file  " B$:Y=OPENOUT(B$)
710 PRINT$Y,Start:PRINT$Y,End:PRINT$Y,Inc:PRINT$Y,Temp
720 FOR D=1 TO P
730 PRINT$Y,Y(D) :NEXT:CLOSE$0:ENDPROC
740 DEF PROCwave
750 a=OPENOUT"START":PRINT$a,Start
760 b=OPENOUT"END":PRINT$b,End
770 c=OPENOUT"INC":PRINT$c,Inc
780 CLOSE$0:ENDPROC
790 DEF PROCREPEAT
800 PRINT"Do you want to repeat the experiment y/n "
810 IF GET$="Y" THEN 350 ELSE ENDPROC
820 ENDPROC
```

```
 10 REM ******************************
 20 REM **                            **
 30 REM **   DECAY LUMINESCENCE       **
 40 REM **                            **
 50 REM ******************************
 60 MODE0
 70 INPUT "Number of data points to be stored , ",N
 80 PRINT:PRINT:PRINT"Time delay per point = 1,2,3 ..... msec."
 90 PRINT:PRINT:INPUT t
100 PRINT:PRINT:INPUT"Temperature of sample ",Temp
110 PRINT:PRINT:INPUT"Wavelength reading ",Wave
120 DIM MC1% 450,Y(N),TALLY%10
130 STORE%=HIMEM-10000
140 PROCMEM :PROCINITIAL :PROCDATA :PROCDRAW
    PROCSAVE :PROCREPEAT
150 CHAIN"LINK":END
160 REM ************************************************
170 REM ******************************
180 REM ****  Initialize memory  ****
190 REM ****      locations.     ****
200 REM ******************************
210 DEF PROCMEM
220 T14=0:XX%=N
230 TALLYLO%=&80:TALLYHI%=&81:TALLYCL%=&82
      TALLYCH%=&83:TALLY%=&84:DELAY =&85
240 ?(TALLYLO%)=STORE%MOD256:?(TALLYHI%)=STORE%DIV256
250 TALLYCL%=((STORE%+XX%+1)MOD256)
    TALLYCH%=((STORE%+XX%+1)DIV256)
260 ENDPROC
270 REM ************************************************
280 REM ******************************
290 REM ****  Assembly language  ****
300 REM ****    for intake of    ****
310 REM ****        points.      ****
320 REM ******************************
330 DEF PROCINITIAL
340 CH=16
350 FOR S=0 TO 2 STEP 2
360 P%=MC1%
370 [ OPT S
380 .GALV  JSR CON
390
400 .ST1   LDA $&00
410        STA &FE6C
420        LDA $&FF
430        STA &FE6D
440        LDA &FE6D
450        AND $&10
460        BEQ ST1
470 .START LDA $0
480        STA TALLY%
490        STA TALLY%+1
500 .TE    LDX $0
510 .LP1   LDA TALLYHI%
520        CLC
```

```
 530         CMP $TALLYCH%
 540         BCS MNO
 550         JMP ET
 560 .MNO    LDA TALLYLO%
 570         CLC
 580         CMP $TALLYCL%
 590         BCS RESET
 600 .ET     CLC
 610         LDA $1
 620         ADC TALLYLO%
 630         STA TALLYLO%
 640         LDA $0
 650         ADC TALLYHI%
 660         STA TALLYHI%
 670 .ST     PHP
 680         PHA
 690         TXA
 700         PHA
 710         LDX $t
 720 .LO     LDA $248
 730         STA DELAY
 740 .LO1    DEC DELAY
 750         BNE LO1
 760         NOP
 770         DEX
 780         BNE LO
 790         NOP
 800         PLA
 810         TAX
 820         PLA
 830         PLP
 840 .TE1    LDA &FCF0
 850         LDA &FCF1
 860         LDX $&00
 870         STA (TALLYLO%,X)
 880         LDA $&CC
 890         STA &FCFC
 900         JMP TE
 910         CLI
 920 .GHI    RTS
 930 .RESET  LDA &FCF0
 940         LDA $&0F
 950         STA TALLY%+1
 960         JMP GHI
 970 .CON    LDA $&C0
 980         STA &FCFB
 990         LDA $T14
1000         STA &FCF4
1010         LDA $0
1020         STA &FCF5
1030         STA &FCF3
1040         LDA $&70
1050         STA &FCF2
1060         LDA $CH
1070         STA &FCF0
1080         LDA &FCF0
```

```
1090         LDA $&EC
1100         STA &FCFC
1110         RTS
1120]
1130 NEXT S
1140 ENDPROC
1150 REM ***********************************************************
1160 DEF PROCDATA
1170 FOR D=1 TO 10
1180 PROCMEM:CALL GALV
1190 FOR I=1 TO N :Y(I)=?(STORE%+I)*16
1200 NEXT:PROCDRAW
1210 NEXTD:ENDPROC
1220 DEF PROCSAVE
1230 MOVE0,30:INPUT" Do you want to save y/n"
1240 IF GET$="Y" THEN 1260 ELSE ENDPROC
1250 PRINT
1260 INPUT" Name of file "B$
1270 X=OPENOUT(B$)
1280 PRINT$X,N:PRINT$X,t:PRINT$X,Temp:PRINT$X,Wave
1290 FOR I=1 TO N :A%=Y(I)
1300 PRINT $X,A%
1310 NEXT:CLOSE$0:ENDPROC
1320 DEF PROCDRAW
1330 CLS:X=0:YMAX=0:PROCCALCULATE
1340 FOR q=1 TO N
1350 Y=((Y(q))*850/YMAX)
1360 MOVE X,Y:DRAW X,Y
1370 X=X+1200/N:NEXT q :ENDPROC
1380 NEXT q
1390 DEF PROCCALCULATE
1400 FOR i%= 1TO N
1410 IF Y(i%)>=YMAX THEN YMAX = Y(i%)
1420 NEXT
1430 ENDPROC
1440 DEF PROCREPEAT
1450 PRINT"Do you want to repeat the experiment y/n "
1460 IF GET$="Y" THEN 60 ELSE ENDPROC
1470 ENDPROC
```

```
 10 REM ************************************************************
 20 REM ****                                                    ****
 30 REM ****    Water vapour absorption spectrum                ****
 40 REM ****                                                    ****
 50 REM ************************************************************
 60 MODE0
 65 CLEAR
 70 PRINT:PRINT:PRINT
 80 PRINT" Water vapour spectrum "
 90 PROCINITIAL:PROCADC:PROCBACKGROUND
100 MODE4
110 DIM Y(P):DIM Y1(P)
120 PROCDATA
130 INPUT "Do you want a copy on chart y/n"
140 IF GET$="Y" THEN PROCDAC
145 PRINT
150 PROCWATERVAP
160 INPUT "Do you want a copy on chart y/n"
170 IF GET$="Y" THEN PROCDAC
175 PRINT
180 PROCDRAW
181 PRINT"Do you want to repeat the experiment y/n"
182 IF GET$="Y" THEN 10 ELSE CHAIN "LINK"
183 END
190 DEF PROCINITIAL
200 PRINT
210 a=OPENIN "START":INPUT$a,Start
220 b=OPENIN "END":INPUT$b,End
230 c=OPENIN "Inc":INPUT$c,Inc
240 CLOSE$0
250 PRINT"Wavelength range ",Start " to  "End
260 PRINT:PRINT"Incremental rate ",Inc
270 INPUT"Do you want to change y/n"
280 IF GET$="Y" THEN PROCNEW
290 P=(End-Start)/Inc+1
300 CLOSE$0:ENDPROC
310 DEF PROCDATA
320 X=0:A1=Start:b=1:d=&FCC0:?(d+3)=128:CLS
330 FOR D=1 TO P
340 ?A=16:?(A+12)=&EC
350 FOR I=1 TO 200:NEXT
360 ?(A+12)=&CE
370 Y(D)=B-(?(A+1)*16+?(A)MOD16)
380 PRINTTAB(5,5)A1
390 MOVE X,Y(D)/2:DRAW X,Y(D)/2
400 X=X+1200/P:A1=A1+Inc:NEXT:ENDPROC
410 DEF PROCDRAW
420 MOVE  0,0:DRAW 0,900
430 DRAW 1200,900:DRAW 1200,0:DRAW 0,0:VDU5
440  MOVE 250,1000:PRINT"Intensity vs Wavelength  "
450  MOVE -10,910:PRINT"|":MOVE 590,910:PRINT"|"
     MOVE 1190,910:PRINT"|"
460  ENDPROC
470 DEF PROCLABLE
480 MOVE -150,950:PRINTStart
```

```
 490 MOVE 900,950:PRINTEnd
 500 VDU4:ENDPROC
 510 ENDPROC
 520 DEF PROCWATERVAP
 530 VDU4
 540 PRINT"correction for absorption"
 550 K=GET
 560 X=0:A1=13401
 570 Slope=(Y(P)-Y(1))/(End-Start)
 580 Intercept=Y(1)-Slope*Start
 590 FOR D=1 TO P
 600 y=Slope*Start+Intercept
 610 Y1(D)=y/Y(D)
 620 Y(D)=Y1(D)*Y(D)
 630 MOVEX,Y(D)/2:DRAW X,Y(D)/2
 640 PRINTTAB(5,5)A1:A1=A1+Inc
 650 X=X+1200/P:Start=Start+Inc:NEXT:*DRIVE2
 660 x=OPENOUT"VAP"
 670 PRINT$x,Start:PRINT$x,End:PRINT$x,Inc
 680 FOR I=1 TO P
 690 PRINT$x,Y1(I):NEXT:CLOSE$0:ENDPROC
 700 DEF PROCDAC
 710 A1=Start
 720 FOR D=1 TO P
 730 V=2048-(Y(D))*1.5
 740 d?b=(V)DIV16
 750 d?2=((V)MOD16)*(1+16*b)
 760 PRINTTAB(5,5)A1:A1=A1+Inc
 770 FOR I=1 TO 200:NEXT
 780 NEXTD:ENDPROC
 790 DEF PROCADC
 800 A=&FCF0:?(A+11)=&C0:?(A+2)=&70
 810 ?(A+4)=6:?(A+5)=0:ENDPROC
 820 ENDPROC
 830 DEF PROCNEW
 840 CLS
 850 INPUT"Wavelength range ",Start,End
 860 INPUT"Incremental rate ",Inc
 870 a=OPENOUT"START":PRINT$a,Start
 880 b=OPENOUT"END":PRINT$b,End
 890 c=OPENOUT"INC":PRINT$c,Inc
 900 ENDPROC
 905
 910 DEF PROCBACKGROUND
 915 CLS
 920 A=&FCF0:?(A+11)=&C0:?(A+2)=&70:?(A+4)=6:?(A+5)=0
 930 C=0:PRINTTAB(5,5) "Check to see if slit is closed ":K=GET
 940 FOR T=1 TO 10:?A=16:?(A+12)=12:?(A+12)=14
 950 a=(?(A+1))*16+(?(A))MOD16
 960 C=C+a:PRINTa:NEXT:B=C DIV10
 970 PRINTTAB(5,15) "Background d.c. voltage = "B:K=GET:CLS
 980 PRINTTAB(5,5) "Adjust for max  signal "
 990 PRINTTAB(5,10) "Type R to continue "
1000 K=GET:?(A+12)=12:?(A+12)=14
1010 IN=?(A+1)*16+?(A)MOD16
1020 PRINTTAB(5,15) "Max  signal  = "B-IN
```

```
1030 IF K<>69 AND K<>82 THEN 1000
1040 IF K=69 THEN 1000
1050 ENDPROC
```

```
 10 REM ***********************************
 20 REM ****                           ****
 30 REM ****    DATA PROCESSING        ****
 40 REM ****                           ****
 50 REM ***********************************
 60 REM
 70 REM
 80 REM
 90 REM
100 MODE3
110 *.
120 INPUT"NAME OF  FILE" ,B$:x=OPENIN(B$)
130 CLS
140 INPUT$x,S:INPUT$x,E:INPUT$x,Inc:INPUT$x,Temp
150 PRINT:PRINT:PRINT"Starting wavelength " ,S
160 PRINT:PRINT:PRINT"Finishing wavelength ",E
170 PRINT:PRINT:PRINT"Incremental rate     ",Inc
180 P=(E-S)/Inc+1
185 FOR I=1 TO 10000:NEXT
190 MODE4:DIM Y(P)
200 FOR I=1 TO P
210 INPUT$x,A%:Y(I)=A%:NEXT:CLOSE$0
220 PROCDRAW :PROCSPIKE:PROCVAP:PROCInten:PROCDRAW :PROCSMOOTH
230 PROCDRAW:PROCSAVE:CHAIN"LINK":END
240 REM ************************************************************
250 REM *********************************
260 REM ***   Spike removal           ***
270 REM *********************************
280 DEF PROCSPIKE
290 X=0:FOR I=1 TO 200:Y(0)=Y(1)
300 IF Y(I)>=Y(I-1)*1.1 THEN Y(I)=(Y(I-1))
310 IF Y(I)<=Y(I-1)/1.1 THEN Y(I)=(Y(I-1)+Y(I-2)+Y(I-3))/3
320 NEXT
330 FOR I=450 TO 2000
340 IF Y(I)>=Y(I-1)*1.1 THEN Y(I)=(Y(I-1)+Y(I-2)+Y(I-3)+Y(I-4))/4
350 IF Y(I)<=Y(I-1)/1.1 THEN Y(I)=(Y(I-1)+Y(I-2)+Y(I-3))/3
360 NEXT:ENDPROC
370 REM ************************************************************
380 DEF PROCDRAW
390 X=0:CLS:FOR I=1 TO P
400 MOVE X,Y(I)/2:DRAW X,Y(I)/2:X=X+1200/P:NEXT:ENDPROC
410 X=X+1200/P:NEXT:ENDPROC
420 REM ************************************************************
430 REM ***********************************
440 REM ***     Smoothing                 ***
450 REM ***********************************
460 DEF PROCSMOOTH
470 FOR I=1 TO P
480 IF I<3 THEN GOTO 520
490 IF I>=1995 THEN 520
500 Y(I)=0.4*Y(I)+0.2*Y(I-1)+0.1*Y(I-2)+0.2*Y(I+1)+0.1*Y(I+2)
510 GOTO 530
520 Y(I)=Y(I)
530 NEXT:PROCDRAW:ENDPROC
540 REM ************************************************************
```

```
550 REM ***************************************
560 REM ***      Correcting    for          ***
570 REM ***   water vapour absorption       ***
580 REM ***************************************
590 DEF PROCVAP
600 y=OPENIN"VAP"
610 CLS:X=0:FOR I=1 TO P
620 INPUT$y,Y:Y(I)=Y(I)*Y
630 MOVE X,Y(I)/2:DRAW X,Y(I)/2:X=X+1200/P:NEXT I:ENDPROC
640 REM ********************************************************************
650 REM ***********************************
660 REM ***    Intensity correction     ***
670 REM ***********************************
680 DEF PROCInten
690 FOR I=1 TO 500:Y(I)=Y(I)*1.02:NEXT
700 FOR I=501 TO 750:Y(I)=Y(I)*1.04:NEXT
710 FOR I=751 TO 1000:Y(I)=Y(I)*1.07:NEXT
720 FOR I=1001 TO 1150:Y(I)=Y(I)*1.15:NEXT
730 FOR I=1151 TO 1250:Y(I)=Y(I)*1.22:NEXT
740 FOR I=1251 TO 1400:Y(I)=Y(I)*1.3:NEXT
750 FOR I=1401 TO 1550:Y(I)=Y(I)*1.45:NEXT
760 FOR I=1551 TO 1700:Y(I)=Y(I)*1.61:NEXT
770 FOR I=1701 TO 1800:Y(I)=Y(I)*2 :NEXT
780 FOR I=1801 TO 1900:Y(I)=Y(I)*2.38:NEXT
790 FOR I=1901 TO 2000:Y(I)=Y(I)*2.78:NEXT
800 PROCDRAW:ENDPROC
810 REM ********************************************************************
820 REM ***********************************
830 REM ***  Saving data files          ***
840 REM ***********************************
850 DEF PROCSAVE
860 PRINT"Do you want to save y/n"
870 IF GET$="Y" THEN 880 ELSE ENDPROC
880 PRINT:INPUT"Name of file "B$
890 Y=OPENOUT (B$)
900 PRINT$Y,S:PRINT$Y,E:PRINT$Y,Inc:PRINT$Y,Temp
910 FOR D=1 TO P
920 PRINT$Y,Y(D)
930 NEXT:CLOSE$Y:ENDPROC
940 REM ********************************************************************
```

```
 10  REM ******************************************
 20  REM *****                                *****
 30  REM *****  Program to analyse   spectra  *****
 40  REM *****                                *****
 50  REM ******************************************
 60 CLS
 70 PRINTTAB(20)    " Analysis  "
 80 PRINTTAB(20)    " ________  "
 90 PRINT:PRINT:PRINT
100 PRINTTAB(20)    " 1.   Semilog plot ln(I/Imax) vs time "
110 PRINT:PRINT:PRINT
120 PRINTTAB(20)    " 2.   Deconvolition { D(t) = E(t) ** i(t) } "
130 PRINT:PRINT:PRINT
140 PRINTTAB(20)    " 3.   Area under curve "
150 PRINT:PRINT:PRINT
160 INPUT "Choice  ",C$
170 IF C$= "1" THEN CHAIN "LIFE"
180 IF C$= "2" THEN CHAIN "DECONVO"
190 IF C$= "3" THEN CHAIN "AREA"
200 GOTO 170
```

```
 10 REM ************************************************************
 20 REM ****                                                    ****
 30 REM ****        Least   square   fit   of   decay          ****
 40 REM ****                          curves                    ****
 50 REM ****                                                    ****
 60 REM ************************************************************
 70 MODE0
 80 *.
 90 PRINT:PRINT:PRINT:
100 INPUT"Name of data file" ,B$
110 L=OPENIN(B$)
120 INPUT$L,N
130 INPUT$L,time
140 INPUT$L,Temp
150 INPUT$L,Wave
160 DIM Y(N),Y1(N),Y2(N)
170 FOR I=1 TO N:INPUT$L,A%:Y(I)=A%:NEXT :CLOSE$0
180 B=0
190 FOR P=1 TO 20 :B=B+Y(P+180):NEXT :B=B/20
200 MODE4
210 PROCCALCULATE:PROCDRAW:PROCINTENSITY
220 CHAIN "ANALY"
230 END
240 DEF PROCCALCULATE
250 YMAX=0:YMIN=100
260 FOR i%= 1TO N
270 IF Y(i%)>YMAX THEN YMAX=Y(i%)
280 IF Y(i%)<=YMIN THEN YMIN=Y(i%)
290 NEXT i%
300 ENDPROC
310 DEF PROCDRAW
320 X=0
330 FOR I=1 TO N
340 MOVE X,(Y(I)-B)/2+100:DRAW X,(Y(I)-B)/2+100
350 X=X+1000/N:NEXT :ENDPROC
360 DEF PROCINTENSITY
370 CLS:VDU4:VDU 29,0;1000;:X=0
380 FOR I=1 TO N
390 IF Y(I)-B<=0 THEN 440
400 Y1(I)=LN((Y(I)-B)/YMAX)
410 Y=Y1(I)*200
420 MOVE X+2,Y+2:DRAW X-2,Y-2
430 MOVE X-2,Y+2:DRAW X+2,Y-2
440 X=X+1000/N:NEXT I
450 INPUT"START POINT"STA:INPUT"FINISH POINT"FIN
460 T=STA*time:P=FIN -STA
470 a=0:b=0:c=0:d=0:e=0
480 REM SLOPE OF SLOW COMPONENT
490 FOR O=STA TO FIN
500 PROCSUM :T=T+time:NEXT O
510 PROCSLOPE:PROCEQ:PROCCALCULATE2
520 T=0 :X=0:FOR O=1 TO N
530 Y1(O)=LN(Y2(O)/Imax):Y=Y1(O)*200 :MOVE X,Y:DRAW X,Y
540 P=200:PROCSUM :T=T+time
550 X=X+1000/N:NEXT O:PROCSLOPE
560 a=0:b=0:c=0:d=0:e=0
```

```
570 INPUT"START POINT"STR:INPUT "FINISH POINT"FIN :T=(time)*STR
580 FOR O=STR TO FIN
590 Y1(O)=(Y(O)-Y2(O))
600 IF Y1(O)<=0THEN GOTO 630
610 Y1(O)=LN(Y1(O)/(YMAX-Imax))
620 PROCSUM
630 T=T+time :NEXT O
640 PROCSLOPE:PROCEQ :ENDPROC
650 DEF PROCSUM
660 a=a+T*Y1(O)       :REM  sum t*y
670 b=b+T             :REM  sum t
680 c=c+Y1(O)         :REM  sum y
690 d=d+Y1(O)*Y1(O)   :REM  sum sqr y
700 e=e+T*T           :REM  sum sqr t
710 ENDPROC
720 DEF PROCSLOPE
730 Slope=(P*a-c*b)/(P*e-b*b)
740 Intercept=(e*c-b*a)/(P*e-b*b)
750 PRINTTAB(0,20)Slope,Intercept
760 ENDPROC
770 DEF PROCEQ
780 T=0:X=0:FOR p=1 TO N
790 Y1(p)=T*Slope+Intercept:Y=Y1(p)*200
800 MOVE X,Y:DRAW X,Y :X=X+1000/N :Y2(p)=EXP(Y1(p))*YMAX
810 T=T+time:NEXT p :ENDPROC
820 DEF PROCCALCULATE2
830 Imax=0:Imin=100
840 FOR i=1 TO N
850 IF Y2(i) > Imax  THEN Imax=Y2(i)
860 IF Y2(i) <= Imin THEN Imin=Y2(i)
870 NEXT i:ENDPROC
```

```
 10 REM ************************************************************
 20 REM ****                                                    ****
 30 REM ****       Deconvolution  of  spectra                   ****
 40 REM ****          { D(t)= E(t)*i(t) }                       ****
 50 REM ****                                                    ****
 60 REM ************************************************************
 70 @%=&20303:CLOSE$0:MODE0
 80 PROCINITIAL:PROCBACKGROUND:PROCDRAW:O=0:PROCchoice:PROCleast
 90 PROCLifetime
100 END
110 DEF PROCINITIAL
120 *.
130 PRINT:PRINT:PRINT:PRINT
140 INPUT " File to be deconvoluated  ",Name$
150 z=OPENIN Name$:Z=OPENIN "DET400"
160 INPUT$Name$,N
170 INPUT$Name$,t
180 INPUT$Name$,Temp
190 INPUT$Name$,Wave
200 MODE4
210 DIM Z(N),X(N),Y1(N),Y(N),Area(N),U(N),D(N)
220 DIM R(N),Chi(100)
230 FOR I = 0 TO N-1
240 INPUT$Z,Z(I):INPUT$z,X(I)
250 NEXT I:CLOSE$Z:CLS
260 MOVE 0,0:DRAW 0,1000:DRAW 1200,1000:DRAW 1200,0:DRAW 0,0
270 ENDPROC
280 DEF PROCBACKGROUND
290 K=0:K1=0:B=0
300 FOR I=1 TO 20:K1=K1+Z(I+180):NEXT
310 K1=K1/20
320 FOR I=1 TO 20:B=B+X(I+180):NEXT
330 B=B/20:ENDPROC
340 DEF PROCDRAW
350 FOR I = 0 TO N-1
360 L=Z(I)/2:DRAW K,L-K1:K=K+1200/N
370 DRAW K,L-K1
380 K=K+1200/N
390 NEXTI:MOVE 0,0
400 MOVE 0,0
410 FOR I = 0 TO N-1
420 L=(X(I)-B)/2
430 MOVE K+2,L+2:DRAW K-2,L-2:MOVE K-2,L+2:DRAW K+2,L-2
440 K=K+1200/N:NEXT:ENDPROC
450 DEF PROCchoice
460 CLS:O=O+1
470 PRINT:PRINT
480 PRINT"Sample  response  given  by  single  (1) or double (2)
                                      exponential "
490 PRINT:PRINT
500 IF GET$="2" THEN PROCdouble
510 PROCsingle
520 ENDPROC
530 DEF PROCsingle
540 PRINT" Sample response is given by -- k1*exp(-t/t1)--  "
```

```
 550 PRINT:PRINT
 560 INPUT" Preexponential factor k1 = ", k1
 570 PRINT:PRINT
 580 INPUT" Lifetime component t1 = ",t1 "msec"
 590 PRINT:PRINT:t2=0:k2=0
 600 S=k1*1E-3:P=EXP(-2/t1)
 610 Y(0)=0:Z(0)=0
 620 X=0:L=0
 630 FOR I=1 TO N
 640 U(I)=(U(I-1)+S*(Z(I)-K1))*P+S*(Z(I-1)-K1)
 650
 660 MOVE X+2,Y(I)/3+2:DRAW X-2,Y(I)/3-2
     MOVE X-2,Y(I)/3+2:DRAW X+2,Y(I)/3-2
 670 MOVE L,(X(I)-B)/3:DRAW L,(X(I)-B)/3
 680 X=X+1200/N:L=L+1200/N
 690 NEXT:ENDPROC
 700 DEF PROCdouble
 710  PRINT"Sample  response  is  given  by  --   k1*exp(-t/t1)  +
                                  k2*exp(-t/t2)--  "
 720 PRINT:PRINT
 730 INPUT" Preexponential factors k1,k2 = ", k1,k2
 740 PRINT:PRINT
 750 INPUT" Short lifetime component t1 = ",t1
 760 PRINT:PRINT
 770 INPUT" Long  lifetime component t2 = ",t2
 780 PRINT:PRINT
 790 REM ************************************
 800 REM *****                          *****
 810 REM *****   Finding area under     *****
 820 REM *****    response  curve       *****
 830 REM *****                          *****
 840 REM ************************************
 850 i=N
 860 FOR I=1 TO i
 870 C=0:h=i*2E-3
 880 h=i*2E-3
 890 IF i<=7 GOTO 970
 900 A=Z(1)-K1+4*(Z(2)-K1)+2*(Z(3)-K1)
 910 B=Z(i)-K1+4*(Z(i-1)-K1)+2*(Z(i-2)-K1)
 920 FOR I1=4 TO i-3
 930 C=C+4*(Z(I1)-K1)
 940 NEXT I1
 950 Area(i)=(h/3)*(A+B+C)
 960 GOTO1030
 970 V=0
 980 FOR P=1 TO i
 990 V=V+Z(P)-K1
1000 NEXT P
1010 Area(i)=(h/i)*V
1020 REM P. Area(i)
1030 i=i-1
1040 NEXTI
1050 M=OPENOUT "AREA"
1060 FOR I=1 TO N
1070 PRINT$M,Area(I)
1080 NEXT:CLOSE$M
```

```
1090 t=0
1100 CLS:FOR I=1 TO N
1110 Y(I)=Area(I)*EXP(-t/t1)
1120 Y1(I)=Area(I)*EXP(-t/t2)
1130 t=t+2E-3:NEXT I
1140 P1=EXP((-2E-3)/t1)
1150 P2=EXP((-2E-3)/t2)
1160 X=0:L=0:t=0:CLS
1170 Z(0)=0:FOR I=1 TO N
1180 a=k1*Y(I)*P1:b=k2*Y1(I)*P2
1190 c=1E-3*(Z(I)-K1)*(k1+k2)+(Z(I-1)-K1)*(k1*P1+k2*P2))
1200 D(I)=a+b+c
1210 MOVE X,D/10:DRAW X,D/10
1220 MOVE L+2,(X(I)-B)/3+2:DRAW L-2,(X(I)-B)/3-2
1230 MOVE L-2,(X(I)-B)/3+2:DRAW L+2,(X(I)-B)/3-2
1240 X=X+1200/N:L=L+1200/N:t=t+2E-3
1250 NEXT:ENDPROC
1260 REM ***************************
1270 REM Statement of least squares
1280 REM ***************************
1290 DEF PROCleast
1300 PRINT"Single (1) or double (2) exponential "
1310 X=0
1320IF GET$="2" THEN GOTO 1410
1330
1340 FOR I=1 TO N
1350 R(I)=X(I)-U(I)
1360 X=X+R(I):NEXT
1370 Chi(O)=X^2
1380 PROCChoice
1390 IF Chi(O) <=Chi(O-1) THEN PROCChoice
1400 IF Chi(O) >Chi(O-1) THEN ENDPROC
1410 FOR I=1 TO N
1420 R(I)=X(I)-D(I)
1430 X=X+R(I):NEXT
1440 NEXT
1450 Chi(O)=X^2
1460 PROCChoice
1470 IF Chi(O) <=Chi(O-1) THEN PROCChoice
1480 IF Chi(O) >Chi(O-1) THEN ENDPROC
1490 DEF PROCLifetime
1500 PRINT "Sample response = "k1 "*exp (-t/" t1")"
                              +  k2"*exp (-t/"t2")"
1510 ENDPROC
```

```
 10 REM ************************************************************
 20 REM ****                                                    ****
 30 REM ****        Program to plot decay spectra on            ****
 40 REM ****                  rikad plotter                     ****
 50 REM ****                                                    ****
 60 REM ************************************************************
 70 MODE3
 80 *.
 90 PRINTCHR$(130)"NAME OF FILE":INPUTB$
100 L=OPENIN(B$)
110 INPUT$L,N:INPUT$L,time:
120 INPUT$L,Temp:INPUT$L,Wave
130 MODE0:X=100:t=N*2
140 DIM Y(N),Y1(N):@%=131850
150 FOR I=1 TO N
160 INPUT$L,A%:Y(I)=A%
170 MOVE X,Y(I)/2:DRAWX,Y(I)/2
180 X=X+1000/N:NEXT I :CLOSE$0 :PROCCAL
190 PRINT"Do you want an intensity or a log plot I/L"
200 IF GET$="L" THEN PROCLOG ELSE PROCPLOT
210 VDU3
220 PRINT"Do you want to plot another spectrum  y/n"
230 IF GET$="Y" THEN 10 ELSE CHAIN "LINK"
240 END
250 DEF PROCCAL
260 YMAX=0:YMIN=100
270 FOR i=1 TO N
280 IF Y(i)>YMAX THEN YMAX=Y(i)
290 IF Y(i)<=YMIN THEN YMIN=Y(i)
300 NEXT i :ENDPROC
310 DEF PROCXAXIS
320 PRINT"M100,100":PRINT"D2500,100,2500,1800,100,1800,100,100"
330 X1=X/3+100
340 FOR I=1TO 3
350 VDU21
360 PRINT"M"+STR$(X)+",80"
370 PRINT"P|"
380 PRINT"M"+STR$(X)+",70"
390 PRINT"S3,3P" STR$(I*t/4)
400 VDU6:X1=X1+X/3:NEXT:ENDPROC
410 DEF PROCYAXIS
420 Y=100:FOR O=0 TO 4:VDU21
430 PRINT"M100,"+STR$(Y)
440 PRINT"P_"
450 PRINT"P"STR$(O/4)
460 VDU6:Y=Y+400:NEXT :ENDPROC
470 DEF PROCPLOT
480 VDU2:X=100:FOR I=1 TO N:VDU21
490 Y=INT(Y(I)*1650/YMAX)+50
500 PRINT"M"+STR$(X)+","+STR$(Y)
510 PRINT"D"+STR$(X)+","+STR$(Y),"B20"
520 X=X+2400/N:X=INT(X):VDU6:NEXT
530 PROCXAXIS:PROCYAXIS:PROCWRITE
540 PROCWRITE1:ENDPROC
550 DEF PROCWRITE
560 PRINT"M1150,30S3,3PTime (msec)"
```

```
570 PRINT"M1700,1600PSample   Si:B 50 ohm cm"
580 PRINT"M1700,1500P  Cu & Zn diffused at "
590 PRINT"M1700,1400P       T=1100.   "
600 PRINT"M1700,1300P Temperature of sample "Temp:PRINT"PK"
610 ENDPROC
620 DEF PROCWRITE1
630 PRINT"M1000,1750S5,5P Intensity vs Time "
640  PRINT"M50,750Q1S3,3PIntensity (arb. units)"
650 PRINT"H":ENDPROC
660 DEF PROCLOG
670 X=100:VDU2:VDU29,0;1000;
680 VDU2
690 FOR I=1 TO N
700 IF Y(I)<=0 THEN 730
710 Y(I)=LN((Y(I))/YMAX)
720 MOVE X,Y(I)*100:DRAW X,Y(I)*100
730 X=X+1000/N:NEXT:PROCCAL:PROCXAXIS
740 Y=1700:FOR O=0 TO 4:VDU21
750 PRINT"M0,"+STR$(Y)
760 PRINT"P "
770 @%=131850
780 o=O*YMIN/4:PRINT"P"o  :Y=Y-400:VDU6:NEXTO
790 X=100
800 FOR I= 1TO N
810 Y(I)=Y(I)*1650/ABS(YMIN)+50
820 Y(I)=INT(Y(I))
830 Y(I)=1600+Y(I)
840 VDU21
850 PRINT"M"+STR$(X)+","+STR$(Y(I))
860 PRINT"D"+STR$(X)+","+STR$(Y(I))
870 X=X+2400/N
880 VDU6:NEXT
890 PRINT"M1000,1700S5,5P LOG(I/Imax)  vs Time"
900 PROCWRITE
910 PRINT"H"
920 VDU3
930 ENDPROC
```

```
 10 REM ************************************************************
 20 REM ****                                                    ****
 30 REM ****       Program to plot spectra                      ****
 40 REM ****                                                    ****
 50 REM ************************************************************
 60 MODE3
 70 *.
 80 PRINTCHR$(130)"NAME OF FILE":INPUTB$
 90 L=OPENIN(B$)
100 INPUT$L,S:INPUT$L,E:INPUT$L,INC:INPUT$L,Temp
110 X=0:P=(E-S)/INC+1
120 MODE4:DIM Y(P)
130 FOR I=1 TO P
140 INPUT$L,A%:Y(I)=ABS(A%)
150 Y(I)=ABS(A%)
160 MOVE X,Y(I)/2:DRAWX,Y(I)/2
170 X=X+1200/P:NEXT I:CLOSE$0:PROCCAL
180 REM PROCSPIKE
190 INPUT"Do you want to look at a specific wavelength range"
200 IF GET$="Y" THEN PROCDIVISION
210 PROCPLOT:PROCXAXIS:PROCYAXIS:PROCWRITE
220 PRINT"H":VDU3
230 PRINT"Do you want to plot another spectrum y/n "
240 IF GET$="Y" THEN 10 ELSE CHAIN "LINK"
250 END
260 DEF PROCCAL
270 YMAX=0:YMIN=100
280 FOR i=1 TO P
290 IF Y(i)>YMAX THEN YMAX=Y(i)
300 IF Y(i)<=YMIN THEN YMIN=Y(i)
310 NEXT i:ENDPROC
320 DEF PROCXAXIS
330 VDU2:X1=X/5+100
340 FOR I=1TO 5
350 PRINT"M"+STR$(X1)+",30":PRINT"S3,3"
360 PRINT"P|"
370 PRINT"M"+STR$(X1)+",0"
380 PRINT"P" STR$(S+INT(I*(E-S)/5))
390 VDU6:X1=X1+X/5:NEXT
400 PRINT"M1000,75":PRINT"P Wavelength (A) "
410 ENDPROC
420 DEF PROCYAXIS
430 VDU2:Y=50
440 FOR O=0 TO 4
450 VDU21
460 PRINT"M95,"+STR$(Y)
470 PRINT"P "
480 PRINT"P"STR$(O/4)
490 Y=Y+400:VDU6:NEXT:ENDPROC
500 DEF PROCPLOT
510 VDU2:X=100
520 FOR I=1 TO P
530 VDU21
540 Y=INT(Y(I)*1600/YMAX)+50
550 PRINT"M"+STR$(X)+","+STR$(Y)
```

```
 560 PRINT"D"+STR$(X)+","+STR$(Y),"B20"
 570 X=X+2500/P:X=INT(X):VDU6:NEXT
 580 REM PRINT"M 1000,1200S5,5PINTENSITY VS WAVELENGTH"
 590 ENDPROC
 600 DEF PROCWRITE
 610 PRINT"M1600,1200PTEMP          "Temp:PRINT"PK"
 620 PRINT"M1000,1650PEnergy (mev)"
 630 X2=X/5+100
 640 FOR I=1 TO 5
 650 PRINT"M"+STR$(X2)+",1800"
 660 PRINT"P|"
 670 PRINT"M"+STR$(X2)+",1750":PRINT"S3,3"
 680 K=S+((E-S)/5)*I
 690 K1=1.243E-3/((K)*1E-10)
 700 @%=131594
 710 PRINT"P"K1
 720 VDU6:X2=X2+X/5:NEXTI
 730 PRINT"M40,700":PRINT"Q1P Intensity (arb. units)"
 740 ENDPROC
 750 PRINT"H"
 760 VDU3
 770 DEF PROCDIVISION
 780 PRINT:PRINT
 790 CLS
 800 INPUT"Wavelength range ", S,E
 810 X=0:S2=S-S+1:E2=E-S
 820 FOR i=S TO E/INC
 830 MOVE X,Y(i)/2
 840 DRAW X,Y(i)/2
 850 X=X+1200/(E-S)
 860 NEXT
 870 PROCCAL
 880 ENDPROC
 890 DEF PROCSPIKE
 900 FOR I=1 TO 100
 910 IF Y(I)>1.05*Y(I-1)  THEN Y(I)=Y(I-1)
 920 NEXT
 930 FOR I=450 TO 1100
 940 IF Y(I)>1.05*Y(I-1) THEN Y(I)=(Y(I-1))
 950 IF Y(I)<Y(I-1)/1.05 THEN Y(I)=Y(I-1)
 960 NEXT
 970 X=0:CLS
 980 FOR I=S1 TO E1/INC
 990 MOVEX,Y(I)/2:DRAW X,Y(I)/2
1000 X=X+1200/(E-S+1):NEXT:ENDPROC
```

```
*************************************************
***                                           ***
***      To Fit an Excitation Impulse         ***
***      to a Series of Exponentials.         ***
***                                           ***
***          N.I.H.E.     DUBLIN,             ***
***                                           ***
*************************************************

      DOUBLE PRECISION   SIGMA, TOL, A(1000,200), B(1000),
                         C(1000,200), WORK(16)
      INTEGER  I, IFAIL, IRANK, LWORK, NIN, NOUT, NRA,
               NA,J,L,K

      CHARACTER *27  TITLE
      WRITE (6,*) " Input data file 001 to 020 "
      READ (5,*)  NA
      WRITE (6,*) " Output files stored at 020 to 040 "
      READ (5,*)  NOUT
      WRITE (6,*) "Input location of matrix A "
      READ (5,*) NIN
      READ (NIN,99999) TITLE
      WRITE (NOUT,99998) TITLE
      NRA=1000
      LWORK=16
      IFAIL=0
      M=200
      N=3
      TOL=5.0E-4

      DO 20  I = 1,M
      READ (NIN,*)  ( A(I,J), J=1,N )
C     WRITE (6,*)  ( A(I,J), J=1,N )
20    CONTINUE

      DO 30  I=1,M
      READ (NA,*)  ( B(I) )
C     WRITE (6,*)  ( B(I) )
30    CONTINUE

C     WRITE (6,*)  ( A(I,J), J=1,N), I=1,M )

      DO 40 K = 1,M
      DO 50 L = 1,N
      C(L,K) = A(K,L)
C     WRITE (6,222)  ( A(K,L) )
50    CONTINUE
40    CONTINUE

C     WRITE (6,222)  (( C(K,L), L=1,M ), K=1,N )

222   FORMAT (3F7.3)
      WRITE (NOUT,99996)
      WRITE (NOUT,99992)  (( A(I,J), J=1,N ), I=1,M )
      WRITE (NOUT 99995)
```

```
      WRITE (NOUT,99992)  ( B(I), I=1,M )

      CALL F04JAF (M,N,A,B,NRA,TOL,SIGMA,IRANK,IFAIL,WORK,LWORK

      WRITE (NOUT,99994)
      WRITE (NOUT,99992)  ( B(I), I=1,N )
      WRITE (NOUT,99993)  SIGMA, IRANK
      STOP  " END OF PROGRAM "

99999 FORMAT ( A35 )
99998 FORMAT ( 2X,/,1X,A35,// "RESULTS" )
99997 FORMAT ( 2F6.2 )
99996 FORMAT ( "MATRIX A" )
99995 FORMAT ( "VECTOR B" )
99994 FORMAT ( "SOLUTION VECTOR" )
99993 FORMAT ( "STANDARD ERROR = ", F10.4, "RANK = ",I2 )
99992 FORMAT ( 1A,3F9.3 )
      END
```

```
C     ************************************************************

                To find the Eigenvalues and Eigenvectors
                    of a complex hermitean matrix.

                              NIHE  DUBLIN.

      ************************************************************

C     OUTPUT OF PROGRAM IS OBSERVED TRANSITION ENERGIES.

      DOUBLE PRECISION AR(12,12),AI(12,12),WR(12),VR(12,12),VI(12,12),
     *  WK1(12),WK2(12),WK3(12),A(12,12),B(12,12),SI(100),DEL(100),
     *  W(12),C(3000),D(3000),E(3000),F(3000),ABS

      REAL Y1,Y2,Y3,Y4

      INTEGER I,N,J,IAR,IVR,IAI,IVI,IFAIL,NOUT,P,Q,L

      NOUT =20
C     OPEN (20,FILE='DATA.',STATUS='NEW')

      IAR=12
      IAI=12
      IVR=12
      IVI=12
      N=12
C     Defining work space for the routine.

      AI=7.8
      BI=22.6
      CI=52.5
      AE=5.8
      BE=11.3
      CE=45.5
C     AI,BI, & CI are parameters accurately known for the
C     free exciton in silicon.
C     Parameters for BE are AE=5.8,BE=11.3,CE=45.5.
C     Parameters for ABC are AE=4.0,BE=15.5,CE=35.5.
C     Stress is positive for tension and negative for compression.
C     Matrix is set up using stress parameters for the transition
C     energy, i.e. if the VB is perturbed to higher electron energy
C     stress term is negative for transition is negatively perturbed.

      ISX=1
      ISY=1
      ISZ=1
C     Internal stress direction.

      ESO=44
      TOL=0.05
      IFAIL=0
      Y1=3.2
      Y2=4.66
      Y3=15.7
      Y4=13.73
      DEL(1)=0.0
      L=1
C     Y1,Y2,Y3,Y4 are energies found in luminescence studies.
```

```
C       The eigenvalues are changed to relative transition erne
C       and compared to Y1.... . The best fit is then obtained.

        DO 10 P=2,1000
        DEL(P)=DEL(P-1)+0.001
        SI(1)=0.0001
        DO 20 Q=2,1000
        SI(Q)=SI(Q-1)+0.0001

        CALL MATR(AR,N,SI,ISX,ISY,ISZ,CI,EGO,DEL,Q,P)
C       Real components of matrix.

        CALL MATI(AI,N,SI,ISX,ISY,ISZ,CI,Q)
C       Imaginary components of matrix.

        CALL F02AXF(AR,IAR,AI,IAI,N,WR,VR,IVR,VI,IVI,WK1,WK2,WK
C       NAG libary routine to diagonalise a hermitean matrix.

        IF (IFAIL.EQ.0) GO TO 30
        WRITE (5,99996) IFAIL
        STOP
C       WRITE (5,99)
C       WRITE (5,99994) (WR(I),I=1,N)
30      C(L)=WR(3)-WR(1)
        D(L)=WR(5)-WR(1)
        E(L)=WR(6)-WR(1)
        F(L)=WR(8)-WR(1)
        WRITE (5,99994) C(L),D(L),E(L),F(L)
        WRITE (5,99994) SI(Q),DEL(P)

        IF(ABS(D(L)-Y2).GT.TOL) GO TO 32
        IF(ABS(E(L)-Y3).GT.TOL) GO TO 32
        IF(ABS(C(L)-Y1).GT.TOL) GO TO 32
        IF(ABS(F(L)-Y4).GT.TOL) GO TO 32

33      WRITE(5,99994) C(L),D(L),E(L),F(L)
C       WRITE(5,99994) Y1,Y2,Y3
        WRITE(5,99994) SI(Q),DEL(P)

32      L=L+1
20      CONTINUE
10      CONTINUE
        STOP



99      FORMAT (' EIGENVALUES')
98      FORMAT (' EIGENVECTORS')
999     FORMAT (F10.5)
99999   FORMAT (A35)
99998   FORMAT (2F8.5)
99997   FORMAT (2X,/1X,A35,///'RESULTS')
99996   FORMAT ('ERROR IN F02AXF IFAIL =',I2)
99994   FORMAT (F10.5,2X,F10.5,2X,F10.5,2X,F10.5,2X)
99991   FORMAT (8F5.5)
        END
```

```
C       REAL PART OF INTERNAL STRESS MATRIX
C       Matrix also has J-J coupling of magnitude DEL (mev)
C       which is defined in the subroutine. ESO is the spin
C       orbit coupling and equals 44 mev.

        XNDX=NDX
        XNDY=NDY
        XNDZ=NDZ
        DNOM=SQRT(XNDX**2+XNDY**2+XNDZ**2)
        DX=XNDX/DNOM
        DY=XNDY/DNOM
        DZ=XNDZ/DNOM
        SXX=SI(Q)*DX*DX
        SYY=SI(Q)*DY*DY
        SZZ=SI(Q)*DZ*DZ
        SXZ=SI(Q)*DX*DZ
        SXY=SI(Q)*DX*DY
        SYZ=SI(Q)*DY*DZ
        STH=(2.0*SZZ-SXX-SYY)*BI/2.0
        SEP=SQRT(3.0)*(SXX-SYY)*BI/2.0
        DO 40 I=1,N
        DO 40 J=1,N
40      A(I,J)=0.0
995     FORMAT (F10.3,2X,F10.3)

C       DEFINE MATRIX ELEMENTS


        A(1,1)=-3.0*DEL(P)/8.0-STH
        A(2,1)=-CI*SXZ/SQRT(3.0)
        A(2,2)=-DEL(P)/8.0+STH
        A(3,1)=-SEP
        A(4,2)=-SEP
        A(5,2)=-DEL(P)*SQRT(3.0)/4
        A(3,3)=DEL(P)/8.0+STH
        A(4,3)=CI*SXY/SQRT(3.0)
        A(4,4)=3.0*DEL(P)/8.0-STH
        A(5,5)=3.0*DEL(P)/8.0-STH
        A(6,3)=-DEL(P)/2.0
        A(6,5)=-CI*SXZ/SQRT(3.0)
        A(6,12)=-CI*SXZ/SQRT(2.0)
        A(6,6)=DEL(P)/8.0+STH
        A(7,4)=-DEL(P)*SQRT(3.0)/4
        A(7,5)=-SEP
        A(7,7)=-DEL(P)/8.0+STH
        A(8,6)=-SEP
        A(8,7)=CI*SXZ/SQRT(3.0)
        A(8,8)=-3.0*DEL(P)/8.0-STH
        A(8,12)=CI*SXZ/SQRT(6.0)
        A(9,1)=CI*SXZ/SQRT(6.0)
        A(9,2)=-STH*SQRT(2.0)
        A(9,3)=-CI*SXZ/SQRT(2.0)
        A(9,4)=-SEP*SQRT(2.0)
        A(9,9)=-DEL(P)/4.0
        A(10,10)=DEL(P)/4.0
        A(11,11)=DEL(P)/4.0
        A(12,12)=-DEL(P)/4.0
        A(10,1)=SEP*SQRT(2.0)
        A(10,2)=-CI*SXZ/SQRT(2.0)
        A(10,3)=STH*SQRT(2.0)
        A(10,4)=CI*SXZ/SQRT(6.0)
```

```
          J=I+4
          A(12,J)=A(10,I)
          A(11,J)=A(9,I)
   60     CONTINUE
          DO 70 I=1,8
          A(I,I)=A(I,I)- ESO/3.0
   70     CONTINUE
          DO 80 I=9,12
   80     A(I,I)=A(I,I)+2.0*ESO/3.0
          DO 82 I=1,N
          DO 81 J=1,N
          A(I,J)=A(J,I)
   81     CONTINUE
   82     CONTINUE

          RETURN
          END


          SUBROUTINE MATI(B,N,SI,NDX,NDY,NDZ,CI,Q)

C         IMAGINARY PART OF MATRIX

          DOUBLE PRECISION B(12,12),SI(50)
          INTEGER Q
          XNDX=NDX
          XNDY=NDY
          XNDZ=NDZ
          DNOM=SQRT(XNDX**2+XNDY**2+XNDZ**2)
          DX=XNDX/DNOM
          DY=XNDY/DNOM
          DZ=XNDZ/DNOM
          SXY=SI(Q)*DX*DY
          SYZ=SI(Q)*DY*DZ

          DO 90 I=1,N
          DO 90 J=1,N
   90     B(I,J)=0.0

C         DEFINE MATRIX ELEMENTS


          B(2,1)=-CI*SYZ/SQRT(3.0)
          B(3,1)=-CI*SXY/SQRT(3.0)
          B(4,2)=-CI*SXY/SQRT(3.0)
          B(4,3)=CI*SYZ/SQRT(3.0)
          B(6,5)=-CI*SYZ/SQRT(3.0)
          B(7,5)=-CI*SXY/SQRT(3.0)
          B(8,6)=-CI*SXY/SQRT(3.0)
          B(8,7)=CI*SYZ/SQRT(3.0)
          B(8,11)=CI*SYZ*SQRT(2.0/3.0)
          B(9,1)=CI*SYZ/SQRT(6.0)
          B(9,3)=CI*SYZ/SQRT(2.0)
          B(9,4)=CI*SXY*SQRT(2.0/3.0)
          B(10,1)=CI*SXY*SQRT(2.0/3.0)
          B(10,2)=-CI*SYZ/SQRT(2.0)
          B(10,4)=-CI*SYZ/SQRT(6.0)
```

```
      J=I+4
      B(11,J)=B(9,I)
      B(12,J)=B(10,I)
110   CONTINUE
      DO 120 I=1,N
      DO 115 J=1,N
      B(I,J)=B(J,I)
115   CONTINUE
120   CONTINUE

99A   FORMAT(E10.3)
      RETURN
      END
```